# Chapter 29: Magnetic Resonance Spectroscopy

> "But because throughout the universe from time everlasting countless numbers of them [*atoms*], buffeted and impelled by blows, have shifted in countless ways, experimentation with every kind of movement and combination has at last resulted in arrangements such as those that created and compose our world."
>
> "at absolutely unpredictable times and places they deflect slightly from their straight course, to a degree that could be described as no more than a shift of movement" Lucretius[1]

Nuclear magnetic resonance and electron spin resonance are distinguished from other forms of spectroscopy by the ability to directly determine molecular connectivity. Molecular connectivity is the pattern of atomic connections that distinguish structural and geometric isomers. Magnetically active nuclei are observed in **nuclear magnetic resonance**, NMR. Unpaired electrons in molecules or ions are observed in **electron spin resonance**, **ESR**. ESR is alternately called **electron paramagnetic resonance, EPR**. Nuclear and electron spins behave analogously when placed in a magnetic field. In a magnetic field, transitions between spin states are observed. The transition frequencies reflect the chemical shifts of the spins and the coupling between the spins.

NMR and Xray diffraction are the most direct and indispensable techniques in molecular structure determination. NMR techniques are well-developed for small and large molecules, including proteins and nucleic acids. NMR and Xray diffraction are the experimental foundation of diverse areas such as natural products chemistry, organometallic chemistry, and Structural Biology. ESR is particularly useful in characterizing paramagnetic metal complexes and reactive intermediates in chemical reactions. Chemical shifts in magnetic resonance spectra provide information about the electronic environments in a molecule or free radical. In addition, the coupling between spins is manifested in spin-spin splitting, which aids the determination of molecular connectivity. Magnetic resonance is also a sensitive probe of molecular motion.

The utility of magnetic resonance techniques is enhanced using pulsed modes of spectral acquisition. In pulsed spectroscopies a short pulse of radiation is used to create a coherent superposition of states. The time evolution of the coherent superposition allows the study of molecular connectivity, state dynamics, and molecular motion. Because NMR is the lowest frequency common form of spectroscopy, coherent techniques have been first introduced in NMR and later applied to ESR, terahertz, and optical spectroscopies. Coherence based spectroscopy uses the careful production and manipulation of known superposition of states, which includes the relative phase of each state in the superposition. Coherent states evolve along a coupled, deterministic, and cooperative path. The intricate control of coherence allows many new forms of spectroscopy that meet critical needs in molecular structure and motion characterization.

## 29.1 Nuclear Magnetic Resonance

*Nuclear Spin States Have Different Energies in a Magnetic Field*: Charged particles that have non-zero angular momentum have a magnetic moment. A nucleus with spin quantum number I has angular momentum with magnitude $\hbar\sqrt{I(I+1)}$, which in an applied magnetic field has projections along the magnetic field axis of $\hbar m_I$ with $m_I = -I, -I+1, .., 0, \ldots, I-1, I$. The number of projections is $2I + 1$, Eq. 24.5.36. The magnetic moment is proportional to the angular momentum. The projection of the nuclear magnetic moment along the applied field, $\mu_z$, is correspondingly quantized:

$$\mu_z = \gamma_n \hbar m_I \qquad m_I = -I, -I+1, .., 0, \ldots, I-1, I \qquad 29.1.1$$

where $\gamma_n$ is the magnetogyric ratio. The magnetogyric ratio, which is also called the gyromagnetic ratio, has units of radians per second per unit field strength in tesla and is characteristic of the given nucleus, Table 29.1.1. Of the naturally occurring elements, only argon has no magnetic isotope.

Table 29.1.1: Typical Magnetic Nuclei with Resonance Frequencies at 9.395 T. The receptivities relative to $^{1}H$ and $^{13}C$ are the relative spectroscopic sensitivities.[2]

| Nucleus | I | Abundance (%) | $\gamma_n$ ($10^6$ $s^{-1}$ $T^{-1}$) | ν (MHz) | Receptivity Recept $^{1}H$ | Receptivity Recept $^{13}C$ |
|---|---|---|---|---|---|---|
| $^{1}H$ | ½ | 99.989 | 267.522 | 400.0 | 1.00 | 5870 |
| $^{2}H$ | 1 | 0.0115 | 41.066 | 61.40 | $1.11 \times 10^{-6}$ | 0.00652 |
| $^{13}C$ | ½ | 1.07 | 67.283 | 100.58 | $1.70 \times 10^{-4}$ | 1.00 |
| $^{14}N$ | 1 | 99.632 | 19.338 | 28.90 | 0.00100 | 5.90 |
| $^{15}N$ | ½ | 0.368 | -27.126 | 40.55 | $3.84 \times 10^{-6}$ | 0.0225 |
| $^{17}O$ | 5/2 | 0.038 | -36.281 | 54.23 | $1.11 \times 10^{-5}$ | 0.0650 |
| $^{19}F$ | ½ | 100 | 251.181 | 376.4 | 0.834 | 4900 |
| $^{31}P$ | ½ | 100 | 108.394 | 161.9 | 0.0665 | 391.0 |
| $^{35}Cl$ | 3/2 | 75.78 | 26.24 | 39.24 | 0.00358 | 21.0 |
| $^{195}Pt$ | ½ | 33.83 | 58.385 | 87.30 | 0.00351 | 20.1 |

Consider first the nuclei of hydrogen atoms, which are protons or equivalently $^{1}H$. Protons have spin quantum number I = ½. When placed in a magnetic field, the magnetic moment of the proton has two orientations with respect to the applied magnetic field, giving angular momentum projections $m_I = \pm ½$, Figure 29.1.1. $^{14}N$ has I = 1, giving three possible projections of the spin angular momentum. $^{35}Cl$ has I = 3/2, giving four possible projections.

The classical energy of interaction of a magnetic moment with an applied magnetic field is:[3]

$$E = -\ \vec{\mu}_n \cdot \vec{B}_o \qquad 29.1.2$$

where $\vec{\mu}_n$ is the magnetic moment vector and $\vec{B}_o$ is the applied magnetic field vector, with magnitude $B_o$. For convenience, we align the direction of the applied magnetic field with the z-axis. The z-axis is then the direction of quantization in Eq. 29.1.1; the projection of the magnetic moment along the z-axis determines the energy. The quantum mechanical Hamiltonian is then derived from the classical expression giving the energy of a single spin as:

$$\hat{\mathcal{H}} = -\gamma_n \hbar \hat{I}_z B_o \qquad 29.1.3$$

where $\hat{I}_z$ is the quantum operator that determines the projection of the angular momentum along the z-axis. The corresponding spin wave functions are eigenfunctions of both $\hat{I}_z$ and the Hamiltonian with energy:

$$E = -\gamma_n \hbar m_I B_o \qquad 29.1.4$$

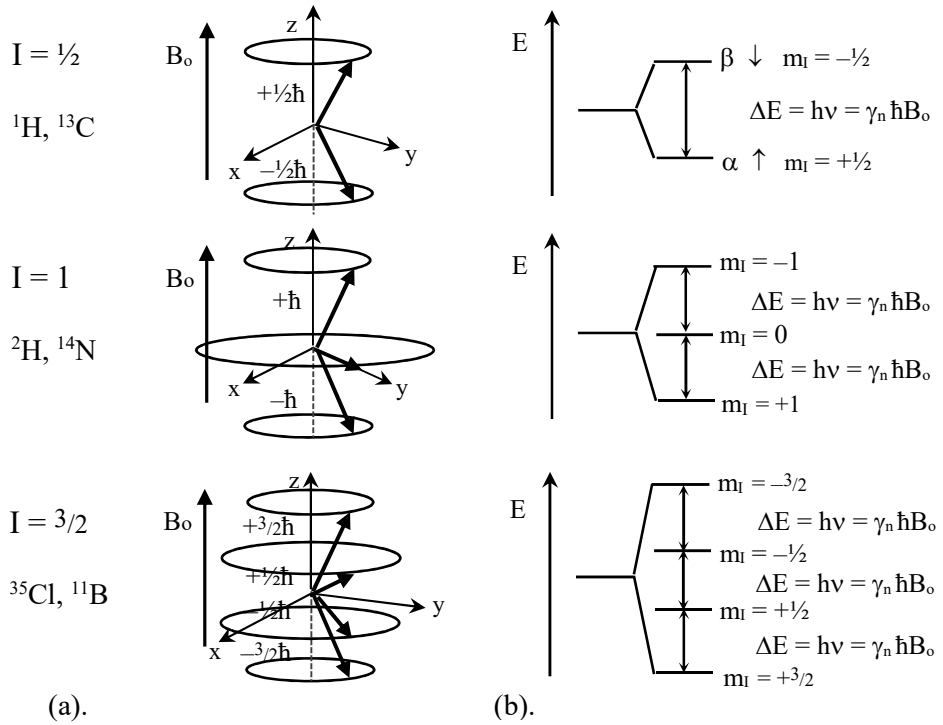


Figure 29.1.1: Energy levels of a nuclear spin in an applied magnetic field. (a). The z-axis projection of the angular momentum is quantized. (b). The energy level diagram has equally spaced spin states corresponding to unit changes in the z-axis angular momentum projection.

For protons and other spin-½ nuclei, the spin wave functions are: $\alpha$ for $m_I = +½$ or "spin-up" and $\beta$ for $m_I = –½$ or "spin-down." Using the spin Hamiltonian, Eq. 29.1.3, gives:

$$\hat{I}_z\,\alpha = +½\,\alpha \quad \text{and} \quad \hat{\mathcal{H}}\alpha = E\,\alpha \quad \text{with} \quad E = –½\,\gamma_n\,\hbar\,B_o$$
$$\hat{I}_z\,\beta = –½\,\beta \quad \text{and} \quad \hat{\mathcal{H}}\beta = E\,\beta \quad \text{with} \quad E = +½\,\gamma_n\,\hbar\,B_o \qquad 29.1.5$$

The specific selection rule requires a unit change in angular momentum for an allowed transition. As a result light absorption and emission cause transitions only between adjacent spin levels. The allowed transition energy differences are, Figure 29.1.1b:

$$\Delta E = h\nu_o = \gamma_n\,\hbar B_o \qquad (\beta \leftarrow \alpha) \qquad 29.1.6$$

where $\nu_o$ is the transition frequency. NMR transition frequencies are in the radio-frequency region of the electro-magnetic spectrum. When the frequency of the exciting radiation matches the transition frequency, energy is absorbed or emitted and spins "flip" going from spin-up to spin-down or spin-down to spin-up, respectively. This frequency matched condition is said to be at resonance, whence the name nuclear magnetic resonance.

The sensitivity of NMR, relative to optical spectroscopies, is quite poor. One cause is that high energy photons are easier to detect than low energy photons. Secondly, the Boltzmann population differences are unfavorable in NMR. For example, at room temperature, the Boltzmann population difference for the $m_I = \pm½$ transition of protons at $\nu = 400$ MHz is:

$$\frac{n_-}{n_+} = e^{-\Delta E/kT} = e^{-\gamma_n \hbar B_o/kT} = e^{-\nu/(kT/h)} = e^{-400x10^6\ s^{-1}/6.2124x10^{12}\ s^{-1}} = 0.999936$$

$$n_+ - n_- = (n_+ + n_-)\left(\frac{1 - 0.999936}{1 + 0.999936}\right) = (n_+ + n_-)\ 3.20x10^{-5} \quad \text{(400 MHz at 298.2 K)} \quad 29.1.7$$

Values of kT/h are tabulated on the inside front cover of this text. The population difference is only 32 out of a million protons. High field strength results in higher transition frequency and larger population differences, which greatly enhance sensitivity. Instruments operating up to 1 GHz for $^1$H at 23.5 T are commercially available. A third cause of the poor sensitivity of NMR is that the natural abundance of many magnetic nuclei is small. Only one out of every 100 carbon atoms is a $^{13}$C. Receptivity, which takes into account the transition energy, population difference, and natural abundance, is a measure of the spectroscopic sensitivity. Relative receptivity as compared to protons or $^{13}$C are commonly tabulated, Table 29.1.1. $^{13}$C NMR is roughly four-orders of magnitude less sensitive than proton NMR. The proton and $^{13}$C spectra of ethanol are shown in Figure 29.1.2.

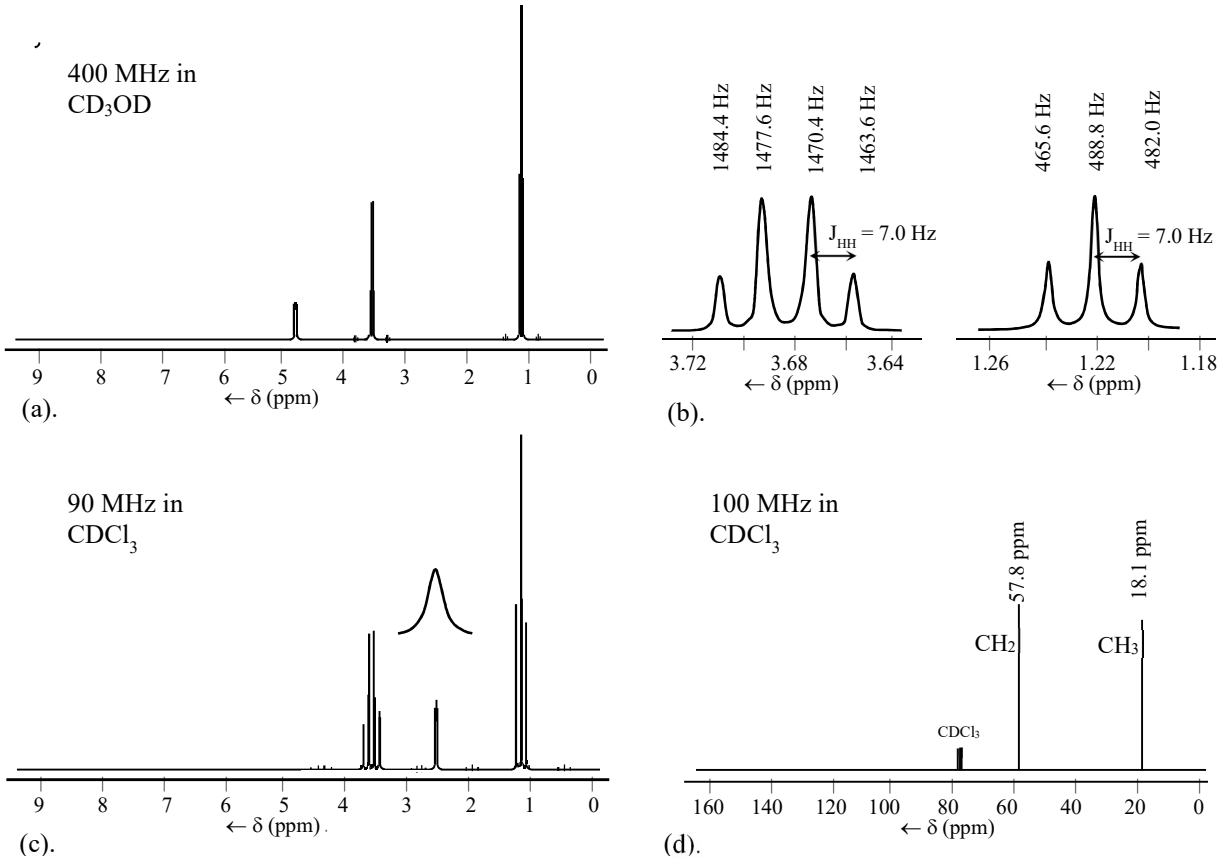


Figure 29.1.2: $^1$H and $^{13}$C NMR spectra of ethanol. (a). $^1$H spectrum at 400 MHz in deuterated methanol. (b). Scale expansions about the chemical shifts for the methylene and methyl groups, respectively. (c). $^1$H spectrum at 90 MH$_z$ in deuterated chloroform. The inset shows the exchange broadened hydroxyl peak on an expanded chemical shift scale. (d). $^{13}$C proton-decoupled spectrum at 100 MHz in deuterated chloroform. The 1:1:1-triplet at 77.4 ppm is the solvent.

*The Chemical Shift is Dependent on Local Electron Denisty:* The proton NMR spectrum of ethanol, Figure 29.1.2a, is a plot of signal intensity, or absorption, versus frequency. For historical reasons, the convention is to plot frequency increasing to the left. At low resolution the spectrum shows three resonances, which correspond to three different chemical environments. The differences between the chemical environments are small. As a result, the horizontal axis is usually presented as relative shifts in parts per million, ppm, instead of directly in frequency. For resonance i, the **chemical shift** in ppm is defined as:

$$\delta_i \equiv \frac{\nu_i - \nu_{ref}}{\nu_{ref}} 1x10^6 \text{ ppm} \qquad 29.1.8$$

where $\nu_i$ is the given resonance frequency and $\nu_{ref}$ is the reference frequency. For $^1$H NMR, tetramethylsilane, TMS, is often chosen as the reference, which by definition is assigned a chemical shift of 0 ppm. The small shift in frequency between different chemical environments is remarkable. For example, a 10 ppm chemical shift at a resonance frequency of 300 MHz corresponds to: 10 ppm(300x$10^6$ Hz)(1/$10^6$ ppm) = 3000 Hz. If TMS resonates at 300.00000 MHz, then 10 ppm corresponds to 400,003,000 Hz. The typical chemical shift range of $^1$H NMR is -1 – 14 ppm.

The integrals under the transitions are proportional to the number of protons in each chemical environment. Using the integrals to identify the chemical environments in ethanol, the most "downfield" resonance at 4.8 ppm is the –OH proton.The resonance at 3.68 ppm is for the methylene protons, -$CH_2$-. The "upfield" resonance at 1.88 ppm is for the methyl protons. The chemical shifts are caused by differences in the electronic environment at each nucleus. The chemical shifts of different chemical environments are amazingly constant from molecule to molecule, Tables 29.1.2-29.1.3. However, because the –OH proton in ethanol is labile, the chemical shift of the –OH proton is variable and the transition is broadened, Figure 29.1.2c. This special case is discussed in the section on chemical exchange.

Table 29.1.2: $^1$H Chemical Shifts of Methyl, Methylene, and Methine Groups.[(DS)4]

| | Methyl protons | $\delta_H$ | Methylene protons | $\delta_H$ | Methine protons | $\delta_H$ |
|---|---|---|---|---|---|---|
| C | $CH_3$–R | 0.9 | R–$CH_2$–R | 1.4 | >CH–R | 1.5 |
| | $CH_3$–C–O | 1.3 | R–$CH_2$–C–O | 1.9 | >CH–C–O | 2.0 |
| | $CH_3$–C=C | 1.6 | R–$CH_2$–C=C | 2.3 | >CH–C=C | 2.6 |
| | $CH_3$–Ar | 2.3 | R–$CH_2$–Ar | 2.7 | >CH–Ar | 3.0 |
| | $CH_3$–C(=O)–R | 2.2 | R–$CH_2$-C(=O)–R | 2.4 | >CH–C(=O)–R | 2.7 |
| | $CH_3$–C(=O)–OR | 2.0 | R–$CH_2$-C(=O)–OR | 2.2 | >CH–C(=O)–OR | 2.5 |
| N | $CH_3$–N | 2.3 | R–$CH_2$–N | 2.5 | >CH–N | 2.8 |
| | $CH_3$–N–Ar | 3.0 | R–$CH_2$–N–Ar | 3.1 | >CH–N–Ar | 3.6 |
| | $CH_3$-N–C(=O)–R | 2.9 | R–$CH_2$–N–C(=O)–R | 3.2 | >CH–N–C(=O)–R | 4.0 |
| O | | | R–$CH_2$–OH | 3.6 | >CH–OH | 3.9 |
| | $CH_3$–OR | 3.3 | R–$CH_2$–OR | 3.4 | >CH–OR | 3.7 |
| | $CH_3$–O–Ar | 3.8 | R–$CH_2$–O–Ar | 4.3 | >CH–O–Ar | 4.5 |
| | $CH_3$–O–C(=O)–R | 3.7 | R–$CH_2$–O–C(=O)–R | 4.1 | >CH–O–C(=O)–R | 4.8 |
| X | | | R–$CH_2$–Cl | 3.6 | >CH–Cl | 4.2 |

R = alkyl, Ar = aromatic ring. Typically ±0.3 ppm for methyl and methylene and ±0.5 ppm for methine unless electronic or anisotropic effects from other groups are strong.

Table 29.1.3: Chemical shift ranges for protons attached to multiple bonds.[4]

| Structure | $\delta_H$ | Structure | $\delta_H$ |
|---|---|---|---|
| RCH=O | 9.4 – 10.0 | >C=CH– | 4.5-6.0 |
| ArCH=O | 9.7 – 10.5 | >C=CHC(=O)– | 5.8 – 6.7 |
| –OCH=O | 8.0 – 8.2 | –HC=CC(=O)– | 6.5 – 8.0 |
| >NCH=O | 8.0 – 8.2 | –HC=C–O– | 4.0 – 5.0 |
| –C≡CH | 1.8 – 3.1 | >C=CH–O– | 6.0 – 8.1 |
| >C=C=CH– | 4.0 – 5.0 | –HC=C–N– | 3.7 – 5.0 |
| ArH | 6.0 – 9.0 | >C=CH–N– | 5.7 – 8.0 |

$^{13}C$ NMR is a commonly used tool, especially in natural products chemistry, Figures 29.1.2d, 29.1.3. $^{13}C$ chemical shifts are roughly 20 times the corresponding proton chemical shifts, with the typical range of 0 to 220 ppm relative to TMS. One advantage of $^{13}C$ spectra is the appearance of resonances for aldehydes, ketones, carboxylic acids, esters, amides, acid anhydrides, and nitriles, which have no corresponding $^{1}H$ equivalent, Table 29.1.4. Quaternary carbons, which have no attached hydrogens, also appear.

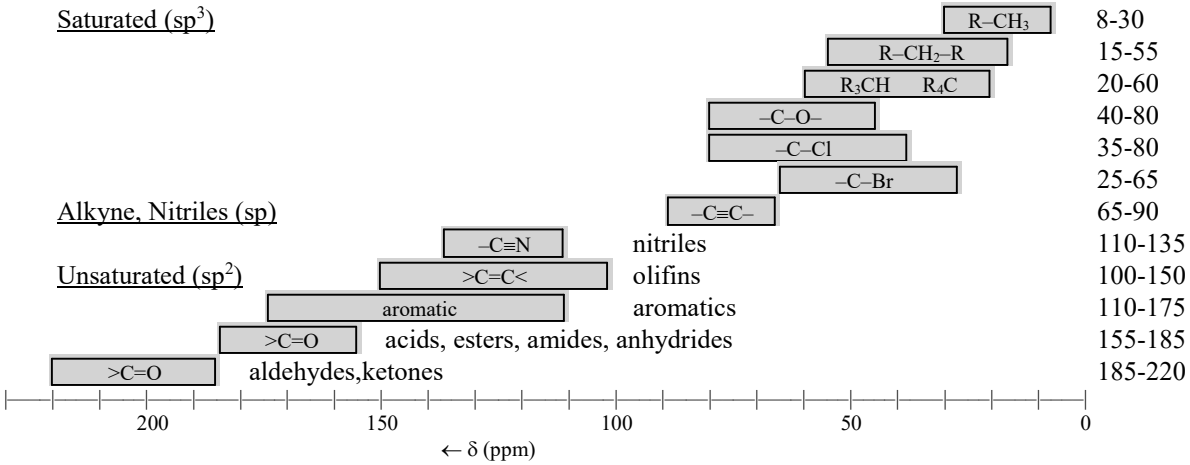


Figure 29.1.3: $^{13}C$-chemical shift ranges using TMS as a reference.[5]

Table 29.1.4: $^{13}C$ Chemical Shifts of Carbonyl Carbons.[(DS) 4]

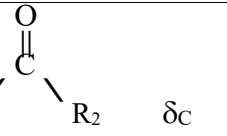

| $R_1$ | $R_2$ | $\delta_C$ |
|---|---|---|
| Et– | –H | 206.0 |
| $CH_2$=CH– | –H | 192.4 |
| Ph– | –H | 192.0 |
| Et– | –Me | 207.6 |
| $CH_2$=CH– | –Me | 197.2 |
| Ph– | –Me | 197.6 |
| Et– | –OH | 180.4 |
| $CH_2$=CH– | –OH | 171.7 |
| Ph– | –OH | 172.6 |

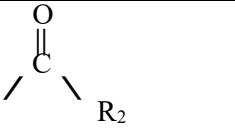

| $R_1$ | $R_2$ | $\delta_C$ |
|---|---|---|
| Et– | –OMe | 173.3 |
| $CH_2$=CH– | –OMe | 165.5 |
| Ph– | –OMe | 166.8 |
| Et– | –$NH_2$ | 174.3 |
| $CH_2$=CH– | –$NH_2$ | 168.3 |
| Ph– | –$NH_2$ | 169.7 |
| Me– | –OAc | 167.3 |
| Ph– | –OAc | 162.8 |
| Et– | –Cl | 174.7 |
| Ph– | –Cl | 168.0 |

A semi-classical descriptive model is useful to understand the origins of the chemical shift. Consider one of the protons in a methyl group, Figure 29.1.4a.

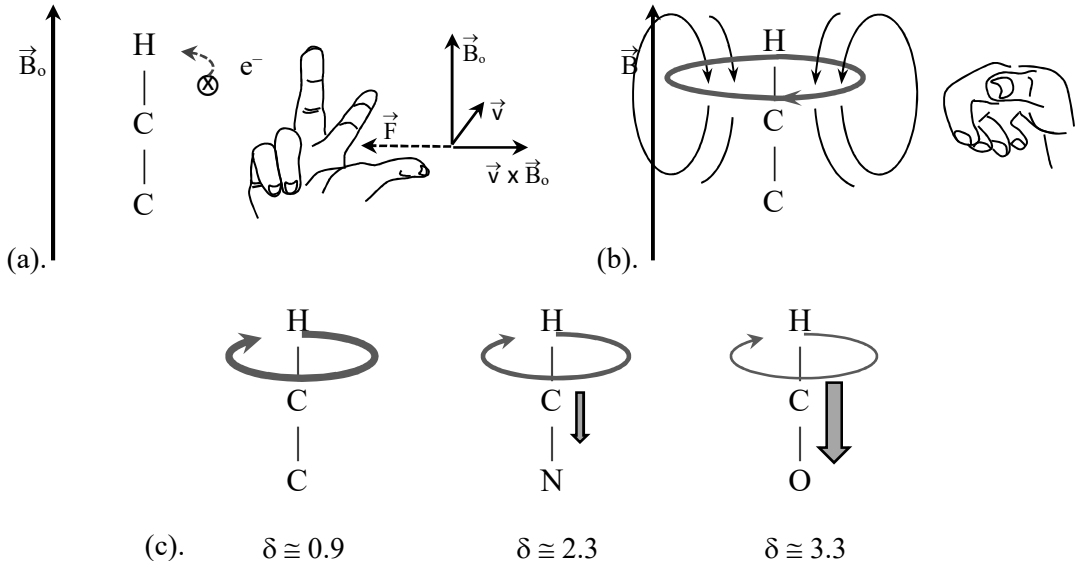


Figure 29.1.4: Diamagnetic shielding of a proton is caused by induced currents in the orbitals forming the C–H bond. (a). The force caused by the velocity of the electron and the applied magnetic field causes a ring current about the C-H bond. (b). The induced magnetic field opposes the external applied magnetic field. (c). Attached electronegative atoms decrease the electron density in the C-H bond, decreasing the ring current, which then decreases the induced magnetic field. The result is a downfield, less diamagnetic chemical shift.

First assume that the methyl group is attached to a neighboring carbon-atom, -C-$CH_3$. When placed in a magnetic field the electrons in the molecular orbitals forming the C –H bond experience a force given by $\vec{F}_B = -e\vec{v} \times \vec{B}_o$, where $\vec{F}_B$ is the force, –e is the charge, and $\vec{v}$ is the velocity vector of the electron. The resulting direction of the force is given by the familiar "right-hand" rule.[3] Assume that the electron has an initial velocity away the viewer, perpendicular to the plane of the paper, Figure 29.1.4a. The corresponding force is towards the nuclei. The subsequent motion of the electron creates a circular orbit about the C–H bond. The result is a **ring current** that is opposite in direction to the electron motion, since the charge of the electron is negative. The ring current in turn produces a magnetic field. The direction of this **induced magnetic field** is given by the corresponding right-hand rule, Figure 29.1.4b. With the thumb in the direction of the current, the fingers curl in the direction of the magnetic flux lines. The direction of the induced magnetic field at the proton is opposed to the applied magnetic field. As a result, the proton experiences a magnetic field that is slightly smaller than the applied magnetic field, $B_o$. The opposition of the induced and applied magnetic fields is called a diamagnetic interaction. The effect is a **diamagnetic shift**, which is upfield, to smaller frequency, and smaller chemical shift (to the right). Alkyl methyl groups are typically the most upfield chemical shifts. If the methyl group is attached to an electronegative element, rather than a carbon-atom, then the difference in electronegativity withdraws electron density away from the C-H bond, which decreases the ring current density, which decreases the induced magnetic field. The result is that

methyl groups attached to N- or O-atoms resonate downfield from alkyl methyl groups, Table 29.1.2. The shift is still diamagnetic, but less so than alkyl groups. Conversely, if the proton is attached to an aromatic ring the result is opposite.

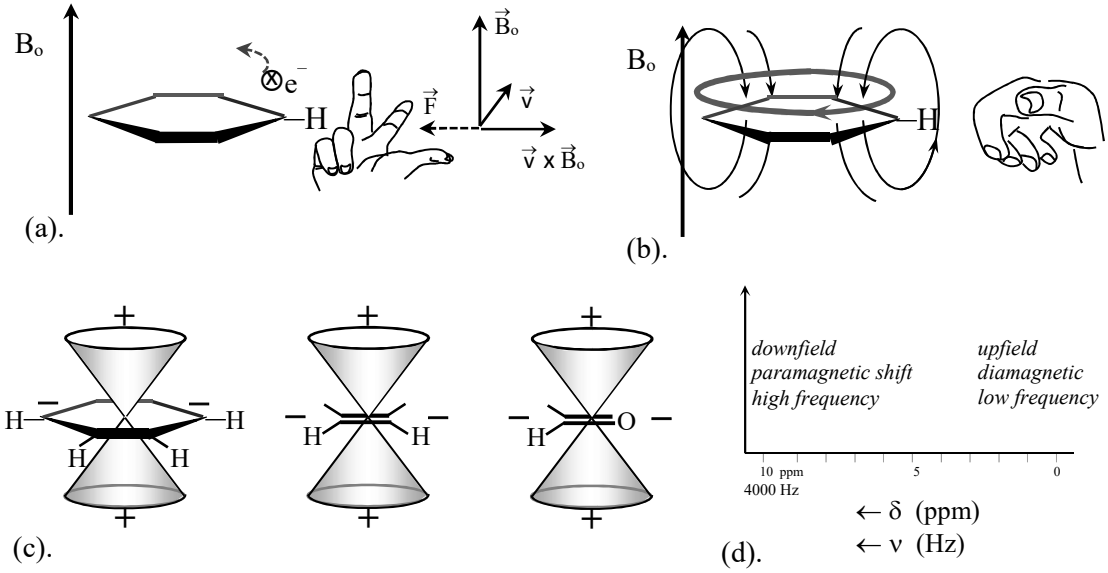


Figure 29.1.5: (a). Delocalized π-electrons give a ring current that (b) induces a magnetic field that adds to the applied field, giving a paramagnetic shift for aromatic protons. (c). Anisotropic chemical shifts depend on location of the nucleus. "+" regions give downfield shifts. (d). Conventional presentation and corresponding chemical shifts for NMR spectra.

Consider a proton attached to an aromatic ring, Figure 29.1.5ab. Assume that the ring is oriented perpendicular to the applied magnetic field. Consider an electron in the delocalized π-molecular orbitals. The force induced by the applied field creates a ring current that circulates above and below the plane of the molecule. Again using the right-hand rule, this aromatic ring current creates an induced magnetic field that runs through the center of the aromatic ring. However, in this instance the position of the protons is in a region where the induced magnetic field is in the same direction as the applied field, $B_o$. As a result, protons attached to aromatic rings experience a larger magnetic field than the applied field. The effect is a **paramagnetic shift**, which is downfield, to larger frequency, and larger chemical shift (to the left). As a result aromatic protons typically resonate near 7 ppm. Alternately, in molecules with an extended geometry, protons can be near the center of the aromatic ring, where they experience a strong upfield shift. Such an orientation is one cause of negative ppm chemical shifts, which are upfield of TMS. The chemical shift clearly depends on the orientation of the proton relative to the aromatic ring current. Such geometric variability is termed **chemical shift anisotropy**. **Isotropic** properties are independent of orientation, while **anisotropic** properties depend on orientation. The orientation dependence of aromatic chemical shifts can be described by anisotropy cones, Figure 29.1.5c. Protons in regions inside the cones experience upfield shifts and regions outside the cones experience downfield shifts. Olefins and aldehydes also show chemical shift anisotropy. Anisotropy effects cause deviations from the tabulated values of chemical shifts,

Tables 29.1.2 and 29.1.3. Never-the-less chemical shifts are an indispensable tool in structure elucidation. Deviations from expected chemical shifts provide useful information concerning 3D-structure.

A change in the spin Hamiltonian, Eqs. 29.1.3-29.1.6, is required to account for chemical shifts. For spin-i:

$$\hat{\mathcal{H}}_i = -\gamma_n \hbar \hat{I}_{z,i} (1 - \sigma_i) B_o \qquad E_i = -\gamma_n \hbar m_{I,i} (1 - \sigma_i) B_o \qquad \Delta E_i = h\nu_i = \gamma_n \hbar (1 - \sigma_i) B_o \tag{29.1.9}$$

where $\sigma_i$ is the parameter that accounts for the change in magnetic field induced by the chemical environment of spin-i. The Hamiltonian and corresponding energy levels are converted into frequency units by substituting $h\nu_i = \gamma_n \hbar (1 - \sigma_i) B_o$ into the Hamiltonian and dividing by h:

$$\frac{\hat{\mathcal{H}}_i}{h} = -\nu_i \hat{I}_{z,i} \qquad \frac{E_i}{h} = -\nu_i m_{I,i} \qquad \text{with} \qquad \nu_i = \frac{\gamma_n}{2\pi}(1 - \sigma_i) B_o \tag{29.1.10}$$

The relationship between the chemical shift expressed as $\sigma_i$ and $\delta_i$ is given by substituting the last expression, with chemical shift $\sigma_i$, and the corresponding expression for the reference, with chemical shift $\sigma_{ref}$, into Eq. 29.1.5:

$$\delta_i \equiv \frac{\nu_i - \nu_{ref}}{\nu_{ref}} 10^6 \text{ ppm} = \frac{\sigma_{ref} - \sigma_i}{1 - \sigma_{ref}} 10^6 \text{ ppm} \cong (\sigma_{ref} - \sigma_i)\ 10^6 \text{ ppm} \tag{29.1.11}$$

The final approximation is excellent, since the chemical shifts are so small: $(1 - \sigma_{ref}) \cong 1$. Chemical shifts are not the only information determined from magnetic resonance spectra.

*The Number of Chemical Shift is the Number of Magnetically Distinct Environments*:
Determining the number of resonances, or chemical shifts, that are observed for a compound is an important first step in predicting spectra. In solution spectra, free rotation about single bonds gives an average environment that generates **chemical equivalence**. For example, free rotation about the C–C bonds to methyl groups averages the environment of each of the methyl protons. As a result the three methyl protons are chemically equivalent and have the same chemical shift. Correspondingly, linear and branched saturated chains with free rotation average the environment of the protons on each atom. The methyl on a given carbon atom and the methylene protons on a given atom have identical chemical shifts, Figure 29.1.6a. Rapid ring flipping also results in chemical equivalence of the methylene protons on cyclohexane, Figure 29.1.6b. However, steric or structural restriction of free bond rotation in rings gives inequivalent methylene protons, of which camphor is an example in Figure 29.1.6c.

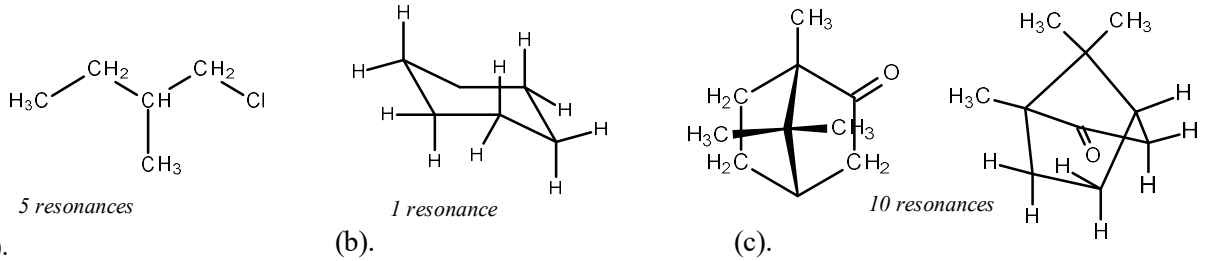


Figure 29.1.6: a.-b. Free rotation about single bonds or ring flips average the chemical environment for protons on each carbon. (c). The methylene protons of camphor are inequivalent because of the rigid ring. Camphor is shown from two perspectives.

Symmetric molecules, those molecules that have a mirror of reflection or a rotational symmetry axis, also result in chemical equivalence, Figure 29.1.7.

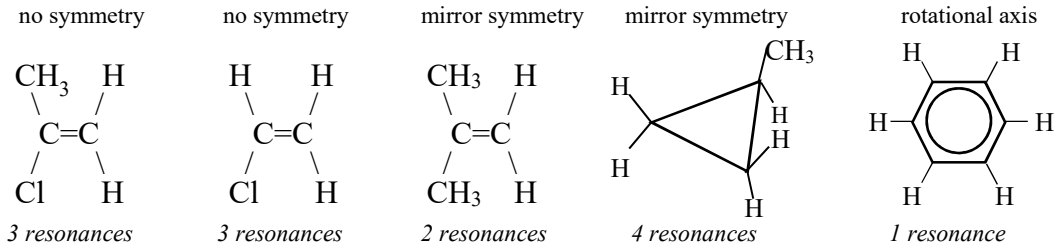


Figure 29.1.7: Molecular symmetry decreases the number of resonances that appear in spectra. The numbers listed are specifically for $^{1}H$ spectra.

A distinction between chemical equivalence and **magnetic equivalence** will be made after the next section.

*Spin-Spin Multiplets are Determined by Connectivity*: At high resolution many resonances are not single lines, but rather groups of related transitions centered on each chemical shift, Figure 29.1.2b. For example in ethanol the resonance at 1.22 ppm is composed of three closely spaced transitions with the intensity ratio of 1:2:1, which is called a triplet. The resonance at 3.68 ppm is composed of four closely spaced transitions in the intensity ratio of 1:3:3:1, which is called a quartet. This fine-structure is called **spin-spin splitting** and results from the interaction of the spins in a given resonance with neighboring spins. The strength of the interaction is given by the spin-spin coupling constant, J, which is usually measured in Hz. The spin-spin coupling constant for proton-proton coupling in ethanol is 7.0 Hz. Spin-spin splitting between nuclei of the same type is called **homonuclear** coupling. For the ethanol example the multiplets arise from the homonuclear splitting of the protons in one chemical environment with other nearby protons, which is measured by the corresponding $J_{HH}$. Spin-spin coupling between nuclei of different types is called **heteronuclear** coupling. For example, $^{13}C$ and proton neighbors can spin-spin couple, which is measured by the corresponding $J_{HC}$. Magnetically equivalent spins do not show spin-spin splitting; the protons in a methyl group do not show spin-spin splitting with each other. Nuclei must experience different chemical environments to show spin-spin splitting.

Consider two inequivalent protons, protons A and B. The resonance of proton A is split into a doublet by the interaction with proton B and the resonance of proton B is split into a doublet by proton A. Doublets result because each proton has spin quantum number I = ½ and correspondingly is either spin-up or spin-down, Figure 29.1.8. Focusing first on proton A, the neighbor B is either spin-up or spin-down, giving the resonance for proton A as a doublet with component frequencies $\nu_A \pm J_{AB}/2$. The frequency difference between the two lines is $J_{AB}$. Focusing next on proton B, the neighbor A is either spin-up or spin-down, also giving the resonance for proton B as a doublet, $\nu_B \pm J_{AB}/2$. For mutually coupled resonances the spin-spin coupling constant is the same for both multiplets; that is $J_{AB} = J_{BA}$.

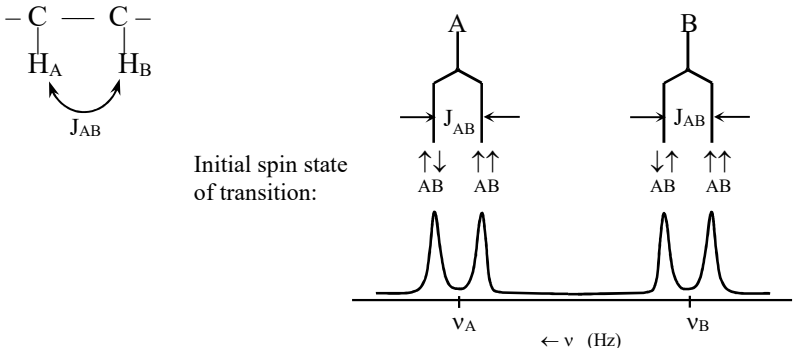


Figure 29.1.8: Spin-Spin splitting. Neighbor B splits the resonance of chemical shift A into a doublet; neighbor B is either spin-up of spin-down. Neighbor A splits the resonance of chemical shift B into a doublet; neighbor A is either spin-up or spin-down. The transition spacing of each mutually coupled multiplet is identical, $J_{AB}$.

A splitting tree is a useful graphical tool for predicting the frequencies and intensities of spin-spin splitting multiplets in more complicated cases. Consider proton A coupled to the three equivalent protons $B_1$, $B_2$, and $B_3$ in an adjacent methyl group, Figure 29.1.9. Since $B_1$, $B_2$, and $B_3$ are equivalent, the coupling constant to A is identical: $J_{AB1} = J_{AB2} = J_{AB3}$. The A resonance is first split into a doublet by proton $B_1$. The resulting two lines are each split into doublets by proton $B_2$. The resulting four lines are each split into doublets by proton $B_3$. Because the coupling constant is the same for each subsequent doublet, the interior lines coincide to give a quartet with relative line intensities of 1:3:3:1.

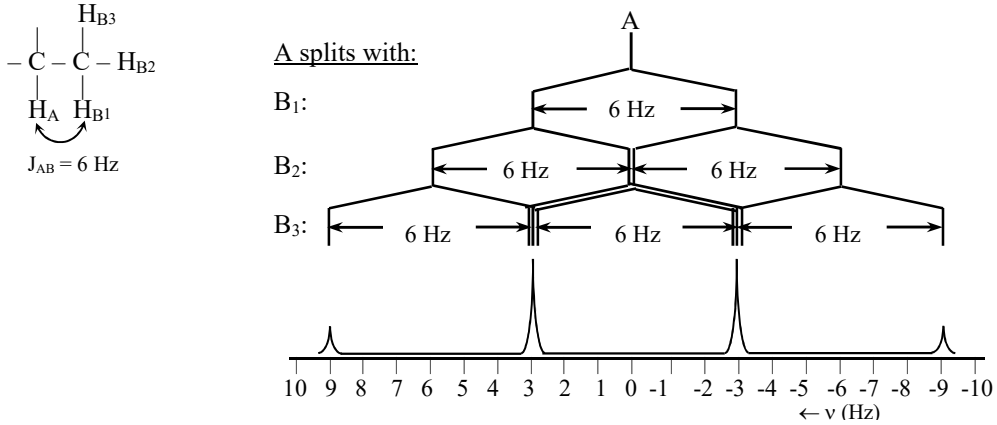


Figure 29.1.9: Splitting tree and resulting multiplet for proton A coupled to three equivalent neighbors, $B_1$, $B_2$, and $B_3$. The coupling constant from A to each equivalent neighbor is $J_{AB}$ = 6 Hz. The interior lines are shown with small offsets to highlight the number of components at each frequency. The doublet for B is not shown.

The expression for the multiplicity of a resonance with n-equivalent neighbors is analogous to Eqs. 25.6.1-25.6.5 with **I**, the total nuclear spin quantum number, replacing S. The total coupled spin angular momentum is $\mathbf{I} = (\Sigma\, m_{I,i})_{max} = n \cdot ½$ giving the multiplicity as:

$$\text{multiplicity} = 2\,\mathbf{I} + 1 = 2\,n\,½ + 1 = n + 1 \qquad \text{(n equivalent spin ½ neighbors)} \quad 29.1.12$$

Equivalent neighbors give the minimum number of lines in a multiplet. Instead, if each coupled proton is inequivalent then the maximum number of lines is observed, which is $2^n$.

The intensity ratios for components within a multiplet for coupling to n-equivalent near-neighbors is predicted using Pascal's triangle, Table 29.1.5. The outer entries in each row are set to one. An intermediate entry in a given row is the sum of the two closest entries in the preceding row. For example, a quintet has the relative line intensities of 1:4:6:4:1.

Table 29.1.5: Intensity Ratios for Multiplets with n Equivalent Near-Neighbors

| n | n+1 | Multiplet | Intensity ratios |
|---|---|---|---|
| 0 | 1 | Singlet | 1 |
| 1 | 2 | Doublet | 1 1 |
| 2 | 3 | Triplet | 1 2 1 |
| 3 | 4 | Quartet | 1 3 3 1 |
| 4 | 5 | Quintet | 1 4 6 4 1 |
| 5 | 6 | Sextet | 1 5 10 10 5 1 |
| 6 | 7 | Septet | 1 6 15 20 15 6 1 |

A variety of multiplet patterns result if not all the neighbors are equivalent. For example, assume proton A has one neighbor B with coupling constant $J_{AB} = 6$ and two equivalent neighbors $C_1$ and $C_2$. Consider two cases: with coupling constant $J_{AC} = 2$ Hz, Figure 29.1.10a, or $J_{AC} = 4$ Hz, Figure 29.1.10b. Starting with the largest coupling constant, B splits A into a doublet and subsequently $C_1$ and $C_2$ split the resulting lines into triplets. A doublet of triplets results. However, the appearance depends on the sizes of the coupling constants.

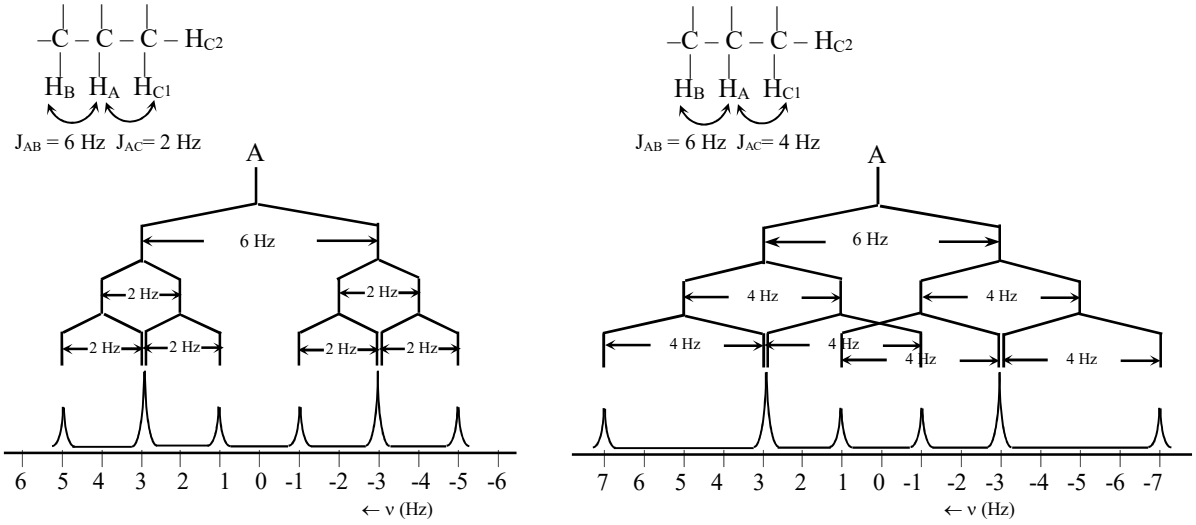


(a). (b).

Figure 29.1.10: Splitting tree and multiplet for proton A coupled to B and two equivalent neighbors $C_1$, and $C_2$ with $J_{AB} = 6$ Hz. (a). The AC coupling constant is $J_{AC} = 2$ Hz. (b). The AC coupling constant is $J_{AC} = 4$ Hz. The doublets for B and C are not shown.

We now present a quantum mechanical treatment of spin-spin splitting, which is helpful in understanding the transitions shown in Figure 29.1.10.

*The Spectrum Results from Transitions Between Total Angular Momentum States*:[6] Consider two inequivalent spins, A and B. The energy of the interaction between the two spins through spin-spin coupling with strength $J_{AB}$ is given by the vector dot-product: $J_{AB}\ \vec{I}_A\cdot\vec{I}_B$. The spin Hamiltonian in frequency units is then:

$$\frac{\hat{\mathcal{H}}}{h} = -\nu_A\,\hat{I}_{zA} - \nu_B\,\hat{I}_{zB} + J_{AB}\,\vec{I}_A\cdot\vec{I}_B \qquad 29.1.13$$

If the difference in chemical shifts is large compared to the coupling constant, the dot product can be approximated using just the z-projections of the spin angular momenta:

$$\frac{\hat{\mathcal{H}}}{h} \cong -\nu_A\,\hat{I}_{zA} - \nu_B\,\hat{I}_{zB} + J_{AB}\,\hat{I}_{zA}\,\hat{I}_{zB} \qquad (|\nu_A - \nu_B| >> |J_{AB}|) \qquad 29.1.14$$

This approximation is called **first-order coupling**. For the two spins the possible spin eigenfunctions are αα, αβ, βα, ββ, where spin A is listed first and B second. Using Eqs. 29.1.10 and 29.1.14 gives the energies of the four spin states as listed and diagrammed in Figure 29.1.11.

| $m_{zA}$ | $m_{zB}$ | AB | no coupling | with coupling | $E/h = -\nu_A m_{zA} - \nu_B m_{zB} + J_{AB}\ m_{zA}\ m_{zB}$ | | |
|---|---|---|---|---|---|---|---|
| –½ | –½ | ββ | | $+J/4$ | $+\frac{\nu_A}{2}$ | $+\frac{\nu_B}{2}$ | $+\frac{J_{AB}}{4}$ |
| –½ | +½ | βα | | $-J/4$ | $+\frac{\nu_A}{2}$ | $-\frac{\nu_B}{2}$ | $-\frac{J_{AB}}{4}$ |
| +½ | –½ | αβ | | $-J/4$ | $-\frac{\nu_A}{2}$ | $+\frac{\nu_B}{2}$ | $-\frac{J_{AB}}{4}$ |
| +½ | +½ | αα | | $+J/4$ | $-\frac{\nu_A}{2}$ | $-\frac{\nu_B}{2}$ | $+\frac{J_{AB}}{4}$ |

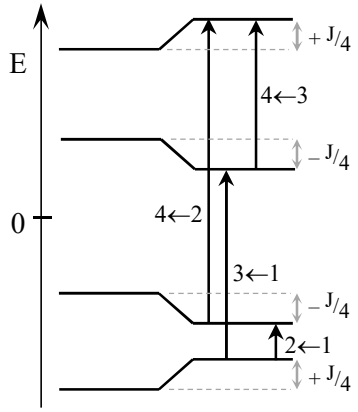


Figure 29.1.11: Two spin-spin coupled protons with different chemical shifts result in two doublets, with the doublet spacing of $J_{AB}$.

From the specific selection rule, the allowed transitions correspond to unit change in angular momentum. Only one spin flip is allowed at a time. The corresponding A-spin transitions are 3←1 for αα to βα, and 4←2 for αβ to ββ. The B-spin transitions are 2←1 for αα to αβ, and 4←3 for βα to ββ:

Transitions:

$$4\leftarrow 2:\ \Delta E/h = \left(+\frac{\nu_A}{2}+\frac{\nu_B}{2}+\frac{J_{AB}}{4}\right)-\left(-\frac{\nu_A}{2}+\frac{\nu_B}{2}-\frac{J_{AB}}{4}\right) = \nu_A+\frac{J_{AB}}{2}$$

$$3\leftarrow 1:\ \Delta E/h = \left(+\frac{\nu_A}{2}-\frac{\nu_B}{2}-\frac{J_{AB}}{4}\right)-\left(-\frac{\nu_A}{2}-\frac{\nu_B}{2}+\frac{J_{AB}}{4}\right) = \nu_A-\frac{J_{AB}}{2}$$

$$4\leftarrow 3:\ \Delta E/h = \left(+\frac{\nu_A}{2}+\frac{\nu_B}{2}+\frac{J_{AB}}{4}\right)-\left(+\frac{\nu_A}{2}-\frac{\nu_B}{2}-\frac{J_{AB}}{4}\right) = \nu_B+\frac{J_{AB}}{2}$$

$$2\leftarrow 1:\ \Delta E/h = \left(-\frac{\nu_A}{2}+\frac{\nu_B}{2}-\frac{J_{AB}}{4}\right)-\left(-\frac{\nu_A}{2}-\frac{\nu_B}{2}+\frac{J_{AB}}{4}\right) = \nu_B-\frac{J_{AB}}{2} \qquad 29.1.15$$

The corresponding spectrum is diagrammed in Figure 29.1.12 using the example parameters: $\delta_A = 3$ ppm, $\delta_B = 1$ ppm, and $J_{AB} = 8$ Hz which is equivalent to 0.02 ppm at 400 MHz.

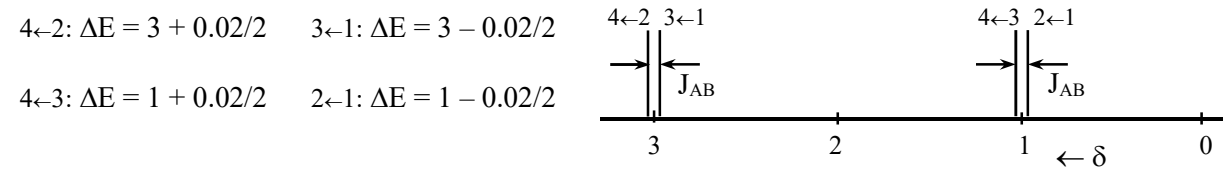


Figure 29.1.12: Spin-spin coupling for an AB system. The doublet spacings are both $J_{AB}$.

The reader should verify that the initial spin state assignments in Figure 29.1.8 agree with Figure 29.1.11. We are now able to understand why equivalent spins don't give an observable splitting. In other words, why is the spectrum of an isolated methylene or methyl group a sharp singlet?

The allowed spin states for two equivalent A spins need to be adjusted to take into account indistinguishability. This process mirrors the requirement placed upon electron configurations by Pauli Exclusion. The allowable spin states of two equivalent spins are the symmetric combinations: $\alpha\alpha$, $^1/\sqrt{2}\,(\alpha\beta + \beta\alpha)$, and $\beta\beta$, while the fourth spin state is antisymmetric: $^1/\sqrt{2}\,(\alpha\beta - \beta\alpha)$. The full Hamiltonian with the dot product, Eq. 29.1.13, must be used in this case to find the energies. The resulting energy levels are diagrammed in Figure 29.1.13. The allowed transitions require the same exchange symmetry; only transitions between adjacent symmetric states are allowed. As a result, even though spin-spin coupling changes the energies of all the levels, the allowed transitions remain at the same frequency as a non-interacting spin system. In other words, equivalent spins don't produce an observable splitting.

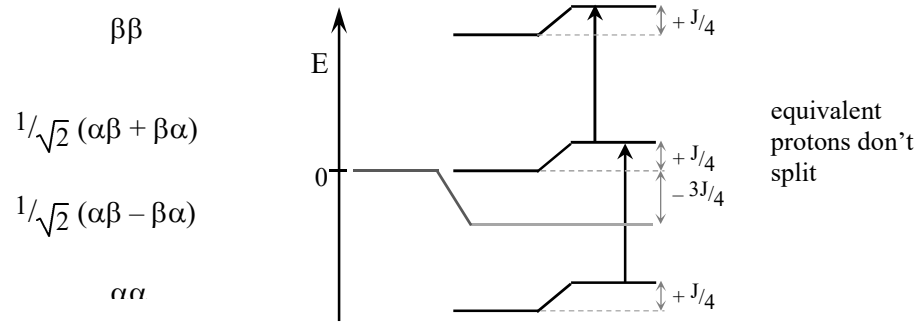


Figure 29.1.13: The symmetric spin-states of two coupled equivalent spins have identical energy shifts. The allowed transitions are unchanged compared to non-interacting spins.

*Spin-Spin Coupling is Primarily Through-Bond*: The most common cause of spin-spin interactions is the **Fermi-contact mechanism**. In Fermi-contact, spin-spin interactions are "through-bond" interactions. The coupling is mediated by interactions of the nuclei with the electrons in the intervening bonds. Fermi-contact interactions are best illustrated using the **Dirac**

**vector model**.[7] Consider first a proton-proton $^1$H-C-$^1$H geminal interaction, Figure 29.1.14a. Thick arrows represent angular momentum vectors of the nuclei and thin arrows represent angular momentum vectors of the electrons. The left-most proton interacts with a nearby electron with the spin-paired orientation (anti-parallel) the most favorable. The two electrons in the molecular orbital localized between the bonded left-H and C-atoms spin-pair, according to the Pauli Exclusion Principle. For the electrons surrounding the C-atom, the lowest energy atomic configuration is determined by Hund's first rule, giving parallel orientations of the electrons the lowest energy. The atomic configuration resulting in $sp^3$ hybridization is: s↑ p↑ ↑ ↑. Finally, the electrons in the right-most C-H bond are once again spin-paired by Pauli Exclusion. The electron-nuclear interaction for the right-most H atom is favorable for spin-paired orientations. Taking account of all the electron-nuclear and electron-electron interactions gives the low energy state with parallel nuclear spins. For such an interaction the αα state is lowest in energy, which corresponds to a negative spin-spin coupling constant in Eqs. 29.1.13 and 29.1.14.

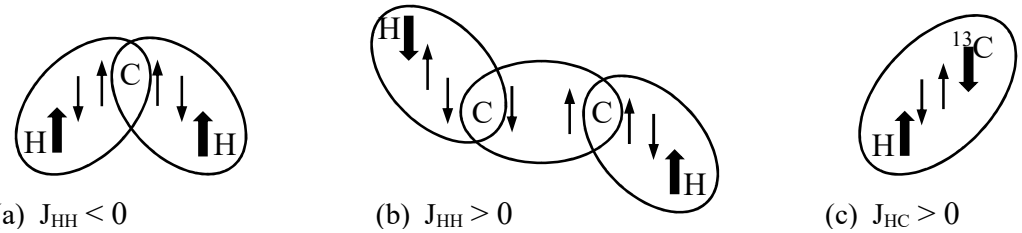


(a) $J_{HH} < 0$ (b) $J_{HH} > 0$ (c) $J_{HC} > 0$

Figure 29.1.14: Spin-spin coupling is mediated by interactions with the electrons in the bonds between the two interacting nuclear spins. Thick arrows are nuclear spins and thin arrows are electron spins. (a). For germinal coupling $J_{AB}$ is negative; the nuclear spin-parallel state is the low energy state. (b) For vicinal interactions $J_{AB}$ is positive. (c). For heteronuclear directly bonded $^1$H–$^{13}$C, the nuclear spin-paired state is lowest energy, predicting a positive $J_{HC}$.

Consider a $^1$H-C-C-$^1$H vicinal interaction, Figure 29.1.14b. The left-most proton interacts with a nearby electron, with the spin-paired orientation the most favorable. The two electrons in each intervening molecular orbital spin-pair, according to the Pauli Exclusion Principle. For the electrons surrounding each C-atom, the lowest energy atomic configuration is determined by Hund's first rule, giving parallel orientations of the electrons near each C-atom the lowest energy. Finally, the electron-nuclear interaction for the right-most H atom is favorable for spin-paired orientations. Taking account of all the electron-nuclear and electron-electron interactions gives the low energy state with anti-parallel nuclear spins. For such an interaction the αβ state is lowest in energy, which corresponds to a positive spin-spin coupling constant. However, the appearance of spectra for positive and negative coupling constants is identical. Some 2D-experiments are sensitive to the sign of the coupling constant.

The heteronuclear coupling constant between directly connected $^1$H and $^{13}$C atoms, $J_{HC}$, is also positive, Figure 29.1.14c. The strength of Fermi-contact coupling decreases with increasing number of intervening bonds. For directly connected $^1$H and $^{13}$C atoms, the typical coupling constant is $J_{HC} \cong 150$ Hz. Geminal coupling constants are typically $J_{HH} \cong 12$-18 Hz, but depend on the hybridization and H-C-H angle about the central C-atom. Vicinal coupling constants are typically $J_{HH} \cong 6$ Hz, but depend on the H-C-C-H dihedral angle. In addition, nearby electron withdrawing groups decrease vicinal coupling constants.

The dihedral angle dependence of vicinal coupling results from the degree of overlap between the intervening molecular orbitals. The **Karplus relationship** applies to vicinal coupling between hydrogens attached to $sp^3$ hybridized C-atoms with dihedral angle $\phi$, Figure 29.1.15:

$$J_{HH} = 8.5\cos^2\phi - 0.28 \qquad 0° \le \phi \le 90°$$
$$J_{HH} = 9.5\cos^2\phi - 0.28 \qquad 90° \le \phi \le 180° \qquad (sp^3\text{-}sp^3) \quad 29.1.16$$

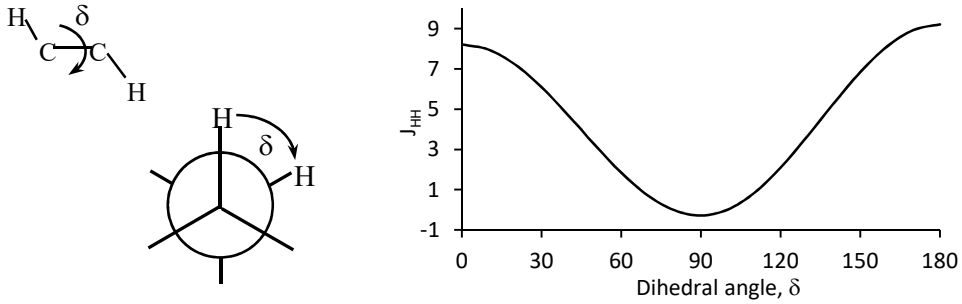


(a). Dihedral angle (b). $^1$H–C–C–$^1$H Spin-spin coupling constant

Figure 29.1.15: (a). Vicinal coupling constants are functions of dihedral angle, shown using a line structure and Newman projection. (b). The Karplus relationship given by Eq. 29.1.16 is specific to vicinal homonuclear $^1$H–C($sp^3$)–C($sp^3$)–$^1$H.

The vicinal $J_{HH}$ coupling constant varies from near zero for dihedral angles close to 90° and increases to ~9 Hz for dihedral angles near 0° or 180°. More accurate relationships that take into account attached electron-withdrawing groups or different carbon atom hybridization have also been developed. Karplus-type relationships are important in natural products chemistry and protein and oligonucleotide structure determination.[8] For cases with free bond rotation, such as sterically unhindered alkyl chains, a torsion-averaged J is observed. Spin-spin coupling constants can be accurately predicted using correlated electronic structure calculations.

*Heteronuclear Spin-Spin Coupling Parallels Homonuclear Coupling*: Nuclei of different types also spin-spin couple. In $^{13}$C spectra using deuterated chloroform as the solvent, the 1:1:1 triplet at 77.4 ppm is an example, Figure 29.1.1d. The $^{13}$C resonance of deuterated chloroform, $CDCl_3$, is a triplet because deuterium has spin quantum number I = 1, giving the multiplicity of the attached $^{13}$C resonance as $2\mathbf{I} + 1 = 3$. In proton spectra, an example is the residual proton resonance of $D_6$-acetone as the solvent. Deuterated solvents for use in NMR are never 100% deuterated; a small amount of protonated acetone, $D_3C(=O)CD_2H$, remains. The result is a small quintet at 2.09 ppm. The total nuclear spin angular momentum of the two deuterium neighbors is $\mathbf{I} = 2\cdot1 = 2$, giving the residual proton resonance as a $2\,\mathbf{I} + 1 = 5$ quintet. This quintet is often used as a reference for chemical shift calibration, if TMS is not added to the solution. Other examples in proton NMR are $^{13}$C-satellites. The one-bond $J_{CH}$ coupling constant is in the range of 100-250 Hz, with 150 Hz typical. Each proton that is directly attached to a $^{13}$C is split into a doublet. However, only one in every 100 carbons is a $^{13}$C, so these doublets are only 1% of the intensity of the main resonance peaks. These doublets are observable as tiny copies of the main resonance spaced at ~75 Hz above and below each main resonance, Figure 29.1.2a.

In $^{13}$C spectra, the one-bond $J_{CH}$ coupling produces a quartet for each methyl $^{13}$C-resonance, a triplet for each methylene $^{13}$C-resonance, and a doublet for each methine $^{13}$C-resonance. These

multiplet splittings are large, 100-250 Hz, which often causes confusion from the overlap of the multiplets with similar chemical shifts. To simplify interpretation and to provide increased signal-to-noise, $^{13}C$ spectra are usually acquired with **proton decoupling**. Weak intensity continuous irradiation of the sample at the proton resonance frequency causes rapid spin-flips of the protons, which averages the spin-spin coupling to zero. As a result, each $^{13}C$ resonance in a proton decoupled spectrum appears as a sharp singlet, independent of the number of attached protons, Figure 29.1.2d.

*Spin-Spin Multiplets Appear Narrower at High Field*: Comparison of Figure 29.1.2a and 29.1.2c shows that the appearance of the methylene and methyl resonances of ethanol change with applied field strength. The chemical shift is plotted on a relative scale in ppm. As a result, the chemical shifts in ppm are unaffected by the field strength. The term in the Hamiltonian for the spin-spin splitting, $J_{AB}\ \vec{I}_A \cdot \vec{I}_B$, in Eq. 29.1.13 is independent of field strength so the spacing between the transitions in a multiplet in Hz are unchanged with increasing field strength. However, the spectral width in Hz does change with field strength. At 60 MHz, 10 ppm corresponds to 600 Hz but at 400 MHz the same 10 ppm corresponds to 4000 Hz. As a result the transitions that make up a spin-spin multiplet are plotted closer together at high field than low field. At high field, spectra at expanded scale about each resonance must be plotted to determine the multiplicity and spin-spin splitting constants of each resonance. The difference in behavior between the plotted chemical shifts and the spin-spin splittings is more than cosmetic. High field provides better clarity. Spin-spin multiplets are easier to see at high field because of less overlap with multiplets that have similar chemical shifts. In addition, second order effects are less pronounced at high field; Eq. 29.1.14 is more generally applicable than Eq. 29.1.13.

*Magnetic Equivalence Requires the Same Coupling Constants*: **Magnetically equivalent** nuclei have the same chemical shift and the same spin-spin coupling constants to each equivalent neighbor. Magnetic equivalence requires chemical equivalence, but magnetic equivalence is more restrictive. Each magnetic environment results in a single chemical shift and magnetically equivalent nuclei don't result in observable spin-spin splitting. The distinction between difluoromethane and difluoroethylene is instructive. The A, A' and B, B'-spin pairs in both difluoromethane and difluoroethylene are chemically equivalent and therefore have the same chemical shifts, Figure 29.1.16.

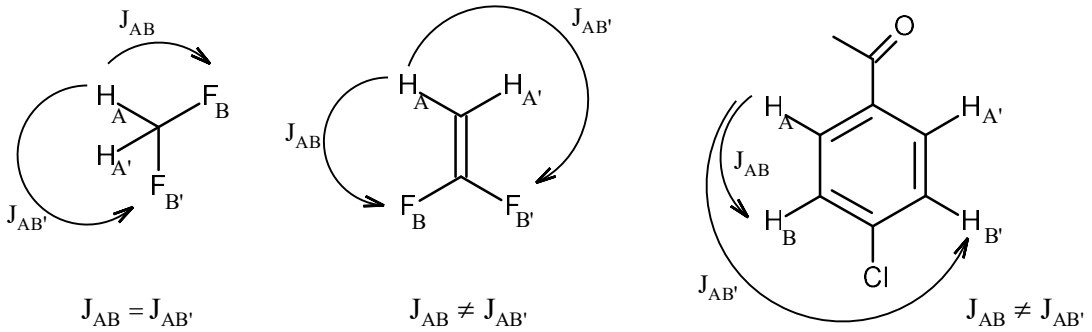


Figure 29.1.16: Magnetic equivalence requires chemical equivalence and the same coupling constants to equivalent spins. The protons in difluoromethane are magnetic equivalents, while the A-A' and B-B' pairs in difluoroethylene and *para*-substituted aromatics are not magnetic equivalents.

However, the protons in difluoromethane are magnetically equivalent, while the protons in difluoroethylene are not. In difluoroethylene, the spin-spin coupling constant of A with B is different than A with B'. As a result B and B' cannot be equivalent. Conversely the coupling constants of B with A is different than B with A'. As a result A and A' cannot be equivalent. However, in difluoromethane the A-B, A-B', A'-B, and A'-B' coupling constants are identical making the proton pair in difluoromethane magnetically equivalent. *Para*-substituted aromatics are also examples of chemically equivalent but magnetically inequivalent spin pairs. $J_{AA'}$ and $J_{BB'}$ have an observable effect on the spin-spin multiplet.[9]

## 29.2 Predicting Chemical Shifts

*Chemical Shifts Depend on the Orientation of the Molecule in the Magnetic Field*: Chemical shifts are orientation dependent; chemical shifts are anisotropic. In the solid state, as single crystals are rotated in the magnetic field the resonances change frequency. This orientation dependence is not normally observed because in solution molecules tumble rapidly and the chemical shifts are motionally averaged. Physical properties are commonly orientation dependent. In general, properties such as the electric and magnetic susceptibilities can be approximated by a series, much like a Taylor power series. The first term in the series is a scalar. This first scalar term is isotropic, independent of orientation. For electric properties the charge on the molecule or ion is the scalar term in the series. The second term in the series is a vector. The electric dipole moment is a vector property with x, y, and z components. The third term in the series transforms as a 3x3 matrix. For electric properties the matrix term is called the electric quadruple moment. Each successive term provides a more complete approximation of the electric distribution of the molecule or ion. A matrix that expresses the directionality of an atomic or molecular property is called a **tensor**. Polarizability, moments of inertia, and NMR chemical shifts are tensor properties. The polarizability tensor that we introduced in Raman spectroscopy is an example, Ch. 27.7. The orientation dependence is given by the rotational properties of the 3x3 matrix (see Problem 2.25 for 2D-rotation). The chemical shift tensor in an arbitrary orientation with respect to the x, y, and z-axes is:

$$\underset{\approx}{\sigma} = \begin{pmatrix} \sigma_{xx} & \sigma_{xy} & \sigma_{xz} \\ \sigma_{yx} & \sigma_{yy} & \sigma_{yz} \\ \sigma_{zx} & \sigma_{zy} & \sigma_{zz} \end{pmatrix} \qquad 29.2.1$$

The $\sigma_{zz}$ component is determined from the spectrum. Analogous to the moment of inertia, Section 27.4, a principal coordinates frame can be found by reorienting the molecule about the axes to give zeros for the off-diagonal components. In the principle coordinates frame, the chemical shift is visualized as an ellipse, with chemical shift components $\sigma_{xx}$, $\sigma_{yy}$, and $\sigma_{zz}$ along the principle axes of the ellipse, Figure 29.2.1. The $\sigma_{xx}$, $\sigma_{yy}$, and $\sigma_{zz}$ values in the principle coordinates frame of reference are the eigenvalues of the chemical shift tensor from an arbitrary orientation.

The trace of a matrix is the sum of the diagonal components: $\mathrm{tr}(\underset{\approx}{\sigma}) = \sigma_{xx} + \sigma_{yy} + \sigma_{zz}$. In solution, small molecules tumble rapidly around all three axes. In solution the motionally averaged chemical shift is calculated from the trace of the chemical shift tensor:

$$\sigma_{soln} = \tfrac{1}{3}\,\mathrm{tr}(\underset{\approx}{\sigma}) = \tfrac{1}{3}\,(\sigma_{xx} + \sigma_{yy} + \sigma_{zz}) \qquad 29.2.2$$

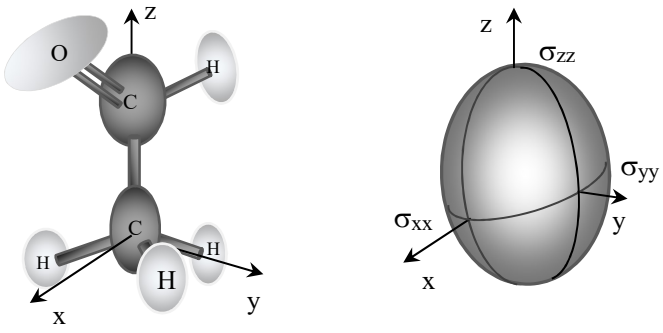


Figure 29.2.1: Acetaldehyde anisotropic chemical shifts. In the principle axes coordinate frame the chemical shift is visualized as an ellipse with principle axes $\sigma_{xx}$, $\sigma_{yy}$, and $\sigma_{zz}$. The carbonyl carbon chemical shift is strongly anisotropic with $\sigma_{zz} > \sigma_{xx} > \sigma_{yy}$. In other words, the ellipse is flattened in the y-direction.

The trace of the chemical shift tensor is invariant to rotation, so the average in Eq. 29.2.2 is independent of the choice of orientation. The averaged value is also called the **isotropic** value. The tensor property of the chemical shift is important for solids and liquids with reduced motional freedom, such as liquid crystals and liquid polymers. The tensor character of the chemical shift also needs to be taken into account when using electronic structure calculations to estimate chemical shifts.

C*hemical Shifts can be Calculated from Molecular Orbital Theory*: The accurate prediction of chemical shifts is often crucial in molecular structure determination. A wide variety of empirical methods have been developed to estimate chemical shifts. These methods are incorporated into commonly used NMR analysis and molecular drawing applications.[10-12] This approach uses tabulated fragment parameters based on functional groups and connectivity (methyl, methylene, methane, etc.)[12] Fragment parameter approaches fail when through-space interactions, such as chemical shift anisotropy and aromatic ring currents, are important. Predicting the proton and $^{13}C$ chemical shifts of heterocyclic aromatic compounds is challenging. Electronic structure methods are available that accurately predict chemical shifts. Two important modifications to commonly used molecular orbital algorithms are necessary. In the theory of electricity and magnetism, the **gauge** of a calculation relates to the orientation of the Cartesian coordinates relative to the atom.[13] The properties of atoms should not depend on the choice of coordinate axes. In other words the calculation must be **gauge invariant**. Modifications must be made to molecular orbital codes to ensure gauge invariance. The results are **gauge invariant atomic orbital**, **GIAO**, methods. Secondly, the effect of the magnetic field on the molecule must be taken into account. This effect is the purely quantum mechanical analog to ring currents, Figures 29.1.4 and 29.1.5. The effect of an applied magnetic field can be thought of in the context of perturbation theory. The magnetic field applies a perturbation to the ground state electronic structure of the molecule. The perturbation series mixes excited states into the ground state to approximate the change in electronic distribution.[13] Remember that the perturbation approach is used to take electron correlation into account in the absence of a magnetic field. The presence of a magnetic field increases the contribution of excited states in excess of that required to account for electron correlation. As result, excited states must be accurately characterized and their effect on the

ground state must be carefully taken into account for successful chemical shift estimation. As a result correlated methods are required as the basis for GIAO calculations. B3LYP is a commonly used method in chemical shift estimation. Because of the need to accurately characterize electron correlation in multiple excited states, GIAO calculations are time consuming.

The output of the B3LYP/6-31G(d) GIAO calculation for acetaldehyde and the corresponding atom numbering is shown in Figure 29.2.2. The full chemical shift tensor with respect to the calculated orientation of the molecule, the eigenvalues, and the resulting isotropic values are listed. The eigenvalues are the components of the chemical shift in the principle coordinates frame. The final shifts are referenced to TMS by subtracting the isotropic value of the given chemical environment from the isotropic chemical shift of TMS, Eq. 29.1.11:

$$\delta_i \text{ (ppm)} = \text{isotropic(TMS)} - \text{isotropic(i)} \qquad 29.2.3$$

The $^{1}$H isotropic chemical shift of TMS is 32.180 ppm and the $^{13}$C isotropic chemical shift is 189.746 ppm at the B3LYP/6-31G(d) level.

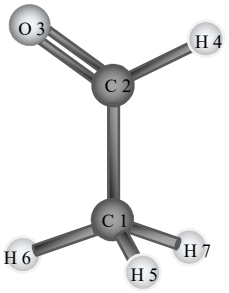


```
SCF GIAO Magnetic shielding tensor (ppm):
1  C  Isotropic = 159.908
      Anisotropy = 49.357
 XX= 146.512  YX= -26.399  ZX=   0.000
 XY= -12.310  YY= 184.723  ZY=   0.000
 XZ=   0.000  YZ=   0.000  ZZ= 148.490
 Eigenvalues: 138.421  148.490  192.813
2  C  Isotropic = 4.222
      Anisotropy = 155.985
 XX= -17.170  YX= -17.424  ZX=   0.000
 XY= -19.158  YY= -78.374  ZY=   0.000
 XZ=   0.000  YZ=   0.000  ZZ= 108.212
 Eigenvalues: -83.424  -12.121  108.212
3  O  Isotropic = -318.923
      Anisotropy = 1015.345
 XX=-900.820  YX= -39.618  ZX=   0.000
 XY= -60.251  YY=-413.922  ZY=   0.000
 XZ=   0.000  YZ=   0.000  ZZ= 357.974
 Eigenvalues: -905.889 -408.854 357.974
4  H  Isotropic = 22.167
      Anisotropy = 4.618
 XX=  20.698  YX=   0.656  ZX=   0.000
 XY=  -3.293  YY=  24.863  ZY=   0.000
 XZ=   0.000  YZ=   0.000  ZZ=  20.941
 Eigenvalues: 20.315  20.941  25.246
5  H  Isotropic = 30.179
      Anisotropy = 4.298
XX=  30.188  YX=   1.339  ZX=   1.485
XY=  -0.704  YY=  28.946  ZY=  -0.470
XZ=   2.842  YZ=   0.178  ZZ=  31.404
 Eigenvalues: 28.352  29.141  33.045
6  H  Isotropic = 30.412
            Anisotropy = 5.244
XX=  29.573  YX=  -0.898  ZX=   0.000
XY=   3.771  YY=  33.432  ZY=   0.000
XZ=   0.000  YZ=   0.000  ZZ=  28.231
 Eigenvalues: 28.231  29.097  33.908
7  H  Isotropic = 30.179
      Anisotropy = 4.298
XX=  30.188  YX=   1.339  ZX=  -1.486
XY=  -0.704  YY=  28.946  ZY=   0.470
XZ=  -2.842  YZ=  -0.178  ZZ=  31.404
 Eigenvalues: 28.352  29.141  33.045
```

Figure 29.2.2: Acetaldehyde GIAO chemical shielding tensors at B3LYP/6-31(d) from Gaussian ’03 (or Spartan/QChem).

The chemical shifts of the carbonyl carbon, C2, and the methyl carbon, C1, are predicted to be:

$$\delta_C\ (C{=}O) = 189.75\ ppm - 4.22\ ppm = 185.5\ ppm$$
$$\text{and} \quad \delta_C\ (CH_3) = 189.75\ ppm - 159.91\ ppm = 29.8\ ppm \qquad 29.2.4$$

The literature $^{13}C$ chemical shifts are 199.7 ppm and 30.9 ppm, respectively, Table 29.1.3$^{(DS)}$. Both predicted values are low at 94% of the observed values. Common practice is to use several compounds as a training set to determine a correction factor, which is then applied to all subsequent calculations at a comparable level of theory. The factor is 1/0.94 = 1.06 in this case. The $^1H$ chemical shifts are:

$$\delta_H\ (HC{=}O) = 32.180\ ppm - 22.167\ ppm = 10.01\ ppm$$
$$\text{and} \quad \delta_H\ (CH_3) = 32.180\ ppm - 30.179\ ppm = 2.00\ ppm$$
$$\delta_H\ (CH_3) = 32.180\ ppm - 30.412\ ppm = 1.77\ ppm$$
$$\delta_H\ (CH_3) = 32.180\ ppm - 30.179\ ppm = 2.00\ ppm \qquad 29.2.5$$

The three methyl protons should have identical chemical shifts. Assuming a small barrier for the torsion, rapid rotation around the C–C bond averages the methyl group chemical shifts to give $\delta_H$ = 1.93 ppm. The literature values are 9.79 ppm and 2.21 ppm, respectively. The agreement of both $^1H$ and $^{13}C$ shifts are sufficient for many purposes. A more complete basis set improves the agreement between predicted and experimental values.

The chemical shift of the carbonyl carbon is highly anisotropic with components -83.42 ppm, -12.12 ppm, and 108.21 ppm, before referencing to TMS. This chemical shift is strongly dependent on the orientation of the molecule in the applied field, as show in Figure 29.2.1.

## 29.3: A Classical Model for the Magnetization

*The Net Magnetization Precesses About the Applied Field*: Magnetic resonance experiments require a detailed description of the behavior of the net magnetization upon interaction with the applied radiofrequency irradiation. The net magnetization, $\vec{M}$, is the vector sum of all the magnetic dipoles of each nuclear spin in the system. The projection of the net magnetization on the z-axis, $M_z$, is proportional to the difference in the populations of the two levels.

$$M_z \propto \text{(spins in lower state)} - \text{(spins in upper state)} \qquad 29.3.1$$

In other words, the net magnetization is given by the difference of the number of up and down-spins. The magnetization is a macroscopically observable quantity. The **Bloch equation** provides a classical description of the behavior of the magnetization in a magnetic resonance experiment:

$$\frac{d\vec{M}}{dt} = \gamma_n\ (\vec{M} \times \vec{B}) \qquad \text{(no spin-relaxation)} \qquad 29.3.2$$

where $\vec{B}$ is the total magnetic field experienced by the nuclear spins, which includes the constant applied field and, if present, the radiofrequency field. The applied magnetic field, $B_o$, is assumed to be in the z-direction. Consider first the behavior of the spin system in the applied magnetic field, without radiofrequency, rf, irradiation. The behavior of the magnetization in the applied magnetic field is analogous to a spinning-top in the field of gravity. Picturing the motion of a top is an aid to understanding the cross-product relationship in Eq. 29.3.2. When placed in the field of gravity, a tilted spinning top precesses about the gravitational field direction, Figure 29.3.1a. When nuclear spins are placed in an applied magnetic field, the net magnetization precesses

about the applied magnetic field direction, Figure 29.8.1b. The projection on the z-axis is $M_z$. The precession of the net magnetic moment about the z-axis is called **Larmor precession**. The frequency of the Larmor precession is the resonance frequency $\nu_i$ in Eq. 29.1.9.

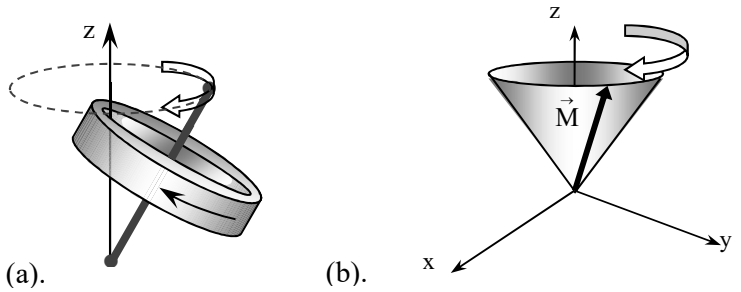


Figure 29.3.1: (a). A tilted top precesses about the gravitational field. (b). A tilted magnetization precesses about the applied field, which is aligned along the z-axis.

The equilibrium position of the net magnetization is stationary and parallel to the z-axis. To observe precession, the magnetization must be tilted away from the z-axis. Tilting of the magnetization is accomplished by an applied rf-field. The rf-field is generated in the probe of the spectrometer by passing an oscillating radiofrequency current though a coil of wire, Figure 29.3.2a. The rf-coil is oriented with the axis perpendicular to the applied field direction. The magnetic field induced in a coil of wire oscillates along the axis of the coil. This linear oscillation is said to be **linearly polarized**. How can a linearly polarized magnetic field interact with the net magnetization, which instead precesses in a circular path about the z-axis? The nuclear precession is said to be **circularly polarized**. The linearly polarized rf-irradiation can be decomposed into two counter-rotating circularly polarized rf-fields of equal strength, Figure 29.3.2b. One of the circularly polarized fields rotates in the same sense as the nuclear precession and is responsible for the interaction with the net magnetization. The other circularly polarized component rotates in the opposite sense and is simply ignored. The applied rf-field rotates in the x-y plane, perpendicular to the applied field. If the applied linear rf-field intensity is $2B_1$, the effective component rotating in the x-y plane has magnetic field strength $B_1$. The rf-field is orders of magnitude weaker than the applied field, $B_1 << B_o$.

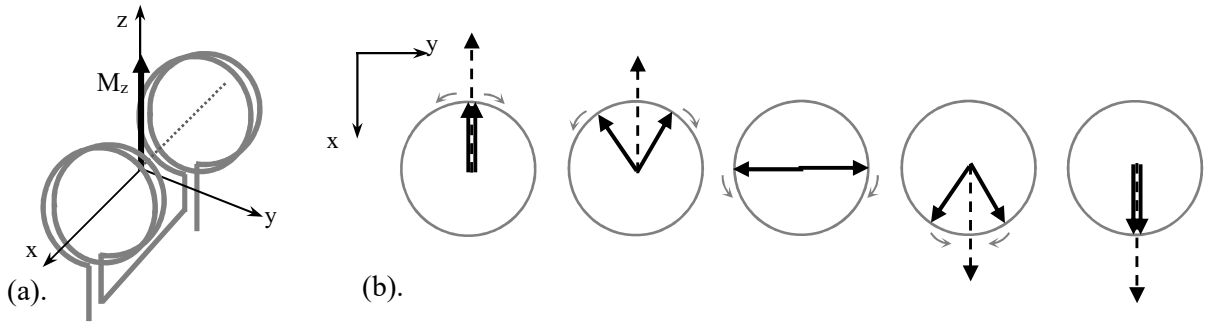


Figure 29.3.2: (a). The rf coil is oriented perpendicular to the main applied field and is wrapped in a Helmholtz configuration to allow sample access from above. (b). A linearly polarized rf-field is composed of two counter-rotating circularly polarized rf-fields. Only the component rotating in the same sense as the magnetization induces transitions.

The applied rf field produces a torque that tilts the net magnetization away from the z-axis. During the rf-pulse, the net magnetization continues to precess about the z-axis, while simultaneously precessing about the applied rf field, as given by the right-hand rule, Figure 29.3.3. The tilted magnetization induces an oscillating rf-current in the rf-coil that when amplified is recorded as the detected signal. The detected signal is called the **free induction decay**, FID. The nuclear magnetization and the rf-coil act as a miniature AC electric generator. The signal intensity is proportional to the magnitude of the precessing magnetization in the x and y-directions, $M_x$ and $M_y$.

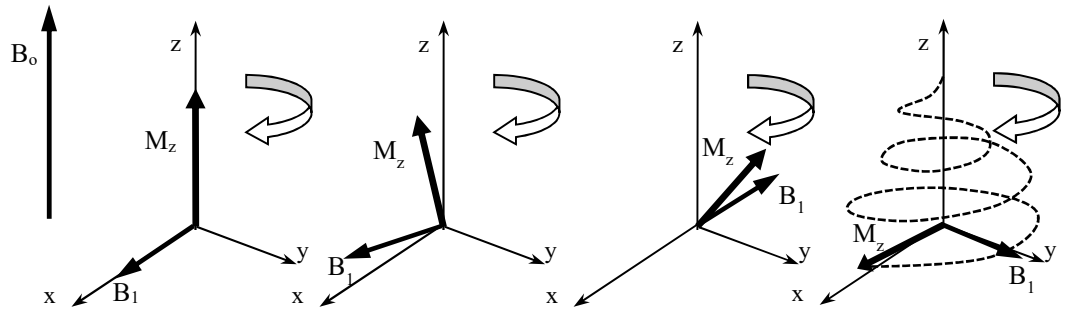


Figure 29.3.3: The rotating component of the applied rf field has magnitude $B_1$ in the x-y plane. The rf field applies a torque, $(\vec{M} \times \vec{B}_1)$, to the net magnetization tilting the magnetization away from the z-axis. A 90° pulse tilts the net magnetization into the x-y plane. After the rf-irradiation is turned off, the precessing net magnetization induces a current in the rf-coil to give the signal, which is the free induction decay, FID.

The projection of the net magnetization on the x-y plane is determined by the tilt angle. A tilt angle of 90° provides the maximum projection of the net magnetization in the x-y plane and correspondingly the biggest signal. The tilt angle is proportional to the length of time that the rf-irradiation is applied. A pulse of rf-irradiation of optimal length tilts the net magnetization by 90°. Such a pulse is called a 90° pulse or equivalently in radians a $\pi/2$ pulse. A pulse of twice the 90° pulse length, a 180° or $\pi$ pulse, tilts the net magnetization to the –z axis. A 180° pulse leaves no projection on the x-y plane and correspondingly no signal is produced. As a result, careful timing of the rf-pulse length is required for optimal signal generation. Rf-pulses of various lengths are used in advanced experiments.

The precession of the magnetization in the preceding figure is complicated. The behavior of the magnetization is most conveniently described in the **rotating frame** of reference.[14] Figure 29.3.3 is drawn in the **laboratory frame** of reference: the observer is stationary while the magnetization precesses about the z-axis. Picture a carousel while you observe from the ground. The horses on the carousel follow a circular path. Now, we jump on the carousel. Observing from the carousel, the horses appear stationary while the surroundings whirl by. The rotating frame of reference is analogous. The observer is rotating at the Larmor frequency, while the laboratory appears to whirl around the observer. In the absence of rf-irradiation, a tiled magnetization at resonance appears stationary to the rotating observer and remains at a fixed tilt angle with respect to the z-axis. In the rotating frame, an applied rf-field at the Larmor frequency also appears stationary in the x-y plane. Assume that the applied rf-field is aligned along the x-axis in the rotating frame, Figure 29.3.4. The torque caused by the rf-field causes the magnetization to rotate in the y-z plane. The tilt angle is proportional to the rf-pulse length.

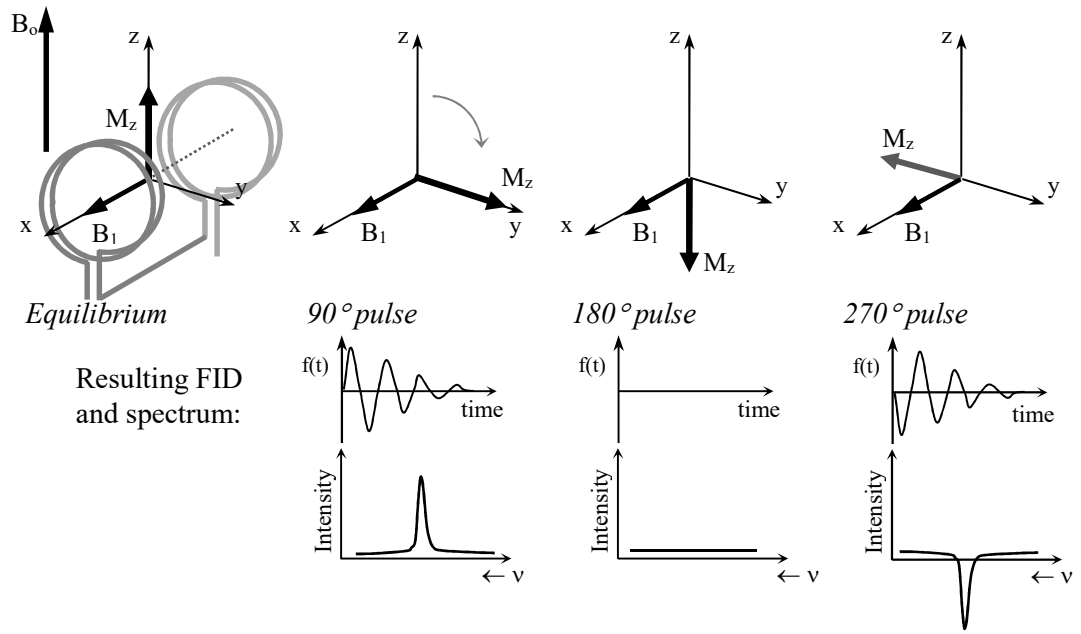


Figure 29.3.4: In the rotating frame, the observer rotates about the z-axis at the Larmor frequency. The effect of a pulse is the precession of the magnetization about the rf-field direction, which for convenience is assumed to lie along the x-axis. The corresponding free induction decays and final spectra are shown beneath the magnetization diagrams. The rf-coils are only shown in the first panel to avoid congestion. The coils are present in each case.

A 90°-pulse tilts the magnetization into the x-y plane along the y-axis. The resulting signal after the pulse is turned off is positive. The 90° phase relationship between the exciting rf and the resulting magnetization is an expectation of all forms of spectroscopy, but in this case the phase shift is easy to visualize. A 180°-pulse tilts the magnetization along the –z-axis, giving no signal. A 270°, or $3\pi/2$-pulse tilts the magnetization along the –y-axis, giving a negative signal. A 360°, or $2\pi$-pulse returns the magnetization to the z-axis as if nothing had happened. In each case, in the absence of relaxation, the magnitude of the net magnetization remains at the equilibrium value of $M_z$.

**29.4: Fourier Transform Spectroscopy**

*Pulsed Spectroscopy: Fourier Transform Techniques Provide a Multiplex Advantage*: Most current NMR and advanced ESR spectrometers make use of pulsed Fourier transform techniques. In pulsed experiments, as we have discussed, a short pulse of radio-frequency radiation at the resonance frequency is applied to the sample, Figure 29.3.3. The sample responds with a transient response in emission, which is the FID, Figure 29.4.1. The Fourier transform of the FID gives the absorption spectrum. Please review Section Ch. 27.3. The FID is the superposition of all the frequencies that make up the spectrum. The Fourier transform is the mathematical technique that unravels all the frequency components in the FID to give the spectrum of the sample. The result, while acquired in emission is equivalent to the spectrum that results from a conventional continuous scan absorption experiment. The advantage of pulsed Fourier NMR experiments is that cw-experiments require minutes per spectrum, while pulsed

techniques require ~5 seconds or less. As a result, pulsed experiments are easily repeated and the results averaged, which allows significant improvement in signal to noise ratio over a single experiment. The signal to noise, s/n, improves as the square root of the number of individual spectra that are averaged, $N_{scans}$:

$$s/n \propto \sqrt{N_{scans}} \qquad 26.4.1$$

Signal averaging is required for the practical acquisition of NMR spectra other than $^{1}H$ and $^{19}F$.

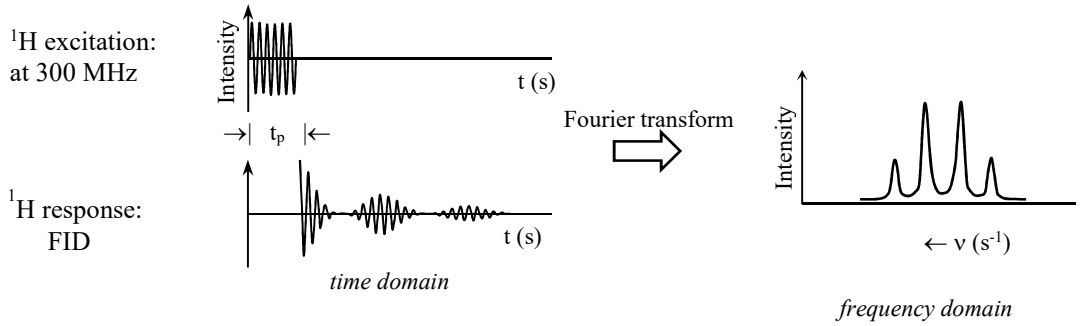


Figure 29.4.1: Pulsed Fourier transform NMR spectroscopy. A radio-frequency pulse at the resonance frequency of the detected nucleus excites a free induction decay, FID. The Fourier transform of the FID gives the spectrum. The envelope of the excitation is a rectangular pulse of length $t_p$.

The time savings of pulsed spectroscopy results because all the frequencies that make up the spectrum are acquired simultaneously, instead of scanning the exciting frequency and measuring the emission or absorption signal one frequency at a time. This time savings is called the **multiplex advantage**.

The Fourier relationship between the FID and the corresponding frequency spectrum are:

$$f(t) = \int_{-\infty}^{\infty} g(\nu) e^{-i2\pi\nu t}\, d\nu \qquad (\textit{time domain}\text{: FID}) \qquad (27.3.8)$$

$$g(\nu) = 2\int_{0}^{\infty} f(t) e^{i2\pi\nu t}\, dt \qquad (\textit{frequency domain}\text{: spectrum}) \qquad (27.3.9)$$

The absorption and dispersion spectra are given by the real and imaginary parts of $g(\nu)$:

$$\text{Absorption} = RE[g(\nu)] \qquad \text{Dispersion} = IM[g(\nu)] \qquad (27.3.10)$$

This real/imaginary terminology is often used in the spectroscopy literature, highlighting the 90° phase shift between the absorptive and dispersive response. The terminology is also used in NMR acquisition software for the two spectral display buffers; both the real and imaginary parts of the spectrum are always calculated (assuming conventional 1D-spectra).

In pulsed NMR a short pulse at the resonance frequency, say at 300.0000 MHz, is applied to the sample. How can all the transitions throughout the spectrum be excited by a pulse at a single frequency? The frequency width of the spectrum of a rectangular pulse is inversely proportional to the pulse width, Figure 27.3.4 and Eq. 27.3.7:

$$\text{full width to first nulls} = \frac{1}{t_p} \qquad 29.4.14$$

The shorter the pulse the wider the range of component frequencies that make up the pulse. A shorter pulse provides broader spectral coverage. In NMR, $^1$H pulse widths are typically near 10 μs, giving a spectral width of $1/10x10^{-6}$ s = $1x10^5$ Hz or 100 kHz. At 10 ppm, the required spectral width is 3000 Hz for a central frequency of 300 MHz. In other words, the spectral coverage of a 10 μs pulse is more than sufficient to span the entire $^1$H chemical shift range.

## 29.5 Magnetic Resonance Relaxation

*Spin-Lattice Relaxation Returns the Spin-System to Equilibrium*:[14-17] Radiofrequency irradiation moves a system away from equilibrium. The spin-system must then undergo transitions from the upper state to the lower state to return to equilibrium, which is called **relaxation**. Energy is conserved by heat transfer to the surroundings, Figure 29.5.1. The surroundings in magnetic resonance are called the **lattice**; therefore the process is called **spin-lattice relaxation**. The characteristic life-time of a spin in the upper state is called the spin-lattice relaxation time $T_1$. Spin-lattice relaxation is essentially identical to non-radiative decay in electronic spectroscopy, except at a much lower frequency, Ch. 28.6.

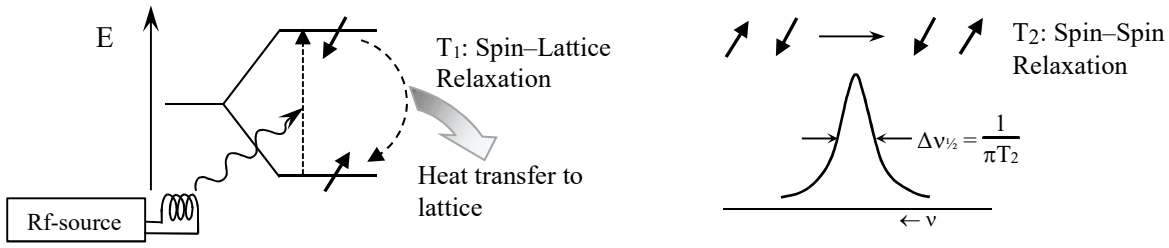


(a). (b).

Figure 29.5.1. (a). Absorption and spin-lattice relaxation, which is caused by non-radiative transitions to the low energy state. Energy is conserved by heat transfer to the lattice. (b). Spin-spin relaxation is caused by mutual spin flips. Energy is approximately conserved in spin-spin relaxation.

One method of measuring $T_1$ is called "saturation recovery," Figure 29.5.2. The net rate of absorption is proportional to the population difference between the lower and upper states, Eq. 27.1.3. At left the molecules start at equilibrium with the largest population difference. A low-intensity radiofrequency source is then turned on, which causes transitions between the two levels. After the rf-source has been on for a few seconds the populations of the two levels are equalized. With equal populations, the two levels are said to be **saturated.** The source is then turned off. Immediately after turning off the rf-source the saturated system gives no resonance signal. However, as time progresses the molecules relax back to equilibrium. With longer delays, the spectrum grows back to the original intensity. About five times $T_1$ is required for the system to return to equilibrium. (Remember that we used this general criterion in Ch. 14.3 "*Internal Constraints for Chemical Reactions*.")

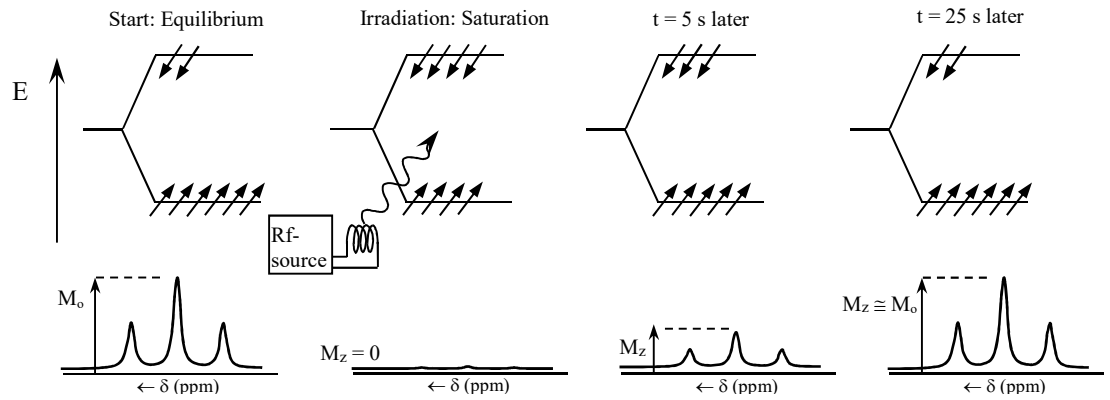


Figure 29.5.2. Saturation-recovery method for $T_1$ measurement. The signal intensity, which is proportional to the projection of the magnetization along the z-axis, is monitored as a function of time after turning off the rf-irradiation at t = 0.

The projection of the net magnetization of the spins along the z-axis, $M_z$, is detected in NMR. The net magnetization is proportional to the difference in the populations of the two levels:

$$M_z \propto \text{(spins in lower state)} - \text{(spins in upper state)} \qquad 29.5.1$$

Spin-lattice relaxation is a first order kinetic process:

$$\frac{dM_z}{dt} = -\frac{1}{T_1}(M_z - M_o) \qquad 29.5.2$$

where $M_z$ is the magnetization at time t and $M_o$ is the magnetization at equilibrium. Integrating Eq. 29.5.2 for the recovery from saturation gives simple exponential growth of the magnetization back to equilibrium:

$$M_z = M_o(1 - e^{-t/T_1}) \qquad 29.5.3$$

Based on this relationship, the $T_1$ relaxation time is derived using curve fitting of the signal intensity as a function of time. A second type of relaxation also plays an important role in magnetic resonance.

*Spin-Spin Relaxation Determines the Transition Line Width*: Spin-spin relaxation occurs through mutual spin-flips. Listing first spin A and then spin B, a mutual spin-flip corresponds to $\uparrow\downarrow \rightarrow \downarrow\uparrow$, Figure 29.5.1b. The characteristic lifetime of a spin in a given spin state is decreased by spin-spin exchange. The characteristic lifetime under spin-spin exchange is called $T_2$. The Heisenberg uncertainty principle relates the energy uncertainty of a state to the lifetime of the state, $\Delta E\, \Delta t \approx \hbar/2$, Eq. 23.4.45. The energy uncertainty of the state corresponds to an uncertainty in the transition line width, $\Delta E = h\, \Delta\nu$, Eq. 23.4.46. The corresponding effect of $T_2$-processes is to cause lifetime broadening. In practical applications, magnetic resonance transitions are also broadened by small spatial variations of the applied magnetic field across the sample. This non-uniformity of the applied magnetic field is called **field inhomogeneity**. The effects of intrinsic lifetime broadening and the applied field inhomogeneity, $\Delta\nu^*$, are combined to give the effective spin-spin relaxation time, $T_2'$:

$$\frac{1}{\pi T_2'} = \frac{1}{\pi T_2} + \Delta\nu^* \qquad \text{(inhomogeneous field)} \qquad 29.5.4$$

In non-viscous solution, a transition at frequency $\nu_A$ is given by the Lorentzian line shape:[12]

$$g(\nu) = \frac{2T_2'}{1 + 4\pi^2 T_2'^2 (\nu - \nu_A)^2} \qquad \text{(solution) (27.3.10)} \qquad 29.5.5$$

where $g(\nu)$ is the intensity at frequency $\nu$, Figure 29.5.1b. The full-width at half-height is:

$$\Delta\nu_{½} = \frac{1}{\pi T_2'} \qquad \text{and} \quad T_2' = \frac{g(\nu)_{max}}{2} \qquad 29.5.6$$

where $g(\nu)_{max}$ is the maximum of the line intensity. Efficient spin-spin relaxation shortens the spin state lifetime, which then broadens the transition. In the solid state, spin-spin relaxation is typically faster or much faster than spin-lattice relaxation, $T_2 << T_1$. However, in non-viscous solution $T_2$ and $T_1$ are approximately equal. What molecular processes control relaxation?

*Spin-lattice Relaxation is a Sensitive Probe of Molecular Motion:* Relaxation is caused by fluctuating magnetic fields in the sample. There are several sources of fluctuating magnetic fields. One source is magnetic dipole-dipole coupling. The strength of the dipole-dipole coupling is changed, or modulated, by molecular motion. Translational diffusion of one molecule past another, whole molecule reorientation, bond torsions, and other vibrations all influence dipole-dipole coupling. We first focus on molecular reorientation. Small molecules tumble rapidly about their axes.

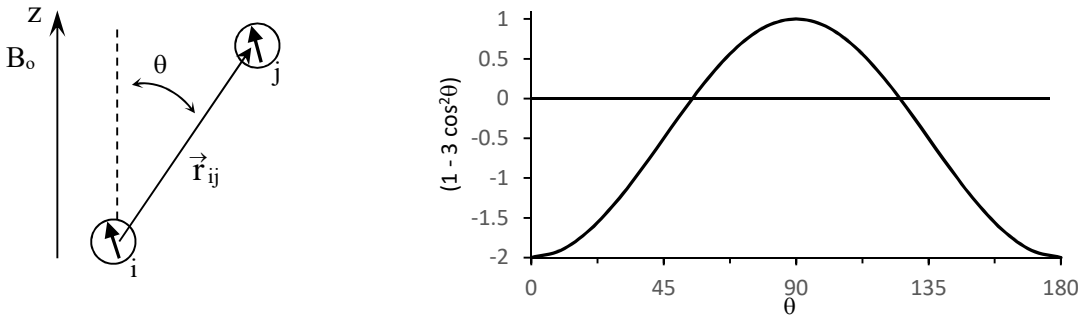


Figure 29.5.3: Magnetic dipole-dipole coupling is a through-space interaction between two magnetic dipoles. In solution, the angle dependence is $(1 - 3\cos^2\theta)$.

Nuclear spins interact through space, Figure 29.5.3. The dipole-dipole interaction is a function of the distance between the spins and the orientation with respect to the applied magnetic field:

$$V_{ij} = \frac{A}{r_{ij}^3}(1 - 3\cos^2\theta) \qquad \text{(solution)} \qquad 29.5.7$$

where $r_{ij}$ is the distance between the two spins, i and j, and $\theta$ is the angle between the applied field and the vector joining the two spins, $\vec{r}_{ij}$. The constant A depends on the magnetic moments of the two coupled spins, which for the interaction of two protons is $A = \gamma_n^2\hbar^2$. When a molecule

tumbles in solution, the angle θ changes rapidly and at random causing a fluctuating magnetic field at each nucleus. This fluctuating magnetic field can bring about relaxation.

Not any fluctuating magnetic field is efficient at bringing about relaxation. To be efficient the fluctuations must have a large component at the frequency of the transition. In Figure 29.5.4a, the transition frequency that corresponds to the magnetic resonance transition, $\nu_o$, is shown at the top. Typical frequencies are 300-500 MHz for protons or 75-125 MHz for $^{13}C$.

Large molecules reorient slowly in solution, so that the angle θ changes slowly, Figure 29.5.4b. The fluctuating magnetic fields caused by the tumbling of large molecules change too slowly to be efficient at relaxation at the transition frequency. The result is a long $T_1$. Intermediately sized molecules tumble at a rate that produce fluctuations with frequency components that match the transition frequency, Figure 29.5.4c. This motion is efficient at causing relaxation and gives a short $T_1$. Small molecules tumble too rapidly, causing fluctuating magnetic fields with frequency components that are too high to cause efficient relaxation, Figure 29.5.4d. Just as in large molecules, in small molecules $T_1$ is long. As a result, the motion of a molecule can be either too fast or too slow to cause efficient relaxation. Only when the motion of the molecule is matched to the transition frequency is relaxation efficient and $T_1$ short.

The motions in a molecule are characterized by a correlation time, $\tau_c$. The correlation time is roughly the average time that a molecule spends in a given orientation. Large molecules tumble slowly and therefore have long $\tau_c$. Small molecules tumble rapidly and therefore have short $\tau_c$. Only when the motion has $\tau_c$ about equal to $1/2\pi\nu_o$ is relaxation efficient.

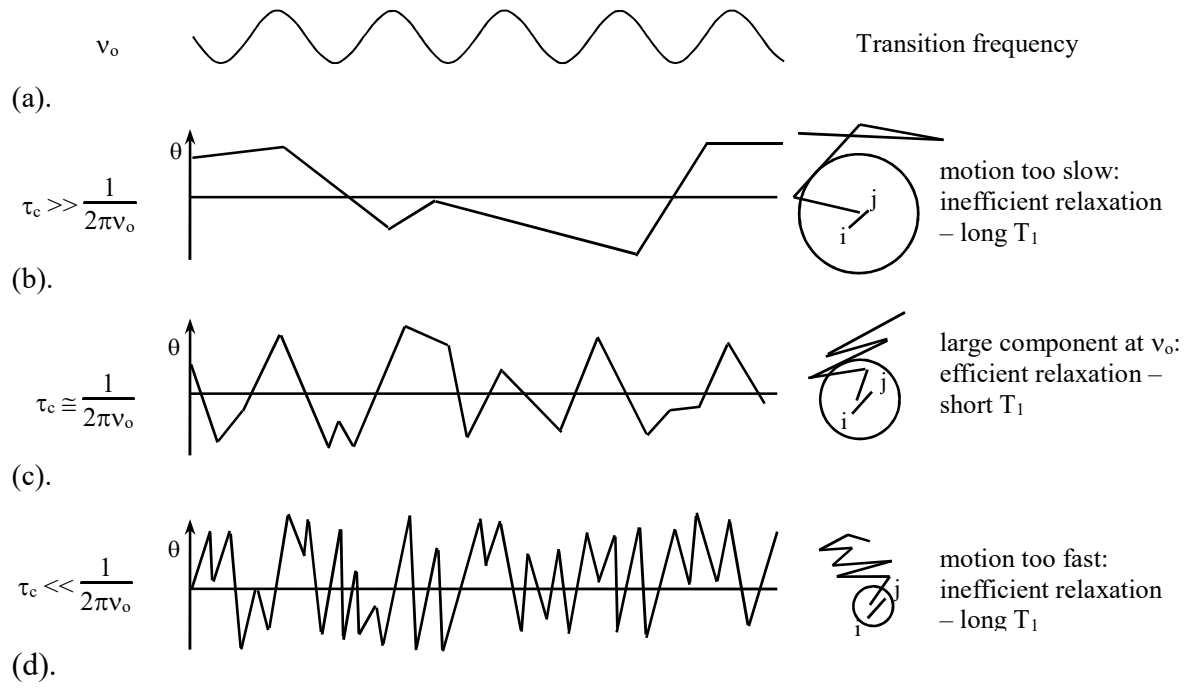


Figure 29.5.4. Effect of motion on relaxation. (a) When motions are slow relaxation is inefficient and $T_1$ is long. (b) When the frequency of the motions match the transition frequency, relaxation is efficient and $T_1$ is short. (c) When motions are too fast, relaxation is once again inefficient and $T_1$ is long. Small molecule reorientations are too fast.

Molecular tumbling is not the only motion that can cause relaxation. Internal motions can be effective at causing relaxation. Most importantly, different parts of a molecule can have different frequencies of motion, because of torsional rotation around single bonds. 1-Bromodecane is a good example of a molecule that has different motional regimes. The $^{13}C$-relaxation times in 1-bromodecane are:[17]

| Br – | $CH_2$ – | $CH_2$ – | $CH_2$ – | $CH_2$ – | $CH_2$ – | $CH_2$ – | $CH_2$ – | $CH_2$ – | $CH_2$ – | $CH_3$ |
|---|---|---|---|---|---|---|---|---|---|---|
| | 2.8 | 2.7 | 1.9 | 2.0 | 2.1 | 2.1 | 2.2 | 3.1 | 3.9 | 5.3 s |
| | *too slow* | | *optimal* | | | | | | *too fast* | |

At the methyl end of the chain the motions are too fast to provide an efficient mechanism for relaxation. Because the bromine is massive, the motions at the bromine end of the chain are slower and are therefore more efficient at relaxation. The minimum relaxation time occurs not next to the bromine, but three carbons away. Motions at the methylenes adjacent to the bromine are too slow for the most efficient relaxation.

As a result of different motions, molecules have multiple correlation times. Diffusion, molecular reorientation, and vibrations all act independently and are characterized by different correlations times. For example, methyl group rotation, which is torsion around the C-C bond leading to the methyl group, is often too fast to provide effective relaxation. However, the C-C bond to the methyl group may be wagging around because the methyl group is attached to a ring. This wagging motion may have the correct frequency components to provide efficient relaxation, leading to a short $T_1$ for the methyl protons. Therefore, all the motions that a particular atom experiences must be considered. Some motions may be too slow, some may be too fast, but if one or a few are just at the right frequency the relaxation will be efficient leading to short $T_1$.

In summary, spin-lattice relaxation times are a sensitive probe of molecular motion. Analysis of relaxation times can tell us whether a given chemical environment is in a rigid portion of the molecule or in a flexible part of the molecule.

However, caution must be exercised when interpreting relaxations times. For $^{13}C$, the biggest effect on relaxation is the number of attached protons. The attached protons are typically the closest spin-active nuclei to a given carbon, providing the largest dipole-dipole coupling. Correlation times being equal, a methyl carbon is expected to relax more rapidly than a methylene, and a methylene relaxes more rapidly than a methine. Quaternary carbons, those with no attached hydrogens, typically have a long $T_1$. For equal correlation times, the expected ratio of $T_1$ values for $^{13}C$ in methine, methylene, and methyl groups is 6:3:2. A simple solution to the problem is to compare carbons with the same number of attached protons. On the other hand, for protons intermolecular relaxation from diffusion is important. For this reason, $^{13}C$ relaxation is preferable for careful studies.

Another source of fluctuating magnetic fields comes from paramagnetic substances in solution. Molecular oxygen is paramagnetic and greatly enhances spin-lattice relaxation. The effect of dissolved $O_2$ is so strong that $O_2$ must be removed by a process called “degassing.”

Having established a qualitative understanding of relaxation, we next take a more quantitative approach. The fundamental process of relaxation progresses through fluctuations caused by the molecular motion.

## *℘ 11*
## *General Pattern*: *Fluctuation Dissipation*[18-21]

Spectroscopic relaxation is governed by the **fluctuation dissipation theorem**: the time evolution of a non-equilibrium system is driven by fluctuations. These fluctuations are the same

as the fluctuations the system experiences at equilibrium. The fluctuations are characterized by a correlation time, $\tau_c$. Rapid random motions have short correlation times and slow random motions have long correlation times. As a specific example we continue with our discussion of spin-lattice relaxation.

Fluctuations are quantitatively characterized by a **correlation function**, $C(\tau)$. The motion can be translational diffusion as characterized by the x, y, z-position of the center of mass, or molecular rotation as characterized by the angles with respect to the x, y or z-axes. The motion can also be vibrational as characterized by the x, y, z-position of each atom. For example, the rotational correlation function describes the orientation of the molecule at time $\tau$ compared to the orientation at time 0. Collisions cause reorientation at random intervals. For example, the rotational correlation time is the average time that a molecule spends in a given orientation. An average is necessary because of the random nature of the motion. For short times, $\tau$, the orientation is similar to the initial orientation at time 0, giving a large value of the correlation function. However, as time progresses collisions cause greater and greater random deviations of the orientation from the value at $t = 0$. At long $\tau$-values the correlation function tends to zero.

Consider the value of the coordinate at time t of a random motion, $f(t)$. Assume the average of the coordinate over time is zero. The correlation function is calculated by comparing the values of the coordinate at times t and $t + \tau$ averaged over a series of measurements:

$$C(\tau) = \langle \overline{f(t+\tau)\, f(t)} \rangle \qquad 29.5.8$$

The overbar indicates a time average from $t = 0$ to $\infty$. For example at one value of t, if both $f(t + \tau)$ and $f(t)$ have the same sign, then the product gives a positive contribution to the time average, Figure 29.5.5. At a subsequent value of t, if $f(t + \tau)$ and $f(t)$ have opposite sign, then the product gives a negative contribution to the time average. For $\tau$ shorter than the correlation time, the system doesn't move much and the signs of $f(t + \tau)$ and $f(t)$ are the same, giving a large $C(\tau)$. For long $\tau$, on average the positive and negative contributions cancel giving $C(\tau \to \infty)$ as zero. Since fluctuations are random, each experiment that is used to calculate the time averages gives a different, though similar, result. If the fluctuations are much faster than the resulting relaxation behavior, we expect the dynamics to be identical with each measurement. To remove the changing repeat behavior, the macroscopic dynamics are given by an **ensemble average** of $\overline{f(t+\tau)\, f(t)}$ in the equilibrium state.[19] The "<" and ">" in Eq. 29.5.8 symbolize the ensemble average. An ensemble is a group of identical systems. A fundamental postulate of statistical mechanics is that the observed value of a macroscopic observable, such as the spin-lattice relaxation time, is given by an ensemble average of the corresponding microscopic, quantum mechanical property (see Chs. 12.1 and 30.1). The ensemble average is calculated by finding $\overline{f(t+\tau)\, f(t)}$ for each system in the ensemble and then averaging the result over the ensemble. The important stipulation of the fluctuation dissipation theorem is that the ensemble is held at equilibrium for the averages.

Under many circumstances, correlation functions decay roughly exponentially with time:

$$C(\tau) = \overline{f(t)^2}\, e^{-\tau/\tau_c} \qquad (\tau > 0) \qquad 29.5.9$$

Where $\overline{f(t)^2} \equiv C(0)$ is the mean square average of the fluctuating coordinate. The exponential time constant $\tau_c$ is the correlation time. Correlation functions are even functions of $\tau$; past behavior is predictive of future behavior. For $\tau < 0$ the exponential factor is instead $e^{\tau/\tau_c}$. Correlation functions can be thought of as measures of persistence. For short time periods the original

orientation persists and C(τ) is large. As time progresses, the molecule loses track of its previous orientation and C(τ) approaches zero, Figure 29.5.5. The Fourier transform of the correlation function gives the frequencies and amplitudes of the underlying fluctuations. The Fourier transform of the correlation function is called the **spectral density**, J(ν). Using Eq. 29.5.9 to find the Fourier transform gives:

$$J(\nu) = 2\int_0^\infty C(\tau)\, e^{-i\,2\pi\nu t}\, d\tau \qquad 29.5.10$$

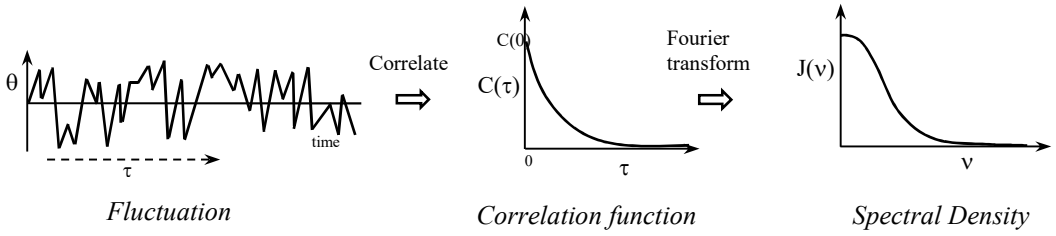


Figure 29.5.5: Random fluctuations are characterized by a correlation function with a correlation time $\tau_c$. The spectral density is the Fourier transform of the correlation function.

The spectral density is the amplitude of the fluctuations at frequency ν. For example, the rate of spin-lattice relaxation at the resonance frequency $\nu_o$ of 300 MHz is directly proportional to the spectral density of the fluctuations at 300 MHz, Figure 29.5.4. Substituting the correlation function, Eq. 29.5.9, into the Fourier transform gives:[18]

$$J(\nu) = 2\int_0^\infty \overline{f(t)^2}\, e^{-\tau/\tau_c}\, e^{-i\,2\pi\nu t}\, d\tau = \overline{f(t)^2}\left(\frac{2\tau_c}{1 + 4\pi^2\nu^2\tau_c^2}\right) \qquad 29.5.11$$

For short or long correlation times the spectral density at the resonance frequency is low, Figure 29.5.6.

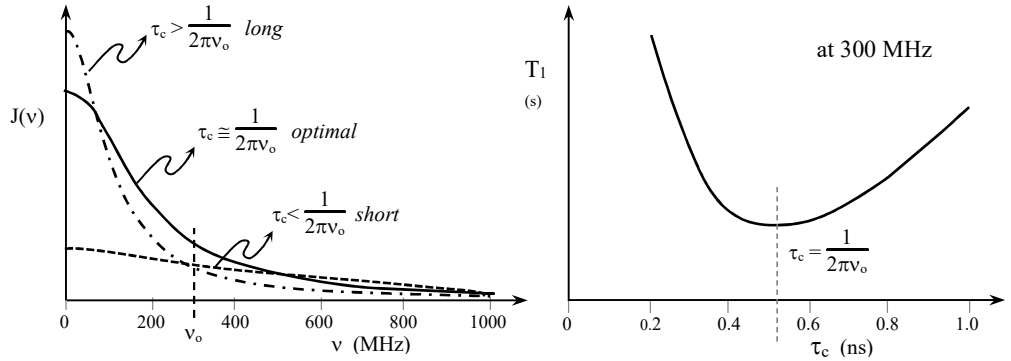


Figure 29.5.6: (a). The spectral density has relatively low amplitude at the resonance frequency, $\nu_o$, for short and long correlation times and is maximal for a correlation time of $\tau_c \cong {}^1/_{2\pi\nu_o}$. (b). $T_1$ passes through a minimum at $\tau_c \cong {}^1/_{2\pi\nu_o}$

The maximum spectral density and minimum $T_1$ result when the correlation time is just right, $\tau_c = 1/2\pi\nu_o$. Relaxation is a "Goldilocks and the three bears" kind of thing. Note that proton and $^{13}C$ NMR sample different frequencies of the spectral distribution. In addition, characterizing the spectral density by studies of the same nucleus at different frequencies is also common (e.g. $^1H$ at $\nu_o$ of 60 MHz, 100 MHz, 300 MHz).

The spectral density function is a generalization of the density of states concept that we used to explain non-radiative processes in electronic spectroscopy. The spectral density approach is appropriate for motions that are essentially random, but the concepts are identical. The relationship between the correlation function and the spectral density, Eq. 29.5.10, is justified by a general mathematical relationship called the **Wiener-Khintchine theorem**.[21] The fluctuation dissipation and Wiener-Khintchine theorems are applied to a wide variety of processes apart from spectroscopy, including reaction dynamics. Electronic and audio noise are also fluctuation phenomena. Historically, the first full introduction of the fluctuation dissipation theorem was the theory of gas phase viscosity.[21] Thinking of the physical world as a bath of fluctuations that drive dynamic processes is a powerful unifying concept.

***℘ 11***

For the spectral density in spin-lattice relaxation, $\overline{f(t)^2}$ in Eq. 29.5.11 is the average square of the fluctuating magnetic field intensities perpendicular to the applied field, $\overline{B_x(t)^2 + B_y(t)^2}$.[18] For a single proton with resonance frequency $\nu_o$ the relationship between the spin-lattice relaxation time and the spectral density from Eq. 29.5.11 is:[18]

$$\frac{1}{T_1} = \frac{\gamma_n^2}{\hbar^2}\,\overline{B_x(t)^2 + B_y(t)^2}\left(\frac{\tau_c}{1 + 4\pi^2\nu_o^2\tau_c^2}\right) \qquad 29.5.12$$

Magnetic dipole-dipole interactions are important sources of the fluctuating magnetic fields at the nucleus. The correlation time is then determined by the details of the molecular motion.

*Inversion-Recovery Experiments Determine $T_1$-Relaxation Times*: The saturation-recovery method for $T_1$ determination was discussed above. A better method, available in pulsed spectrometers, is the inversion-recovery pulse sequence.[14] The pulse sequence is a 180° pulse followed at time $\tau$ by a 90° pulse, Figure 29.5.7. The 180° pulse in the inversion-recovery sequence inverts the magnetization, which causes all the up-spins to become down-spins, and visa-versa. This 180° pulse creates a population inversion in which there are more spins in the high energy state than in the low energy state. After time $\tau$ the FID is acquired by applying a 90° pulse. The $\tau$-interval is called an **evolution period**, during which the spins relax towards equilibrium. For short $\tau$-values the peaks in the spectrum are negative; the combined result of the two pulses is effectively a 270° pulse. For long $\tau$–values, the system is able to regain equilibrium before the second pulse and the spectrum appears normally at full intensity.

The spectra at various $\tau$ values are often plotted on the same chart, giving the so-called partially relaxed spectra for the system, Figure 29.5.8. The $T_1$ value of each chemical environment is obtained by fitting the corresponding peak intensity as function of $\tau$ to:

$$\ln(M_o - M_z) = \ln(2M_o) - \frac{\tau}{T_1} \qquad 29.5.13$$

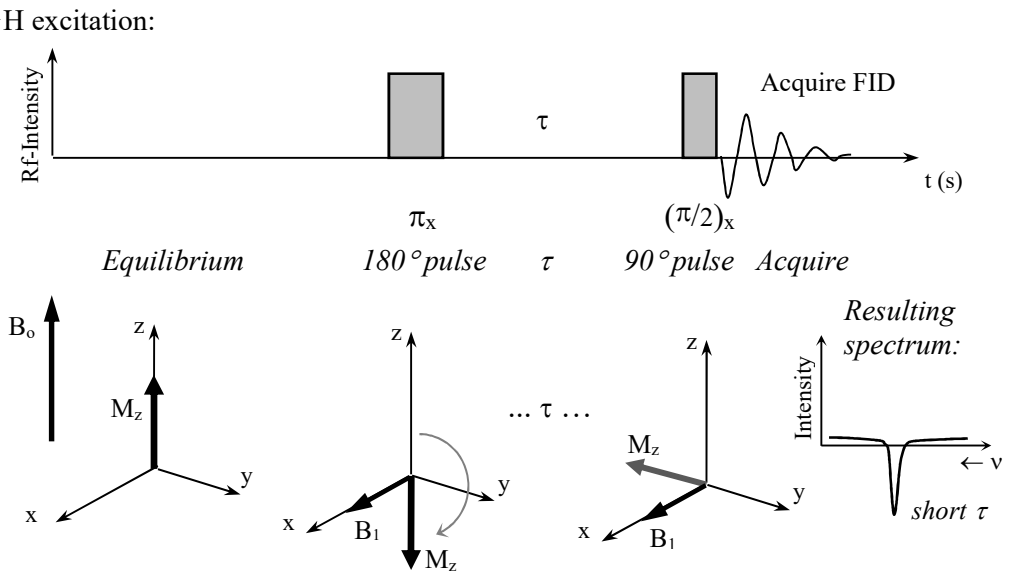


Figure 29.5.7: Inversion-recovery sequence for $T_1$ determination. The pulse profiles are shown; the final pulses are at the resonance frequency (e.g. 300 MHz). The 180° pulse inverts the magnetization. The system relaxes towards equilibrium during the evolution period τ, after which the spectrum is obtained by applying a 90° pulse.

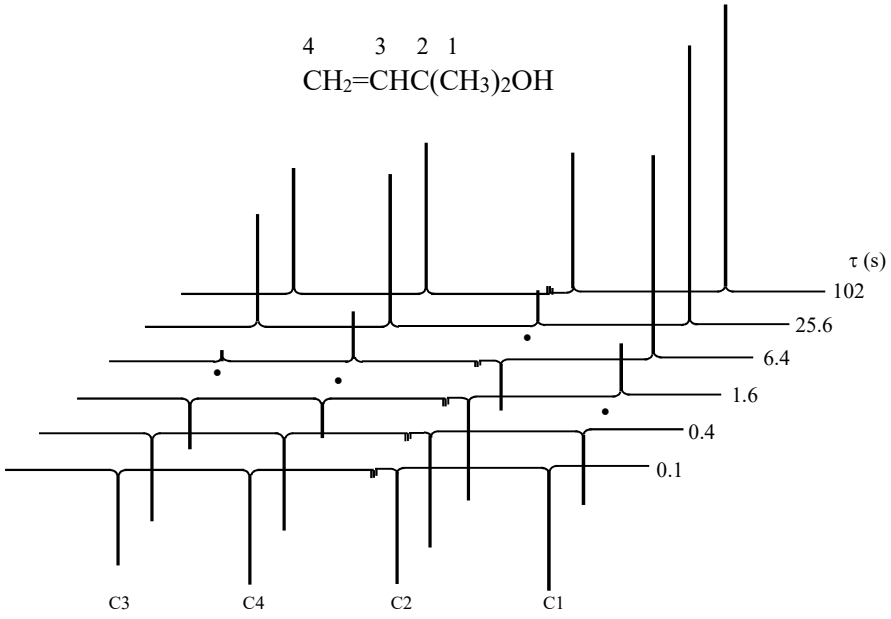


Figure 29.5.8: Partially relaxed inversion-recovery $^{13}C$-spectra.[22] The zero-crossing τ-values, for which $\tau = T_1 \ln 2$, are shown by "•" symbols.

By comparison, taking the logarithm of both sides of Eq. 29.5.3 gives $\ln(M_z)=\ln(M_o) - \tau/T_1$. The difference is that in the inversion-recovery method, the signal for small $\tau$ is negative. The point when a peak changes from negative to positive is a rough measure of the $T_1$, which from setting Eq. 29.5.13 equal to zero gives $\tau = T_1 \ln 2$.

## 29.6 Chemical Exchange[23-26]

*Chemical Exchange Broadens Transitions*: The hydroxyl resonance in ethanol, Figure 29.1.3ab, is significantly broader than the methylene and methyl resonances. The chemical shift of the hydroxyl is strongly temperature dependent and also shifts with changes in solvent; compare Figure 29.1.3a to 29.1.3c. The cause of this variable behavior is that the hydroxyl protons are **labile**. The hydroxyl proton on one ethanol molecule is rapidly exchanged with the hydroxyl proton on another alcohol molecule or with the protons from trace amounts of water, which is absorbed from the atmosphere. The exchange of labile protons is an example of a dynamical process called **chemical exchange**. The protons on carboxylic acids, amines, amides, ammonium, quanidinium, and thiol groups are similarly labile and exchangeable. NMR is one of the most commonly used spectroscopic tools for studying chemical exchange, which also includes conformational changes and chemical reactions.[23] Examples of conformational studies are the boat-chair interconversions in cyclohexanes and *cis-trans* isomerization. Chemical reaction types include keto-enol tautomerization and complexation. There are two requirements for the applicability of dynamic NMR. The magnetically active nucleus must change environments so that the chemical shift of the nucleus differs from one environment to another. The time scale of the exchange must also be slow enough or fast enough to cause the NMR transitions to be broadened. The time scale for broadening is called the **NMR time scale**. The utility of dynamic NMR studies is twofold. First, dynamic aspects of systems that are at equilibrium can be studied. For example, rate constants can be obtained for "virtual" reactions, such as the *cis-trans* isomerization of N,N-dimethylacetamide in which reactants and products are chemically identical:

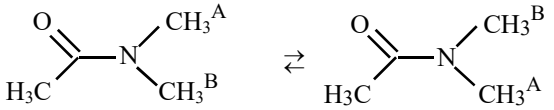


29.6.1

Secondly, the NMR time scale corresponds to reaction rate constants in the range of $10^{-1}$-$10^{-5}$ $s^{-1}$, which are too fast for classical kinetics studies.[24]

*The Exchange Rate Constant is Determined by Line Widths*: If two groups of nuclei are exchanged, the broadening of the transitions is a function of the difference in their resonance frequencies, $\Delta\nu = \nu_A - \nu_B$, and the exchange rate constant, k. The exchange lifetime is defined as $\tau_e = {}^1/_{2k}$. At low temperatures the exchange is slow, $\tau_e >> {}^1/_{\Delta\nu}$, giving two sharp singlets at $\nu_A$ and $\nu_B$, Figure 29.6.1a. At high temperatures the exchange is fast, $\tau_e << {}^1/_{\Delta\nu}$, and a single sharp transition is observed, Figure 29.6.1d. At intermediate temperatures the spectrum consists of two significantly broadened overlapping lines, Figure 29.6.1b. At the **coalescence temperature** the two transitions broaden sufficiently that the two transitions merge into a single broad peak.

In the absence of chemical exchange, spin-spin relaxation and magnetic field inhomogeneity determine the width of an NMR transition. Chemical exchange shortens the lifetime of each spin state, additionally contributing Heisenberg uncertainty broadening of $\Delta\nu_{½} = {}^1/_{2\pi\tau}$, in analogy

with Eq. 23.4.46. The line shape that results from the exchange process is derived from the Bloch equations.[24,25] The resulting line shape in the case of two exchanging groups with equal probability of occurrence and no spin-spin coupling is:[25]

$$g(\nu) = \frac{K\tau\,(\nu_A - \nu_B)^2}{\left(\tfrac{1}{2}(\nu_A + \nu_B) - \nu\right)^2 + 4\pi^2 T_{2,\text{eff}}^2 (\nu_A - \nu)^2\,(\nu_B - \nu)^2} \qquad (50{:}50,\ J_{AB} \cong 0,\ \text{slow})$$

$$\text{with} \quad \frac{1}{T_{2,\text{eff}}^2} = \frac{1}{T_{2A}'^2} + \frac{1}{\tau} \qquad 29.6.2$$

where $g(\nu)$ is the intensity at frequency $\nu$, K is a normalization constant, and $T_{2,\text{eff}}$ combines the effective spin-spin relaxation time and chemical exchange. Nonlinear curve fitting of the observed line shape to Eq. 29.6.2 is used to determine $\tau$, $\nu_A$, and $\nu_B$. Approximations are also commonly made that apply over different ranges of exchange rates.

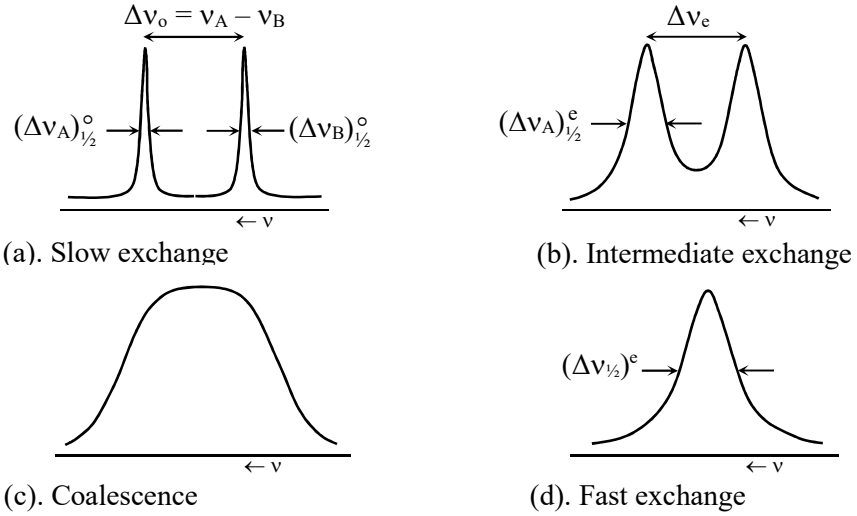


Figure 29.6.1. Effect of chemical exchange on NMR line shapes. The two transitions just merge to give a single peak at the coalescence temperature, such that $k = \pi\Delta\nu_o/\sqrt{2}$.

The full widths at half-height, as defined in Figure 29.6.1, are used in approximate methods to find the exchange lifetime and exchange rate constant. The line widths of the two transitions are assumed to be identical. In the slow exchange limit the spectrum consists of two sharp lines. For the A-transition at frequency $\nu_A$, Eq. 29.6.2 reduces to:[25]

$$g(\nu) \cong \frac{KT_{2A}'}{1 + 4\pi^2 T_{2A}'^2\,(\nu_A - \nu)^2} \qquad (\tau >> 1/\Delta\nu,\ \text{slow}) \qquad 29.6.3$$

where $T_{2A}'$ is the effective spin-spin relaxation time. A parallel equation holds for the B-transition. Comparing Eq. 29.6.3 to Eq. 29.6.2 shows that the linewidth of the transition at $\nu_A$ is:

$$(\Delta\nu_A)_{1/2}^{\circ} = \frac{1}{\pi T_{2A}'} \qquad (\tau >> 1/\Delta\nu,\ \text{slow}) \qquad 29.6.4$$

In the intermediate range,[26] exchange results in additional broadening of $1/\pi\tau$:

$$(\Delta\nu_A)^e_{½} = \frac{1}{\pi T_{2A}'} + \frac{1}{\pi\tau} \qquad \text{(intermediate)} \qquad 29.6.5$$

The exchange rate constant is determined by comparing linewidths of exchanging peaks to those recorded at temperatures at which the rate of exchange is negligible:

$$k \cong \frac{\pi}{\sqrt{2}}\left[(\Delta\nu_A)^e_{½} - (\Delta\nu_A)^\circ_{½}\right] \qquad \text{(intermediate)} \qquad 29.6.6$$

Often $T_{2A}'$ is long (≈ 5 s) so that the second term in Eq. 29.6.6 can be dropped. The exchange rate constant is also related to the change in peak separation:

$$k \cong \frac{\pi}{\sqrt{2}}\left[\Delta\nu_o^2 - \Delta\nu_e^2\right]^{½} \qquad \text{(intermediate)} \qquad 29.6.7$$

where $\Delta\nu_o$ is the peak separation in the absence of exchange, at low temperature, and $\Delta\nu_e$ is the peak separation with intermediate exchange. At the coalescence temperature the rate constant is:

$$k \cong \frac{\pi\Delta\nu_o}{\sqrt{2}} \qquad \text{(coalescence)} \qquad 29.6.8$$

In other words the NMR time scale is determined by the chemical shift differences with $\tau = {}^1/_{2k}$. In the fast exchange limit, at temperatures above the coalescence temperature, the spectrum consists of a single peak. In this region $k << (\nu_A - \nu_B)$ and Eq. 29.6.2 reduces to:

$$g(\nu) \cong \frac{KT_2'}{1 + 4\pi^2 T_2'^2 (\nu_A + \nu_B - 2\nu)^2} \qquad (\tau << {}^1/\Delta\nu, \text{ fast}) \qquad 29.6.9$$

with the average ${}^1/T_2' = ({}^1/T_{2A}' + {}^1/T_{2B}')/2$. The fast exchange limit is called **extreme narrowing**. If the signal is not completely collapsed, exchange is slow enough to contribute to the width but much faster than the rate corresponding to separate signals, then:

$$k \cong \frac{\pi\Delta\nu_o^2}{2}\,\frac{1}{\left[(\Delta\nu_{½})^e - (\Delta\nu_A)^\circ_{½}\right]} \qquad (\tau << {}^1/\Delta\nu, \text{ fast}) \qquad 29.6.10$$

---

**Example 29.6.1:** *Chemical Exchange*

For N,N-dimethylacetamide at low and intermediate temperatures, the -$N(CH_3)_2$ group gives two resonances, Eq. 29.6.1. One N-methyl group is *cis* to the carbonyl and the other is *cis* to the acetyl methyl group. The spectrum is acquired at three temperatures. The full width at half height and difference in peak maxima for the corresponding transitions in slow, intermediate, and fast exchange are given schematically below at 400 MHz. Calculate the exchange lifetimes and rate constants at the temperatures with intermediate and fast exchange.

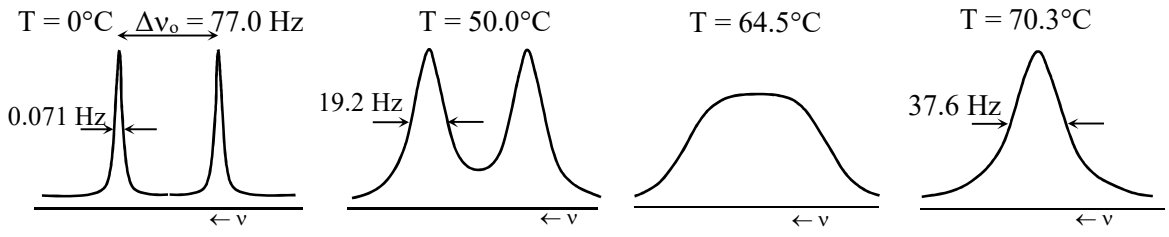


Figure 29.6.2: N, N-dimethylacetamide –$N(CH_3)_2$ proton resonances at 400 MHz.

*Answer*: The lowest temperature gives the effective spin-spin relaxation time in the absence of chemical exchange, Eq. 29.6.4:

$$(\Delta\nu_A)^{\circ}_{½} = \frac{1}{\pi T_{2A}'} \qquad \text{which gives } T_{2A}' = 4.5\ s^{-1}$$

In intermediate exchange, at 50.0°C, the line width is 19.2 $s^{-1}$, so that Eq. 29.6.6 gives:

$$k \cong \frac{\pi}{\sqrt{2}}\left[(\Delta\nu_A)^{e}_{½} - (\Delta\nu_A)^{\circ}_{½}\right] = \frac{\pi}{\sqrt{2}}\left[19.2\ s^{-1} - 0.071\ s^{-1}\right] = 42.5\ s^{-1} \qquad \text{or} \quad \tau_e = 11.8\ ms$$

At coalescence, 64.5°C: $k \cong \frac{\pi\Delta\nu_o}{\sqrt{2}} = \frac{\pi\ 77.0\ s^{-1}}{\sqrt{2}} = 171.\ s^{-1}$ or $\tau_e = 2.92$ ms

In fast exchange, at 70.3°C, the line width is 37.6 $s^{-1}$, so that Eq. 29.6.10 gives:

$$k \cong \frac{\pi\Delta\nu_o^2}{2}\ \frac{1}{\left[(\Delta\nu_{½})^{e} - (\Delta\nu_A)^{\circ}_{½}\right]} = \frac{\pi(77.0\ s^{-1})^2}{2}\ \frac{1}{(37.6\ s^{-1} - 0.071\ s^{-1})} = 248.\ s^{-1} \quad \text{or} \quad \tau_e = 2.02\ ms$$

The activation energy for the exchange is given by the torsional energy barrier. Assuming Arrhenius behavior, the temperature dependence of the rate constant is used to determine the activation energy of the torsion. A plot of ln k vs. $^1/_T$ gives $E_a$ from the slope: slope = $-E_a/R$.

---

**29.7 Electron Spin Resonance**

ESR is best explained by drawing a direct analogy between proton-NMR and ESR, Table 29.7.1. An electron with spin quantum number s = ½ has angular momentum with magnitude $|S| = \hbar\sqrt{½(½+1)}$, which in an applied magnetic field has projections of $m_s = \pm½\hbar$ along the field axis, Figure 29.7.1. The magnetic moment is proportional to the angular momentum. The projection of the electron spin magnetic moment along the applied field, $\mu_z$, is correspondingly quantized:

$$\mu_z = \gamma_e\, \hbar\, m_s \qquad \text{or alternatively} \qquad \mu_z = g_e\, \mu_B\, m_s \qquad \text{(isolated electron)} \qquad 29.7.1$$

where $\gamma_e$ is the magnetogyric ratio of the electron. In the alternative relationship, the proportionality constant is given by the isolated electron g-factor, $g_e$, and the **Bohr magneton**:

$$\mu_B = \frac{-e\hbar}{2\, m_e} \qquad 29.7.2$$

Comparing the two relationships in Eqs. 29.7.1 gives $\gamma_e\, \hbar = g_e\, \mu_B$. The g-factor of an isolated electron is 2.0023. The **nuclear magneton** can also be defined in an analogous expression, Table 29.7.1, using the mass of the proton instead of the mass of the electron. The nuclear and Bohr magnetons are opposite in sign, because the nucleus is positively charged and the electron is negatively charged. In the applied field, $B_o$, the isolated electron energy levels are:

$$E = g_e\, \mu_B\, B_o\, m_s \qquad \text{(isolated electron)} \qquad 29.7.3$$

Because of the smaller mass of the electron, the Bohr magneton is roughly ~ 2000 times larger than the nuclear magneton. As a result the energy level spacing in ESR, $\Delta E = g_e\, \mu_B\, B_o$, is much larger than in proton-NMR. Depending on the applied field strength, ESR spectra occur in the

microwave and mm-wave regions of the electromagnetic spectrum. Microwave frequencies are in the gigahertz range, 1 $GH_z = 1x10^9$ Hz, and mm-wave frequencies extent to the terahertz range, 1 THz = $1x10^{12}$ Hz. By comparison Bluetooth networks operate at 2.4 GHz.

Table 29.7.1: Correspondence between $^1$H-NMR and ESR Expressions.

| property | NMR, I | ESR, s=½ |
|---|---|---|
| angular momentum | $\lvert I \rvert = \hbar\sqrt{I(I+1)}$ | $\lvert S \rvert = \hbar\sqrt{½(½+1)}$ |
| magnetic moment | $\lvert \mu \rvert = \gamma_n \hbar\sqrt{I(I+1)}$ | $\lvert \mu_e \rvert = \gamma_e \hbar\sqrt{½(½+1)}$ |
| projection on z-axis | $\mu_z = \gamma_n \hbar m_I$ | $\mu_z = \gamma_e \hbar m_s$ |
| | $\mu_z = g_n \mu_n m_I$ | $\mu_z = g_e \mu_B m_s$ |
| nuclear or Bohr magneton | $\mu_n = \frac{e\hbar}{2 m_p}$ for $^1$H | $\mu_B = \frac{-e\hbar}{2 m_e} \approx 2000\ \mu_n$ |
| energy $E = -\vec{\mu}\cdot\vec{B}_o = -\mu_z B_o$ | $E = -\gamma_n \hbar B_o M_I$ | $E = g_e \mu_B B_o M_s$ |
| chemical shift | $\Delta E = \gamma_n \hbar B_o (1-\sigma)$ | $\Delta E = g \mu_B B_o$ |

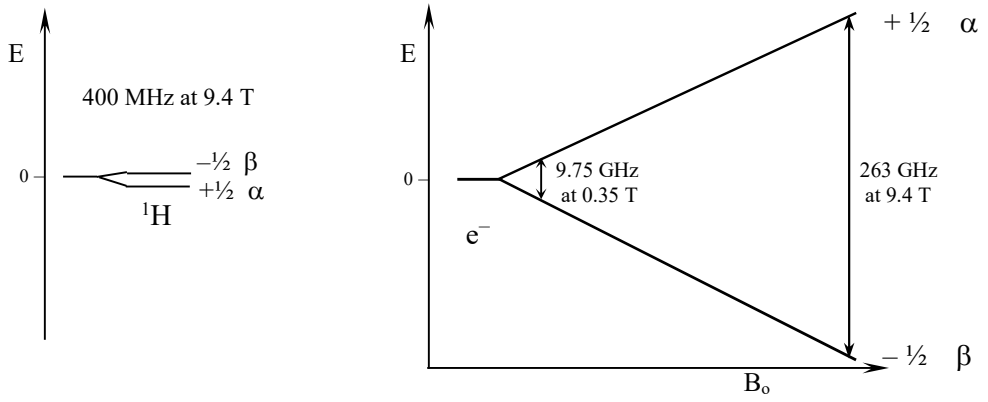


Figure 29.7.1: Correspondence between $^1$H-NMR and ESR of a one-electron radical. Resonance occurs when the magnetic field increases the level spacing to equal the fixed microwave frequency. The energy scale of the NMR plot is 1/20 the scale of the ESR plot.

Table 29.7.2: NMR and ESR Resonance Frequencies at Common Field Strengths.

| Band | X | Q | W | D | mm-wave |
|---|---|---|---|---|---|
| λ (mm) | 30 | 8.5 | 3.2 | 2.1 | 1.1 |
| ESR: $\nu_o$ (GHz) | 9.75 | 34.0 | 94 | 140 | 263 |
| $^1$H: $\nu_o$ (MHz) | 15 | 52 | 143 | 213 | 400 |
| $B_o$ (T) | 0.35 | 1.24 | 3.35 | 5.0 | 9.4 |

*The g-Factor and Hyperfine Splitting*: For an unpaired electron in a molecule, we need to take into account the local effective magnetic field. The electron experiences a net magnetic field that has shifts in analogy to the nuclear chemical shift. To account for chemical shifts, the g-factor $g_e$ of an isolated electron is replaced by an effective g-factor, g:

$$\Delta E = g\, \mu_B\, B_o \qquad \text{(molecule)} \qquad 29.7.4$$

The applied magnetic field in ESR is chosen over a wide range. The resulting ESR transition frequencies of a one-electron radical with $g \cong 2.00$, are given in Table 29.7.2. The corresponding proton NMR frequencies in the same field are tabulated for comparison. The early development of ESR was based on advances in radar technology. The frequency ranges for ESR are named based on the ranges, or bands, typical in radar. The most common band for ESR is X-band at 9.75 GHz requiring a magnetic field strength of 0.35 T. In the same magnetic field, proton-NMR occurs at 15 MHz, which is a factor of 650 times smaller. The historical trend to higher field strengths in ESR is three-fold. ESR spectra have higher resolution and sensitivity at higher field strength. Higher field strengths also facilitate simultaneous NMR and ESR experiments.

ESR spectra are acquired on solids, liquids, and gases. Spectra of solutions are typical, either at room temperature or frozen at cryogenic temperatures. The biggest difference between NMR and ESR is that the occurrence of molecules or ions with unpaired electrons is rare. All molecules have magnetically active nuclei, subject to natural abundance, so that NMR spectra are universal. For organic molecules, on the other hand, few room-temperature stable odd-electron radicals are known. Instead, radical species must be generated in the sample tube or in flow systems by chemical reactions, electrochemistry, or photochemistry. The lifetimes of radicals and triplet states are usually short at room temperature, but radical lifetimes are lengthened at low temperature. As a result low temperature ESR spectra of solids or solid solutions is common. In spite of the lack of generality, ESR is a powerful and common tool in the laboratory. The detection of free radical intermediates using ESR is often a key step in finding the mechanism of complex reactions. Many, if not most, transition metal, lanthanide, and actinide complexes have unpaired electrons. Another advantage is that the typical high frequencies make ESR orders of magnitude more sensitive than proton-NMR, Eq. 29.1.7. Compared to proton NMR, unpaired electron species are easily detected in small numbers.

ESR spectra are commonly acquired by keeping the irradiation frequency constant while scanning the applied magnetic field, $B_o$. Historically, scanning the magnetic field was electronically easier than scanning the frequency. This mode is called continuous wave mode, **cw**. As the applied magnetic field increases, the spacing between the levels increases. A transition occurs when the spacing between the levels matches the fixed irradiation frequency, $\Delta E = h\nu_o$, Figure 29.7.1. The horizontal axis in ESR spectra is usually magnetic field strength in Tesla or Gauss, where $1\ T = 10^4$ G. Pulsed Fourier transform instruments are also available. In cw-mode for odd-electron radicals, the magnetic field sweep range is typically small, up to a maximum of 50-700 mT (500 to 7000 G) depending on the instrument. Note that 1 mT = 10 G. Detection of triplet states requires wide field scan ranges, because zero-field splitting of triplet states is variable (see below).

*Field Modulation Produces a Derivative Line Shape*: The tradition in ESR spectroscopy is to display the derivative of the absorption signal. The derivative signal results because magnetic **field modulation** is used to enhance signal to noise. In field modulation a constant amplitude, weak, oscillating magnetic field is applied to the sample along with the slowly swept main magnetic field. The modulation frequency is typically 100 kHz and the spectrum sweep time is

generally minutes. The detected signal follows the combined magnetic fields. Consider a $B_o$ value near the beginning of the absorption line, Figure 29.7.2a.

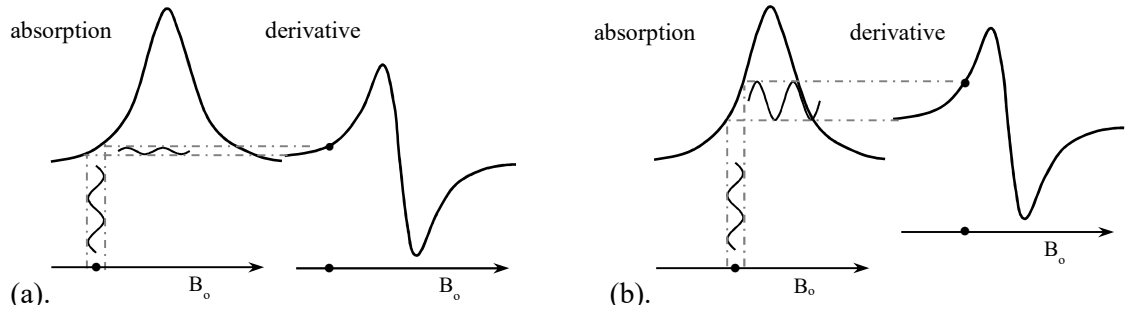


Figure 29.7.2: ESR spectra are commonly recorded as derivatives using magnetic field modulation. A constant amplitude, weak, oscillating-field is superimposed on the slowly swept main field, which causes the detected signal to oscillate proportionally to the change in absorbance for the fixed modulation of the magnetic field, $^{dA}/_{dB}$.

The modulation causes a small change in signal because the slope of the signal is small. Next consider a $B_o$ value at a steep portion of the absorption line, Figure 29.7.2b. The modulation causes a large change in output signal, because the slope of the signal is large. The amplitude of the detected signal is displayed as a function of $B_o$. The slope at the maximum of the absorption signal is zero, giving a zero value for the derivative in the middle of the transition.

Spin-spin splitting occurs in both ESR and NMR. In the ESR context, spin-spin splitting is called **hyperfine structure**. In ESR the spin of the odd electron interacts with nearby magnetic nuclei. Electron-nuclear coupling with a single proton gives a doublet, coupling with equivalent methylene protons gives a triplet, and coupling with methyl protons gives a quartet. As in NMR, electron-nuclear coupling with n-equivalent nuclear spins with spin quantum number I gives the multiplicity of 2nI + 1, Figure 29.7.3.

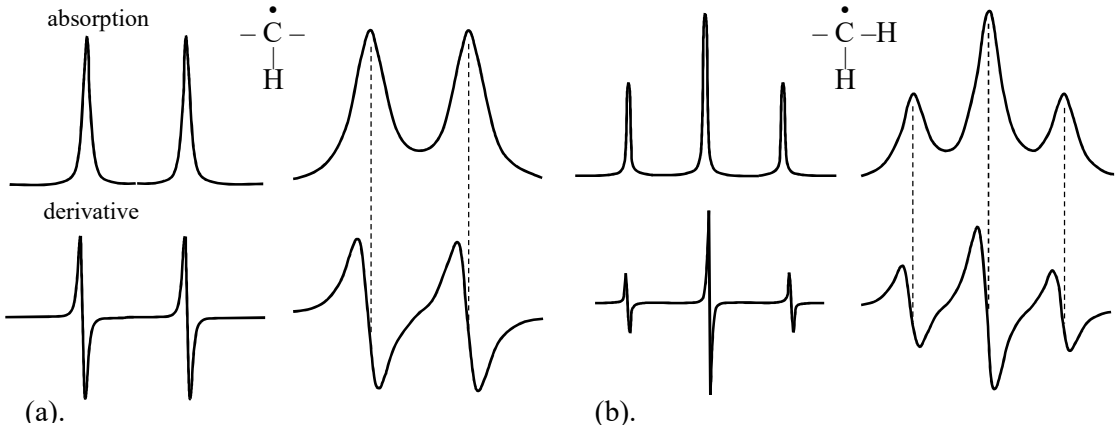


Figure 29.7.3: The derivative passes through zero at the absorption maximum. The multiplicity is equal to the zero crossings of the signal: (a). doublets and (b). triplets.

The spin-spin coupling constant, or **hyperfine-structure constant**, is given the symbol *a*, as a distinction with J in NMR. The multiplicity of a resonance is easy to determine from the derivative spectra, if the line-width is much less than the peak spacing, Figure 29.7.3. However, broad line width causes the derivative signals to overlap, which at first may appear confusing. A quick trick to find the multiplicity is to count the zero-crossings of the signal, Figure 29.7.3b.

The NMR spectrum of ethanol and the ESR spectrum of the 1-hydroxyethyl radical highlight the similarity and differences between NMR and ESR, Figure 29.7.4. The radical was created by oxidation of ethanol with $H_2O_2$ using Ti(III) as a catalyst. NMR spectra typically have multiple chemical shifts. Secondarily, the resonances often show spin-spin splitting. Interpreting the chemical shifts of the different environments in the molecule is the first step in molecular structure determination. In ESR of an odd-electron radical, however, there is only one chemical shift, because there is only one unpaired electron. The g-factor does shift with chemical environment, but the primary information in most circumstances is a single hyperfine-structure multiplet. For the 1-hydroxyethyl radical, the largest splitting is between the electron and the protons of the methyl group at 22.0 G, which gives a 1:3:3:1 quartet. Additional splitting between the electron and the single remaining methylene proton is 15.0 G, giving the final multiplet as a quartet of doublets.

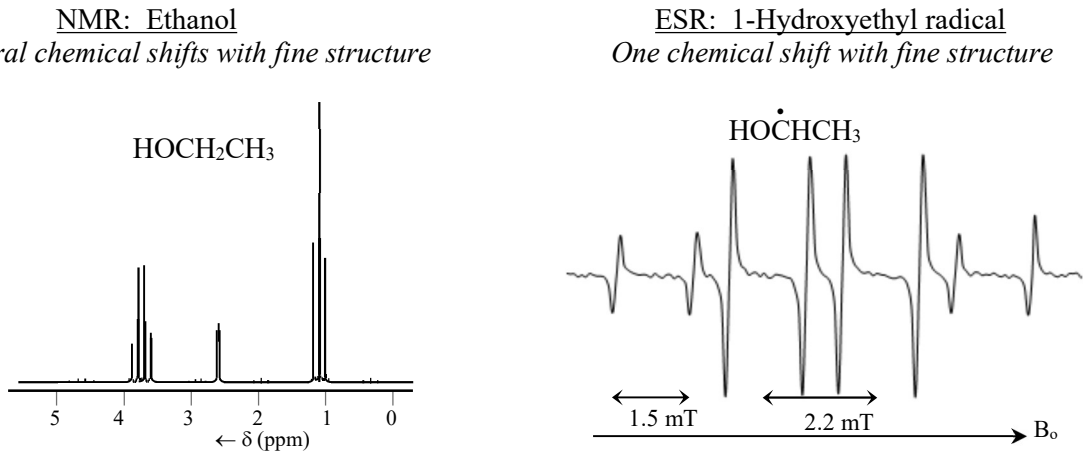


Figure 29.7.4: Comparison of NMR and ESR spectra. Electron-nuclear hyperfine structure (spin-spin splitting) is often the primary information obtained using ESR.[27]

The ESR spectrum of the ammonia radical, produced by X-ray irradiation, shows a triplet of quartets, Figure 29.7.5a. The triplet results from coupling with $^{14}N$, which has a spin of I = 1. Additional splitting by the three methyl protons gives the triplet of quartets.

The nature of the chemical shifts and spin-spin interactions determined by NMR and ESR are another difference. The NMR chemical shift is a measure of the electronic environment in a localized part of the molecule adjacent to the given nucleus. In contrast, in ESR the odd-electron in a radical is often delocalized over many nuclei, because the electron is often in a delocalized molecular orbital. As a result, the multiplicity of a radical is often an indicator of the extent of delocalization of the electron, Figures 29.7.5b, 29.7.6ab. Each of the three examples shows extensive electron-delocalization over all the $sp^2$-centers. The radical structures shown in each case are just one of several possible resonance structures.

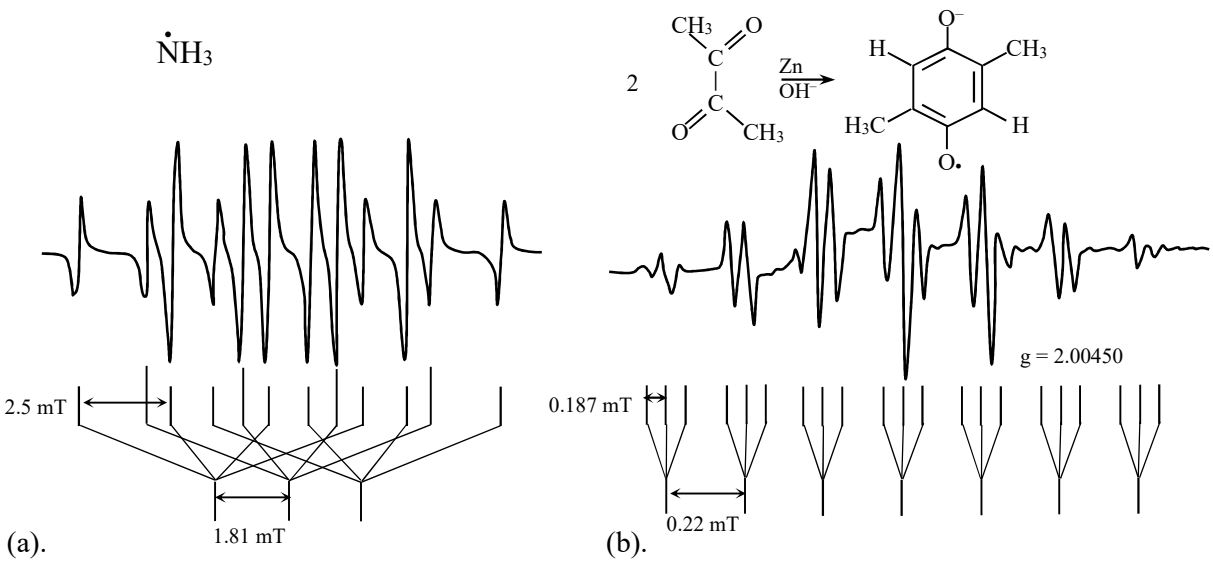


Figure 29.7.5: ESR spectra (X-band). (a). X-ray irradiation of solid ammonium perchlorate. (b). Semiquinone radical formed from reduction of 2,3-butanedione.[28]

In the semiquinone radical, Figure 29.7.5b, the methyl groups are equivalent and the ring-protons are equivalent by delocalization. The two equivalent methyl groups give a septet, 2nI+1 = 2(6)(½)+1 =7. Additional splitting by the two equivalent ring-protons give a final septet of triplets. The hyperfine coupling constant to the methyl-protons is larger than to the ring protons, because the ring protons lie in the nodal plane of the delocalized π-orbital.

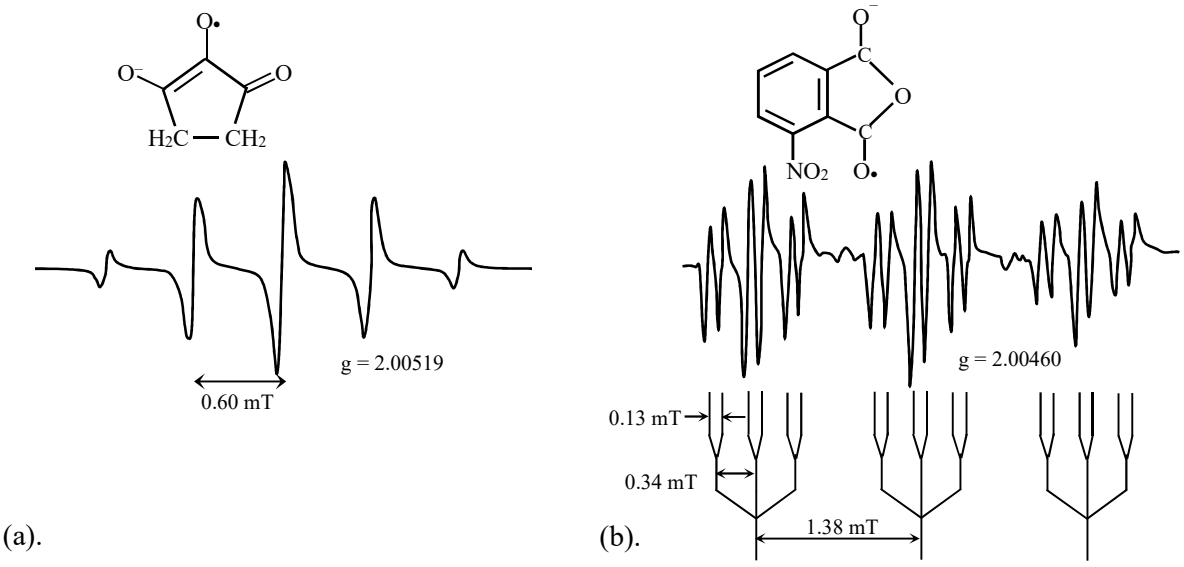


Figure 29.7.6: ESR spectra (X-band). (a). Oxidation of reductic acid with $H_2O_2$.[29] (b). Reduction of 3-nitrophthalic anhydride with Zn.[28]

In the radical anion produced by $H_2O_2$ oxidation of reductic acid, Figure 29.7.6a, delocalization makes the two methylenes equivalent. As a result the hyper-fine pattern is a 1:4:6:4:1 quintet. The alkaline oxidation of 3-nitrophthalic anhydride produces a radical anion with extensive delocalization over both rings, Figure 29.7.6b. The $^{14}N$ from the nitro-group produces a triplet, which is additionally split by two approximately equivalent aromatic ring protons into a triplet, and again by the remaining aromatic-proton into doublets.

A block diagram of an ESR spectrometer is shown in Figure 29.7.7. Microwaves dissipate rapidly traveling along short wires; short wires are effective antennas for microwaves. As a result, the electronic paths for microwaves are usually constructed from waveguides. Waveguides are metallic tubes with rectangular cross section. The width of the waveguide is approximately the wavelength of the microwaves, Table 29.7.2. The sample tube for an ESR study is placed in the middle of a rectangular cavity at the end of a length of waveguide. The microwave cavity is placed between the pole pieces of a magnet. Iron-core electromagnets are usually used for X and Q-band instruments. In bench-top spectrometers, smaller rare-earth permanent magnets are used. High frequency ESR depends on superconducting magnets, as does NMR. Sample absorption is measured by determining the reflected power from the cavity using a reflectance bridge.

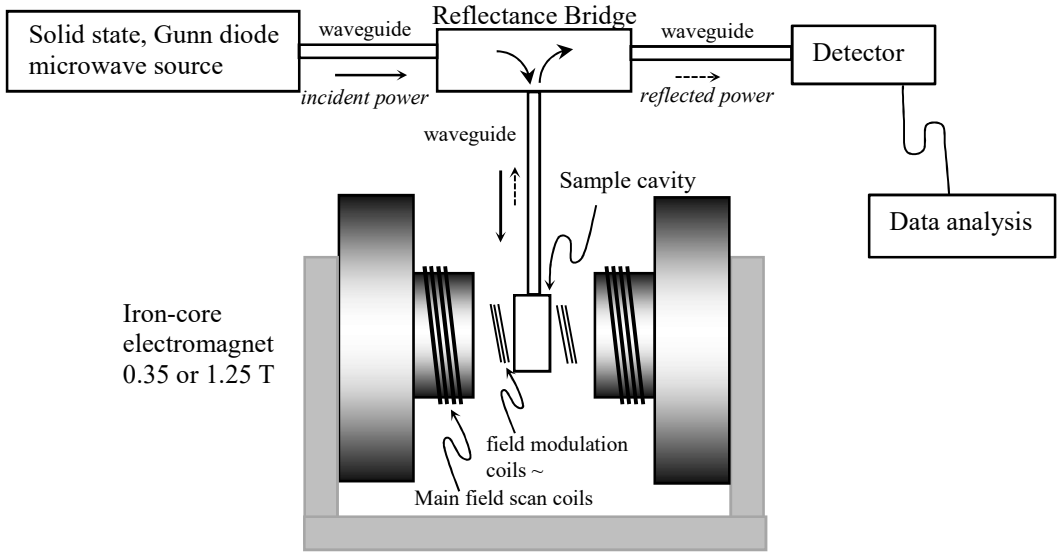


Figure 29.7.7: A typical X- or Q-band ESR spectrometer. The sample is placed in the middle of a rectangular cavity at the end of a waveguide. Sample absorption decreases reflected power from the cavity. Field modulation coils are placed on the exterior of the cavity. Field scan coils sweep the main applied magnetic field linearly over a ~500 mT (~5000 G) range.

In our discussion so far we have emphasized the spectra of odd-electron radicals. ESR of triplet states is also common and distinct from the one-electron case.

*Triplet States Often Give Three ESR Resonances*:[30] The electron spin wave functions of a triplet electronic state are:

$$\begin{array}{ll} \alpha\alpha & m_s = +1 \\ {}^1/_{\sqrt{2}}(\alpha\beta + \beta\alpha) & m_s = 0 \\ \beta\beta & m_s = -1 \end{array} \qquad (25.4.20)$$

First consider a triplet state in the absence of an applied magnetic field. If the interaction between the two electrons is small, the three spin-states are degenerate. However, for many triplet states magnetic dipole-dipole coupling between the two electrons breaks the degeneracy. The energy difference between the resulting degenerate (or nearly degenerate) $m_s = \pm 1$ states and the $m_s = 0$ state is given by the **zero-field splitting**.[30] This interaction occurs in the absence of an applied field. In the presence of an applied magnetic field the $m_s = \pm 1$ levels split in proportion to the strength of the field (see also Ch. 25.6-25.7). With no zero-field splitting, the two $\Delta m_s = \pm 1$ transitions are at the same frequency, and only one resonance is detected, Figure 29.7.8a. The $\Delta m_s = \pm 2$ is not allowed. With moderate zero-field splitting, at fixed frequency, two different $\Delta m_s = \pm 1$ transitions are observed. If the zero-field splitting is small compared to the microwave frequency, a third transition with $\Delta m_s = \pm 2$ is then magnetic dipole allowed.[30] The three transitions are usually at significantly different applied fields, Figure 29.7.8b. As a result, ESR spectrometers designed for the study of triplet states do not use fixed-field main magnets, such as those found in bench-top spectrometers. The necessary magnetic field scan range is over many tesla. Most importantly, as in the one-electron radical case, each transition can also carry electron-nuclear hyperfine-structure, which shows the extent of delocalization.

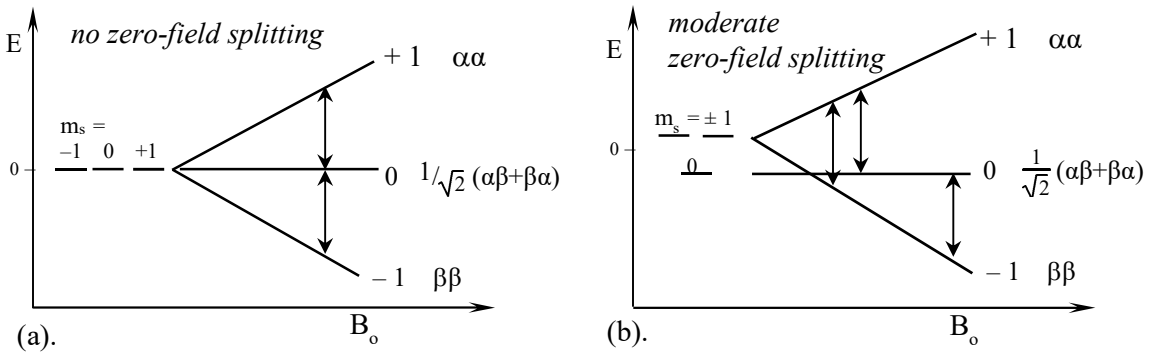


Figure 29.7.8: (a). Triplet states with negligible zero-field splitting give one resonance. (b). Triplet states with moderate zero-field splitting give two $\Delta m_s = \pm 1$ resonances and, if the zero-field splitting is small, a $\Delta m_s = \pm 2$ transition. (*zfs ordering assuming* $B_o$ || *z-axis*)

## 29.8 Coherence

*A Strong Oscillating Field Produces a Superposition of States*: The vector model described by the Bloch equation presents a classical model of a fundamentally quantum mechanical phenomenon. What is the quantum mechanical description of the response of the spin system to a short, strong pulse of rf irradiation? Consider the energy level diagram of a spin-½ system, Figure 29.8.1. The average number of spins in each level is N and the population difference is Δ. The rf-field promotes transitions from the lower level to the upper level in absorption and from the upper level to the lower level in stimulated emission. The net result is a change in populations of the two states. The rf-field couples the two states with the populations oscillating in proportion to the length of the rf-field pulse, $t_p$:

$$P_{+½} = N + \frac{\Delta}{2}\cos\theta \qquad P_{-½} = N - \frac{\Delta}{2}\cos\theta \qquad \text{with } \theta = 2\pi\gamma_n B_1 t_p \qquad 29.8.1$$

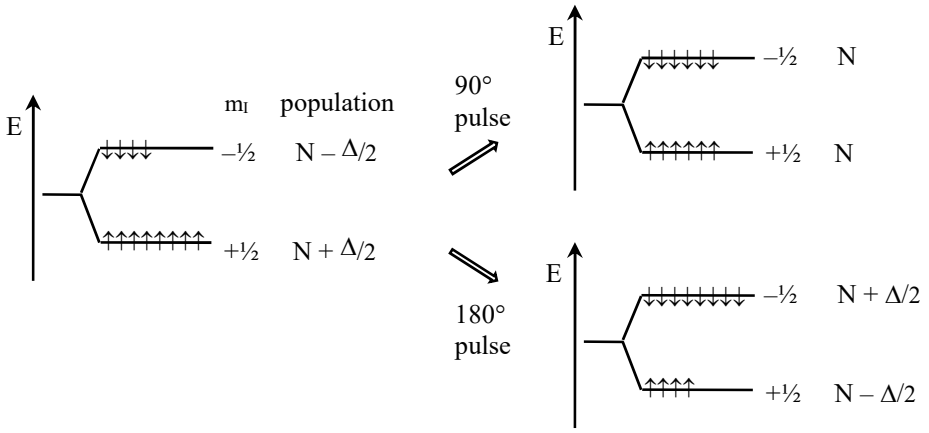


Figure 29.8.1: The populations of the two coupled states oscillate with frequency $\gamma_n B_1$.

A 90° pulse gives equal populations, Figure 29.8.1. A 180° pulse corresponds to a population inversion, giving more spins in the upper state than the lower state. With continuous radiation of a weak field, the populations are equalized giving a saturated transition that produces no signal. However, a strong 90° pulse gives a maximum signal, as correctly predicted by the vector model. If the states have equal populations after a strong 90° pulse, why does the spin system give a strong signal? The answer is that irradiation with a strong rf-field creates a **coherent superposition** of spin states that has a large effective magnetic moment in the x-y plane. The precession of this magnetization produces the free induction decay after the pulse is stopped. What is meant by a coherent superposition? In the presence of irradiation, the state of a spin is no longer purely spin-up or spin-down, but rather a linear combination of the two with coefficients that evolve sinusoidally with time: $\Psi(t) = \cos(2\pi\gamma_n B_1 t_p)\,\alpha + \sin(2\pi\gamma_n B_1 t_p)\,\beta$. The coupling of the two states has important implications for the relative phases of the individual spin magnetization vectors.

At equilibrium, each individual spin has a fixed z-axis projection with a few more spin-up than spin-down, as given by the Boltzmann distribution. The x and y-axis projections of the individual nuclear magnetic moments are distributed at random. The ends of the individual spin magnetization vectors precess around the top and bottom of the cones corresponding to $m_I = \pm½$, Figure 29.8.2a. A strong rf-pulse has the effect of causing the x and y-projections of the magnetization to bunch-up. Because of the coherent superposition, the spin-up and spin-down states are not independent, the phases are held in step. The result is a net magnetization in the x-y plane, Figure 29.8.2b. The synchronization of the x and y-axis projections of the individual spin moments is called temporal coherence. Before the pulse, the individual spins precess at random. The strong rf-field causes the phase of the precession of each individual spin moment to synchronize. In the vector model the generation of coherence is pictured as the tilt of the magnetization away from the z-axis, generating a component of the magnetization in the x-y plane. In both models, angular momentum is conserved by maintaining a constant magnitude of the magnetization vector at any tilt angle.

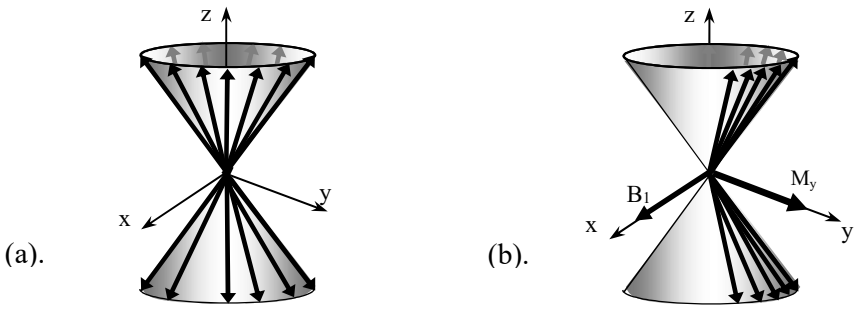


Figure 29.8.2: (a) Before irradiation, the $M_x$ and $M_y$ projections of the individual spin magnetizations are randomly distributed. A strong rf field synchronizes the precessional phases generating a resultant magnetization in the x-y plane. (Rotating frame perspective)

*Coherence Maintains Phase Relationships, Remember $e^{-iEt/\hbar}$*: The quantum mechanical temporal phase is determined by the time-dependent part of the wave function. For a stationary energy state of a single particle, the time dependence is given by Eqs. 23.7.32-23.7.34:

$$\Psi(t) = e^{-iEt/\hbar} = e^{-i\,2\pi\nu_o t} \qquad \text{with } E = h\nu_o \tag{23.7.32}$$

The factor of $2\pi\nu_o t$ is the phase angle in radians, Eq. 23.7.33. However for multiple spins, in the absence of irradiation, each spin has a random phase offset, $\eta$:

$$\Psi(t) = e^{-i(2\pi\nu_o t + \eta)} \qquad \text{(multiple spins)} \qquad 29.8.2$$

At equilibrium $\eta$ is randomized by $T_2$ spin-spin interchanges. The presence of an rf-field synchronizes the phases giving a narrow distribution of phase offset angles. However, in many experiments, the vector model is an easier way of visualizing the evolution of coherence generation and decay. The motion of the magnetization vector describes the creation and evolution of the coherent superposition of states prepared by the applied rf-pulses.

*Temporal Coherence Can Be Observed in UV/Visible and Infrared Spectroscopy*: Temporal coherence is not specific to magnetic resonance. Coherence is observable in pulsed UV/visible, infrared, and microwave spectroscopy, which gives a powerful tool for the study of the effects of molecular motion on relaxation processes. In magnetic resonance, an oscillating magnetic field pulse creates the coherent superposition. In electronic, vibrational, and rotational spectroscopy, the electric field of the pulse creates the superposition of the ground and excited states. Temporal coherence is observable when the irradiation field strength is sufficient to provide tilt angles near 90° in times short compared to the active relaxation times (the equivalent of $T_2$ processes). Relaxation in electronic and vibrational spectroscopy is orders of magnitude faster than in NMR. As a result, high power lasers with picosecond or shorter pulse widths are necessary to observe coherence in pulsed optical spectroscopy.

## 29.9 Summary – Looking Ahead

Magnetic resonance is an immense field with strategic implications for the characterization of structure and motion in all the molecular sciences. Developing the principles of magnetic resonance has also greatly advanced quantum mechanics, statistical mechanics, and spectroscopy

in general. The developments in coherence, non-equilibrium dynamics, and non-linear spectroscopy are especially noteworthy. We have only had the opportunity to present the briefest of introductions to this important field.

The fluctuation dissipation theorem provides an important window into the relationship between microscopic, quantum mechanical processes and macroscopically observable behavior. Dynamic processes, in the absence of driving forces such as applied electromagnetic fields, evolve by isoenergetic transfers of energy to fluctuations in the surroundings. Fluctuations are caused by the wiggling and jiggling of the atoms in the system caused by translation, rotation, and vibration. The important motional frequencies are those that are matched to the frequency of the transition. In non-radiative electronic transitions, the important fluctuations are high frequency vibrations. In NMR and ESR relaxation, the important fluctuations are much slower: translations, rotations, and low-frequency torsional vibrations. The fluctuations that occur in the system at equilibrium drive the dynamics of non-equilibrium processes. In other words, non-equilibrium and equilibrium systems are not distinct. Systems relax to equilibrium using the same fluctuations that exist in and maintain the system at equilibrium.

Detailed Balance, the Gibbs Phase Rule, the Pauli Exclusion Principle, and the Fluctuation Dissipation Theorem are fundamental principles that govern all chemical phenomena. These four, central generalizations describe the interrelationships between different aspects of chemical processes. Each principle is a simple statement with wide ranging ramifications. We will see in the next chapter that the fluctuations of the system about the equilibrium configuration are small. The equilibrium state is the most probable state, which is calculated using an ensemble average of the quantum mechanical properties of the molecules that comprise the system.

The quote at the beginning of this chapter from Lucretius's *On the Nature of the Universe* is prescient in stating the centrality of fluctuations in the dynamic processes that drive the universe. The quotes are poetic pronouncements of the underlying form of nature as based on the statistical probability of random events. Lucretius wrote his six book poem in the first century B.C.E.

## Chapter Summary

1. The projection of the nuclear magnetic moment along the applied field, $\mu_z$, is quantized:

$$\mu_z = \gamma_n \hbar m_I \qquad \text{with} \quad m_I = -I, -I+1, .., 0, \ldots, I-1, I$$

2. The Hamiltonian of a single spin is: $\hat{\mathcal{H}} = -\gamma_n \hbar \hat{I}_z B_o$, where $\hat{I}_z$ is the operator for the projection of the angular momentum along the z-axis.

3. The spin wave functions are eigenfunctions of $\hat{I}_z$. For spin-½ nuclei: $\alpha$ for $m_I = +½$ or "spin-up" and $\beta$ for $m_I = -½$ or "spin-down":

$$\hat{I}_z \alpha = +½ \alpha \quad \text{and} \quad \hat{\mathcal{H}}\alpha = E \alpha \quad \text{with} \quad E = -½ \gamma_n \hbar B_o$$

$$\hat{I}_z \beta = -½ \beta \quad \text{and} \quad \hat{\mathcal{H}}\beta = E \beta \quad \text{with} \quad E = +½ \gamma_n \hbar B_o \quad \text{that is:} \quad E = -\gamma_n \hbar m_I B_o$$

4. The specific selection rule requires a unit change in angular momentum $\Delta E = h\nu_o = \gamma_n \hbar B_o$.

5. The sensitivity of NMR is poor, because of low energy photons, unfavorable Boltzmann population differences, and the natural abundance of many magnetic nuclei is small.

6. For resonance i with frequency $\nu_i$ and reference frequency $\nu_{ref}$, the chemical shift in ppm is

$$\delta_i \equiv \frac{\nu_i - \nu_{ref}}{\nu_{ref}} 1x10^6 \text{ ppm}$$

7. The transition integral is proportional to the number of nuclei in the chemical environment.

8. The chemical shift of a non-labile nucleus in a specific chemical environment is predictable from model compounds.

9. The chemical shift of a labile nucleus is variable, spin-spin multiplets are often collapsed, and the transition is often broadened by chemical exchange (e.g. hydroxyl protons).

10. Chemical shifts are a function of the electron density at the nucleus. Diamagnetic shifts are upfield, to smaller frequency, smaller $\delta$ and are caused by induced magnetic fields that are opposed to the applied magnetic field at the nucleus.

11. Paramagnetic shifts are downfield, to larger frequency, larger $\delta$ and are caused by induced magnetic fields that are additive to the applied magnetic field. The induced magnetic field is produced by ring currents of the electrons in the molecular orbitals of the molecule.

12. Chemical shifts show chemical shift anisotropy; they depend on the orientation of the nucleus relative to functional groups in the molecule. The chemical shift of a nucleus near a $\pi$-orbital depends on the orientation and distance with respect to the orbital.

13. The spin Hamiltonian and transition energy including the chemical shift $\sigma_i$ of spin-i is:

$$\hat{\mathcal{H}}_i = -\gamma_n \hbar \hat{I}_{z,i} (1 - \sigma_i) B_o \qquad E_i = -\gamma_n \hbar m_{I,i} (1 - \sigma_i) B_o \qquad \Delta E_i = h\nu_i = \gamma_n \hbar (1 - \sigma_i) B_o$$

The Hamiltonian and corresponding energy levels converted into frequency are:

$$\frac{\hat{\mathcal{H}}_i}{h} = -\nu_i \hat{I}_{z,i} \qquad \frac{E_i}{h} = -\nu_i m_{I,i} \qquad \text{with} \qquad \nu_i = \frac{\gamma_n}{2\pi}(1 - \sigma_i) B_o$$

14. The chemical shift expressed as $\sigma_i$ and $\delta_i$ is: $\delta_i = \dfrac{\sigma_{ref} - \sigma_i}{1 - \sigma_{ref}} 10^6 \text{ ppm} \cong (\sigma_{ref} - \sigma_i)\, 10^6 \text{ ppm}$

15. Chemically equivalent nuclei have the same chemical shift. Chemical equivalence results from free bond rotation that averages the chemical environments of the equivalent protons and from molecular symmetry (mirror planes or axes of rotation).

16. Magnetically equivalent nuclei have the same chemical shift and the same coupling constants to each equivalent neighbor. Magnetically equivalent nuclei couple, but the effects of the coupling have no effect on the spectrum.

17. Spin-spin splitting is the interaction of spins in a given resonance with neighboring spins. The strength is given by the spin-spin coupling constant, J, usually in Hz.

18. The spin-spin multiplicity of a resonance with n-equivalent neighbors is $2\,\mathbf{I} + 1 = n + 1$.

19. Equivalent neighbors give the minimum number of lines in a multiplet. All inequivalent neighbors give the maximum number of lines, $2^n$.

20. The spin Hamiltonian for nuclei A and B is: $\dfrac{\hat{\mathcal{H}}}{h} = -\nu_A \hat{I}_{zA} - \nu_B \hat{I}_{zB} + J_{AB} \vec{I}_A \cdot \vec{I}_B$

If $|\nu_A - \nu_B| >> |J_{AB}|$ the first-order approximation is valid: $\dfrac{\hat{\mathcal{H}}}{h} \cong -\nu_A \hat{I}_{zA} - \nu_B \hat{I}_{zB} + J_{AB} \hat{I}_{zA} \hat{I}_{zB}$

21. Magnetically equivalent nuclei don't split because levels of the same symmetry shift equally.

22. In Fermi-contact, spin-spin interactions are "through-bond" interactions mediated by interactions of the nuclei with the electrons in the intervening bonds.

23. For positive J ($^1$J and $^3$J) the low energy state of the coupled nuclei is spin-paired (↑↓). For negative J ($^2$J - germinal) the low energy state of the coupled nuclei is spin-parallel (↑↑).

24. Spin-spin coupling is a function of dihedral angle. The Karplus relationship gives the vicinal coupling between protons attached to $sp^3$ C-atoms with dihedral angle $\phi$ as approximately:

$^3J_{HH} = 8.5\cos^2\phi - 0.28$ for $0° \le \phi \le 90°$ and $^3J_{HH} = 9.5\cos^2\phi - 0.28$ for $90° \le \phi \le 180°$

25. Proton decoupled $^{13}$C spectra are acquired with weak intensity continuous irradiation at the proton $\nu_o$, which causes rapid spin-flips of the protons that average $J_{HC}$-coupling to zero.

26. Spin-Spin multiplets appear narrower at high field with the spectrum plotted in ppm.

27. Chemical shifts are a tensor interaction, which correspondingly depend on the orientation of the molecule in the applied magnetic field. The isotropic shift is $\frac{1}{3}\,\mathrm{tr}(\underset{\approx}{\sigma}) = \frac{1}{3}(\sigma_{xx} + \sigma_{yy} + \sigma_{zz})$.

28. Gauge invariant atomic orbital, GIAO, chemical shift calculations mix excited state character with the ground state to approximate the electronic distribution in the applied magnetic field.

29. The Bloch equation is a classical description of the behavior of the magnetization:

$$\frac{d\vec{M}}{dt} = \gamma_n (\vec{M} \times \vec{B}) \qquad \text{(no spin-relaxation)}$$

where $\vec{B}$ is the total magnetic field, which includes the applied field and the radiofrequency field.

30. The net magnetization precesses at the Larmor frequency about the applied field. Application of rf-irradiation adds concurrent precession about the rotating rf-field direction.

31. In the rotating frame, the net magnetization appears stationary in the absence of rf-irradiation. An applied rf-field at the Larmor frequency appears stationary in the x-y plane in the rotating frame. Application of rf-irradiation gives precession about the rf-field direction.

32. A 90° rf-pulse ($\pi/2$ pulse) flips the net magnetization into the x-y plane giving the maximum FID. A 180° pulse ($\pi$ pulse) flips the net magnetization to the –z-axis giving no signal.

33. Precession of the component of the net magnetization in the x-y plane gives the free induction decay, FID. The Fourier transform of the FID gives the spectrum.

34. Spin-lattice relaxation, $T_1$, returns the populations of the spin states to equilibrium, conserving energy by energy exchange with the lattice (the surroundings).

35. Spin relaxation is a first-order kinetic process, with $M_z$ the magnetization at time t and $M_o$ the equilibrium magnetization:

$$\frac{dM_z}{dt} = -\frac{1}{T_1}(M_z - M_o) \qquad \text{giving exponential growth} \qquad M_z = M_o(1 - e^{-t/T_1})$$

36. Spin-spin relaxation, $T_2$, progresses through energy conserving mutual spin flips that shorten the life time of the spin states. Shortened lifetime gives Heisenberg broadening, intrinsic lifetime broadening, of spin transitions with full-width-at-half-height: $\Delta\nu_{½} = {}^1/_{\pi T_2}$.

37. Intrinsic lifetime broadening and applied field inhomogeneity, $\Delta\nu^*$, give the effective spin-spin relaxation time, $T_2'$:

$$\frac{1}{\pi T_2'} = \frac{1}{\pi T_2} + \Delta\nu^*$$

37. In non-viscous solution, a transition at $\nu_A$ is Lorentzian: $g(\nu) = \dfrac{2T_2'}{1 + 4\pi^2 T_2'^2 (\nu - \nu_A)^2}$

38. Relaxation is caused by fluctuating magnetic fields in the sample. The most effective fluctuations match the frequency of the transition.

39. One source of fluctuating magnetic fields that drive relaxation are magnetic dipole-dipole interactions, with $r_{ij}$ the distance between the spins and θ the angle between the internuclear vector and the applied magnetic field. In solution:

$$V_{ij} = \frac{A}{r_{ij}^3}(1 - 3\cos^2\theta) \qquad \text{for } {}^1H - {}^1H: \quad A = \gamma_n^2\hbar^2$$

40. The fluctuating magnetic fields caused by the tumbling of large molecules give long correlation times and change too slowly to be efficient at relaxation at the transition frequency. Small molecules tumble too rapidly giving short correlation times causing fluctuating magnetic fields with frequency components that are too high to cause efficient relaxation.

41. Diffusion, molecular reorientation, and vibrations act independently and are characterized by different correlations times. Some motions are too slow, some are too fast, but if one or a few are at the right frequency the relaxation will be efficient leading to short $T_1$.

42. The biggest effect on relaxation is the number of nearby protons.

43. *Fluctuation Dissipation theorem*: the time evolution of a non-equilibrium system is driven by fluctuations that the system experiences at equilibrium.

44. A correlation function compares the values of a coordinate at times t and t + τ averaged over a series of measurements: $C(\tau) = \langle \overline{f(t+\tau)f(t)} \rangle$. The overbar is a time average from t = 0 to ∞. The "<" and ">"symbolize the ensemble average; an ensemble is a group of identical systems.

45. Correlation functions often decay exponentially with time: $C(\tau) = \overline{f(t)^2}\, e^{-\tau/\tau_c}$, where $\overline{f(t)^2} = C(0)$ is the mean square average of the fluctuating coordinate and $\tau_c$ is the correlation time.

46. *Wiener-Khintchine theorem*: The spectral density is the amplitude of fluctuations at frequency ν, which is given by the Fourier transform of the correlation function:

$$J(\nu) = 2\int_0^\infty C(\tau)\, e^{-i\,2\pi\nu t}\, d\tau$$

47. The spectral density of an exponential correlation function is a Lorentzian based on $\tau_c$:

$$J(\nu) = 2\int_0^\infty \overline{f(t)^2}\, e^{-\tau/\tau_c}\, e^{-i\,2\pi\nu t}\, d\tau = \overline{f(t)^2}\left(\frac{2\tau_c}{1 + 4\pi^2\nu^2\tau_c^2}\right)$$

48. The maximum spectral density and minimum $T_1$ result with correlation time $\tau_c = 1/2\pi\nu_o$.

49. For a proton at frequency $\nu_o$, $1/T_1$ is the product of average squared magnitude of the fluctuating magnetic field (e.g. from dipole-dipole interactions) and the spectral density:

$$\frac{1}{T_1} = \frac{\gamma_n^2}{\hbar^2}\overline{B_x(t)^2 + B_y(t)^2}\left(\frac{\tau_c}{1 + 4\pi^2\nu_o^2\tau_c^2}\right)$$

50. Inversion-recovery determines $T_1$-relaxation using a 180° -τ - 90° pulse sequence giving:

$$\ln(M_o - M_z) = \ln(2M_o) - \tau/T_1$$

51. Transitions are broadened by chemical exchange if the nucleus experiences environments having different chemical shifts, $\Delta\nu_o$, and the rate of exchange is roughly $k \cong \pi\Delta\nu_o/\sqrt{2}$.

52. Given the line width with slow exchange $(\Delta\nu_A)^\circ_{1/2}$ and the line width with intermediate exchange, $(\Delta\nu_A)^e_{1/2}$, the exchange rate constant is: $k \cong \pi\,[(\Delta\nu_A)^e_{1/2} - (\Delta\nu_A)^\circ_{1/2}]/\sqrt{2}$

52. The peak separation, $\Delta\nu_e$, with intermediate exchange gives: $k \cong \pi\,[\Delta\nu_o^2 - \Delta\nu_e^2]^{1/2}/\sqrt{2}$

53. The exchanging transitions coalesce at exchange rate: $k \cong \pi\Delta\nu_o/\sqrt{2}$.

54. If exchange contributes to the width but is faster than the coalescence rate, $\tau << 1/\Delta\nu_o$, then:

$$k \cong \frac{\pi \Delta \nu_o^2}{2} \frac{1}{[(\Delta \nu_{½})^e - (\Delta \nu_A)^\circ_{½}]}$$

55. The projection of the electron spin magnetic moment along the applied field, $\mu_z$, is quantized:

$$\mu_z = \gamma_e \hbar m_s \qquad \mu_z = g_e \mu_B m_s \qquad \text{(isolated electron)}$$

where $\gamma_e$ is the magnetogyric ratio of the electron, $g_e = 2.0023$ is the isolated electron g-factor, and the Bohr magneton is defined as:

$$\mu_B = \frac{-e\hbar}{2 m_e}$$

56. Including chemical shifts, the transition energy is $\Delta E = g \mu_B B_o$ with $g \cong 2.0$. The chemical shift changes the g-factor.

57. ESR spectra occur in the microwave and mm-wave regions. X-band is 9.75 GHz with $B_o$ = 0.35 T and a waveguide dimension of 30 mm.

58. The signal-to-noise ratio of cw-ESR is enhanced using magnetic field modulation, which produces a derivative line shape.

59. A spin-spin splitting multiplet in ESR is called hyperfine structure, with hyperfine constant *a*.

60. Zero-field splitting is the energy difference between the $m_s = \pm 1$ and the $m_s = 0$ state for triplet states interacting through magnetic dipole-dipole coupling between the two electrons.

61. Depending on the zero-field splitting, a triplet state can give three ESR transitions at widely different applied magnetic field strengths.

62. Irradiation by a strong rf-field creates a coherent superposition of states. Coherence results when the phases of the individual spin moments synchronize: the time dependent wave functions of the spins, $\Psi(t) = e^{-i(2\pi\nu_o t + \eta)}$, have a narrow distribution of phase angles, $\eta$.

63. The fluctuation dissipation theorem relates microscopic, quantum mechanical processes and macroscopically observable behavior. Dynamic processes, in the absence of driving forces such as applied electromagnetic fields, evolve by isoenergetic transfers of energy to fluctuations in the surroundings. The important motional frequencies are those that are matched to the frequency of the transition. Systems relax to equilibrium using the same fluctuations that exist in and maintain the system at equilibrium.

## Literature Cited


1. S. Greenblatt, *The Swerve: How the World Became Modern*, W. W. Norton, New York, NY, 2011, pp. 188. Also Titus Lucretius Carus, *De Rerum Natura* (translated as "On the Nature of Things" or "On the Nature of the Universe"), trans. M. F. Smith, Hackett Press, Indianapolis, IN, 2001, pp. 40-41: passages 1.1024-28 and 2.218-20.
2. R. K. Harris, *Encyclopedia of Nuclear Magnetic Resonance*, D. M. Granty and R. K. Harris, (eds.), vol. 5, Wiley, Chichester, UK, 1996.
3. Halliday, R. Resnick, J. Walker, *Fundamentals of Physics, 6th Ed.*, Wiley, New York, NY, 2001, Ch. 29.
4. D. H. Williams, I. Fleming, *Spectroscopic Methods in Organic Chemistry. 4th Ed.*, McGraw Hill, London, UK, 1987. Tables 3.13, 3.17
5. D. L. Pavia, G. M. Lampman, G. S. Kriz, Jr., *Introduction to Spectroscopy: A Guide for Students of Organic Chemistry, 3rd. Ed.,* W. B. Saunders, Philadelphia, PA, 2001. Figure 4.1, p. 168.

6. J. D. Roberts, *An Introduction to the Analysis of Spin-Spin Splitting in High-Resolution Nuclear Magnetic Resonance Spectra*, W. A. Benjamin, New York, NY, 1962. Ch. 2, pp. 25-60.

7. A. Carrington, A. D. McLachlan, *Introduction to Magnetic Resonance*, Harper & Row, New York, NY, 1967. pp. 182-197. pp. 80-85

8. K. Wüthrich, *NMR of Proteins and Nucleic Acids*, Wiley, New York, NY, 1986.

9. J. D. Roberts, *An Introduction to the Analysis of Spin-Spin Splitting in High-Resolution Nuclear Magnetic Resonance Spectra*, W. A. Benjamin, New York, NY, 1962. Ch. 2, pp. 90-101.

10. "ChemDraw, 15.1," Perkin Elmer Corp., Shelton, Connecticut, 2016; "ACD/Spectrus Processor," Advanced Chemistry Development, Inc., Toronto, Canada, 2016.

11. P. S. Beauchamp, R. Marquez, "A General Approach for Calculating Proton Chemical Shifts for Methyl, Methylene, and Methine Protons When There Are One or More Substituents within Three Carbons," *J. Chem. Ed*., **1997**, *74(12)*, 1483-1485, as implemented in "$^{1}$H Chemical Shift Prediction," "H1pred.html" applet on the text book Web site.

12. B. Shoulders, S. C. Welch, "A Very Brief, Rapid, Simple, and Unified Method for Estimating Carbon-13 NMR Chemical Shifts," *J. Chem. Ed.*, **1987**, *64(11)*, 915-918: as implemented in "$^{13}$C Chemical Shift Prediction," "C13chemshift.html" applet on the text book Web site.

13. R. Ditchfield, "Self-consistent perturbation theory of diamagnetism: I. A gauge-invariant LCAO method for N.M.R. chemical shifts," *Mol. Phys.*, **1974**, *27*, 789-807.

14. T. D. W. Claridge, *High Resolution NMR Techniques in Organic Chemistry*, 2nd Ed., Elsevier, Oxford, UK, 2009. Chapter 2

15. E. D. Becker, *High Resolution NMR: Theory and Chemical Applications, 2nd. Ed.*, Academic Press, New York, NY, 1980. Ch. 8

16. J. A. Pople, W. G. Schneider, H. J. Bernstein, *High-resolution Nuclear Magnetic Resonance*, McGraw-Hill, New York, NY, 1959. Ch. 3.5 p. 31, Ch. 9, pp.199-204.

17. E. Breitmaier, W. Voelter, *Carbon 13 NMR Spectroscopy,3rd Ed.,* VCH, Weinheim, DE, 1987. Sec. 3.3.2, pp. 166-181.

18. A. Carrington, A. D. McLachlan, *Introduction to Magnetic Resonance*, Harper & Row, New York, NY, 1967. pp. 182-194.

19. N. Davidson, Statistical Mechanics, McGraw-Hill, New York, NY, 1962. pp. 290-295.

20. J. M. Deutch, I. Oppenheim, "Time Correlation Functions in Nuclear Magnetic Resonance," J. M. Waugh, Ed., *Advances in Magnetic Resonance*, Vol. 3,

21. F. Reif, *Fundamentals of Statistical and Thermal Physics*, McGraw-Hill, New York, NY, 1965, Chapter 15. Reprinted by Waveland Press, Long Grove, IL, 2009.

22. E. D. Becker, *High Resolution NMR: Theory and Chemical Applications, 2nd. Ed.*, Academic Press, New York, NY, 1980. Figure 10.7, p. 234.

23. L. M. Jackman, "Rotation About Partial Double Bonds in Organic Molecules," in *Dynamic Nuclear Magnetic Resonance Spectroscopy*, L. M. Jackman, F. A. Cotton, Eds., Academic Press, New York, NY, 1975. Chapt. 7, pp. 203-252.

24. H. A. Pople, W. G. Schneider, H. J. Bernstein, *High Resolution Nuclear Magnetic Resonance*, McGraw-Hill, New York, 1967. Chaps. 3 and 10, 35-37, 218-224.

25. A. Carrington, A. D. McLachlan, *Introduction to Magnetic Resonance*, Harper and Row, New York, NY, 1967. pp. 204-210.

26. E. S. Johnson Jr., "Chemical Rate Processes and Magnetic Resonance," in *Advances in Magnetic Resonance*, J. S. Waugh, Ed., Academic Press, New York, **1956**, Volume 1, Chapter 2, pp. 33-102.

27. W. T. Dixon, R. O. C. Norman, "Electron spin resonance studies of oxidation. Part I. Alcohols," *J. Chem. Soc.*, **1963**, 3119-3124. Spectrum simulated using $a(CH_3)$ = 22.0 G and $a$(CH) = 15 G.

28. M. Adams, M. S. Blois, R. H. Sands, "Paramagnetic Resonance Spectra of Some Semiquinone Free Radicals ," *J. Chem. Phys*., **1958**, *28(5)*, 774-776.

29. G. P. Laroff, R. W. Fessenden, R. H. Schuler, "The Electron Spin Resonance Spectra of Radical Intermediates in the Oxidation of Ascorbic Acid and Related Substances," *J. Amer. Chem. Soc*., **1972**, *94(26)*, 9062-9073.

30. R. S. Drago, *Physical Methods for Chemists, 2nd. Ed*., Saunders, Ft. Worth, TX, 1992. Chs. 9, 13.

31. S. P. McGlynn, T. Azumi, M. Kinoshita, *Molecular Spectroscopy of the Triplet State*, Prentice-Hall, Englewood Cliffs, NJ, 1969. pp. 46-51, 329-348.

## Further Reading

*Organic and Biochemical Spectroscopic Identification:*

Timothy D. W. Claridge, *High-Resolution NMR Techniques in Organic Chemistry*, Pergamon, Oxford, 2009.

D. L. Pavia, G. M. Lampman, G. S. Kriz, Jr., *Introduction to Spectroscopy: A Guide for Students of Organic Chemistry, 3rd. Ed.,* W. B. Saunders, Philadelphia, PA, 2001.

D. H. Williams, I. Fleming, *Spectroscopic Methods in Organic Chemistry. 4th Ed.*, McGraw Hill, London, UK, 1987.

E. Breitmaier, W. Voelter, *Carbon 13 NMR Spectroscopy*, *3rd. Ed.*, VCH, New York, NY, 1987.

K. Wüthrich, *NMR of Proteins and Nucleic Acids,* Wiley, New York, NY, 1986.

*Magnetic Resonance Relaxation*:

A. Carrington, A. D. McLachlan, *Introduction to Magnetic Resonance*, Harper & Row, New York, NY, 1967. Chapter 11: pp. 176-194; Appendices E-G: pp. 252-259.

N. Davidson, Statistical Mechanics, McGraw-Hill, New York, NY, 1962. Chapter 14: pp. 265-295.

*ESR/EPR*:

A. Carrington, A. D. McLachlan, *Introduction to Magnetic Resonance*, Harper & Row, New York, NY, 1967. Chapters 6-11.

Weil and Bolton, *Electron Spin Resonance; Elementary Theory and Practical Applications, 2nd Ed.* 2007.

R. S. Drago, *Physical Methods for Chemists, 2nd. Ed*., Saunders, Ft. Worth, TX, 1992. Chapters. 9, 10, 13.

## Chapter 29: Magnetic Resonance Problems.

1. Deuterium NMR, $^{2}H$, is quite common. High field instruments have a channel for protons, one or two channels for $^{13}C$ or other nucleus, and an additional channel for deuterium. The deuterium channel is used for acquiring the resonance frequency of a peak from the deuterated solvent and using that frequency in maintaining a constant magnetic field. This process is called field-locking. The deuterium channel is also used for magnetic field shimming, which adjusts the uniformity of the magnetic field to achieve the narrowest, and hence most intense, transitions. Shimming enhances the resolution of the spectrum. Draw the energy level diagram for deuterium

in an applied magnetic field and calculate the resonance frequency of protons and deuterium at a magnetic field of 7.046 T.

2. The spin quantum number of $^{35}Cl$ is I = 3/2. For a single $^{35}Cl$, assuming no spin-spin coupling, how many transitions are observed for $^{35}Cl$?

3. A spectral width of at least 10 ppm is required to cover the $^{1}H$-NMR spectra of many compounds. (a). Calculate the spectral width in Hz if the resonance frequency of protons is 60 MHz and if the resonance frequency is 500 MHz. (b). The resonance frequency of $^{13}C$ is ¼ the resonance frequency of protons at the same field strength. A spectral width of 160 ppm is required to cover the $^{13}C$-spectra of many compounds. Calculate the spectral width in Hz if the resonance frequency of $^{13}C$ is 75 MHz (300 MHz for protons) and if the resonance frequency is 125 MHz (500 MHz for protons).

4. In a given instrument, the NMR resonance frequency of a proton in a methyl group is centered at 399,095,832 Hz. The resonance frequency of TMS at the same field strength is 399,095,432 Hz. (a). Calculate the chemical shift of the methyl group. (b). The methyl group is split into a triplet by an adjacent methylene with a spin-spin coupling constant of 7.0 Hz. Calculate the spin-spin splitting in ppm assuming the same resonance frequency as part (a).

5. The NMR chemical shift of a methyl group is centered at 1.240 ppm at a 60 MHz resonance frequency and the spin-spin splitting constant with an adjacent methylene is 7.0 Hz. (a). Calculate the multiplet peak positions in ppm assuming TMS at 60 MHz. (b). Calculate the multiplet peak positions in ppm with TMS at 500 MHz. (c). Describe the difference in appearance between the spectrum at 60 MHz and 500 MHz.

6. (a). Derive Eq. 29.1.7 for the population difference of the spins states of a spin-½ nucleus. (b). Determine the number of spins in the upper and the lower spin states for protons at 400 MHz at 298.2 K. Assume $10^6$ total spins. (c). Table-top, permanent magnet NMR spectrometers commonly operate at 60 MHz. Determine the number of spins in the upper and the lower spin states for protons at 60.0 MHz at 298.2 K. Assume $10^6$ total spins.

7. (a). Give the peak intensities in a sextet that result from coupling to equivalent spins. (b). Give the peak intensities in a doublet of triplets. (Don't worry about the transition frequencies.) (c). How many spins are coupled to the observed resonance if the multiplet is a doublet of quartets? Assume each quartet has intensity ratios: 1:3:3:1.

8. Show the spin-spin splitting pattern for nucleus A in the following molecular fragment. Assume $J_{AB}$ = 10 Hz and $J_{AC}$ = 15 Hz. Indicate the relative intensities. Assume first-order behavior.

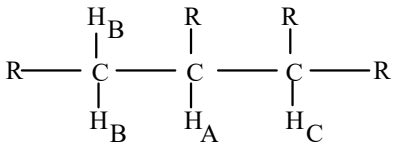

9. Show the spin-spin splitting pattern for nucleus A in the following molecular fragment with $J_{AB}$ = 5 Hz and $J_{AC}$ = 10 Hz. Indicate the relative intensities. Assume first-order behavior.

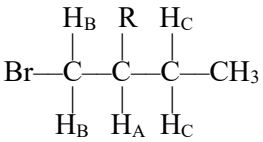


10. In an isolated ethyl group, $-CH_2CH_3$, there is no spin-spin coupling through the attachment point. Examples include ethyl alcohol, ethylbromide, diethylether, and ethylacetate. An isolated ethyl gives characteristic spin-spin splitting patterns of a quartet and triplet, in the order $-CH_2CH_3$. Give the characteristic splitting patterns of isolated *n*-propyl, *iso*-propyl, *n*-butyl, *sec*-butyl, *iso*-butyl, *tert*-butyl, and *iso*-amyl. Assume the vicinal spin-spin coupling constants are approximately equal, with no longer range coupling, and free rotation about the bonds. (Note: *iso*-propyl = 1-methylethyl, *sec*-butyl = 1-methylpropyl, *iso*-butyl = 2-methylpropyl, *tert*-butyl = 1,1-dimethylethane, *iso*-amyl = 3-methylbutyl )

11. The geminal coupling constant between inequivalent methylene protons on $sp^3$-hybridized carbons is often large, ~12 Hz. (a). Use the Karplus relationship to estimate the $J_{AC}$ and $J_{AD}$ spin-spin coupling constants of the labeled protons in camphor, below. (b). Sketch the expected multiplet pattern of proton-A based on your estimated geminal and vicinal coupling constants. Note that proton-B will also give a similar multiplet that will likely overlap with the multiplet of proton-A. We don't consider the proton-B multiplet in this problem for simplicity. (In practice the appearance of the spectrum is sensitive to the exact values of all the parameters. The purpose of this exercise is to give just one reasonable prediction of the appearance of the spectrum.)

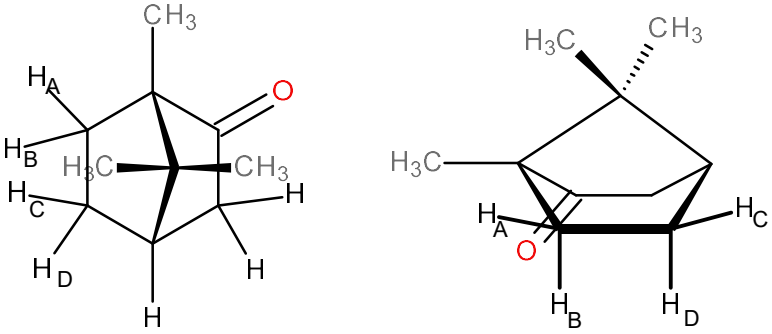


Dihedral angles: $\phi_{AC} = 0°$ and $\phi_{AD} = 120°$

12. Determine the structure of the following compound. The spectrum was acquired at 200 MHz, so the spin-spin multiplets are easy to see. The degree of unsaturation is a useful starting point if the formula of the compound is known. The degree of unsaturation is equal to the sum of the number of double bonds and rings: dbr = (2c – h + 2 + n – x)/2, where c is the number of carbons, h the number of hydrogens, n the number of nitrogens, and x the number of monovalent atoms, which includes F, Cl, and I.

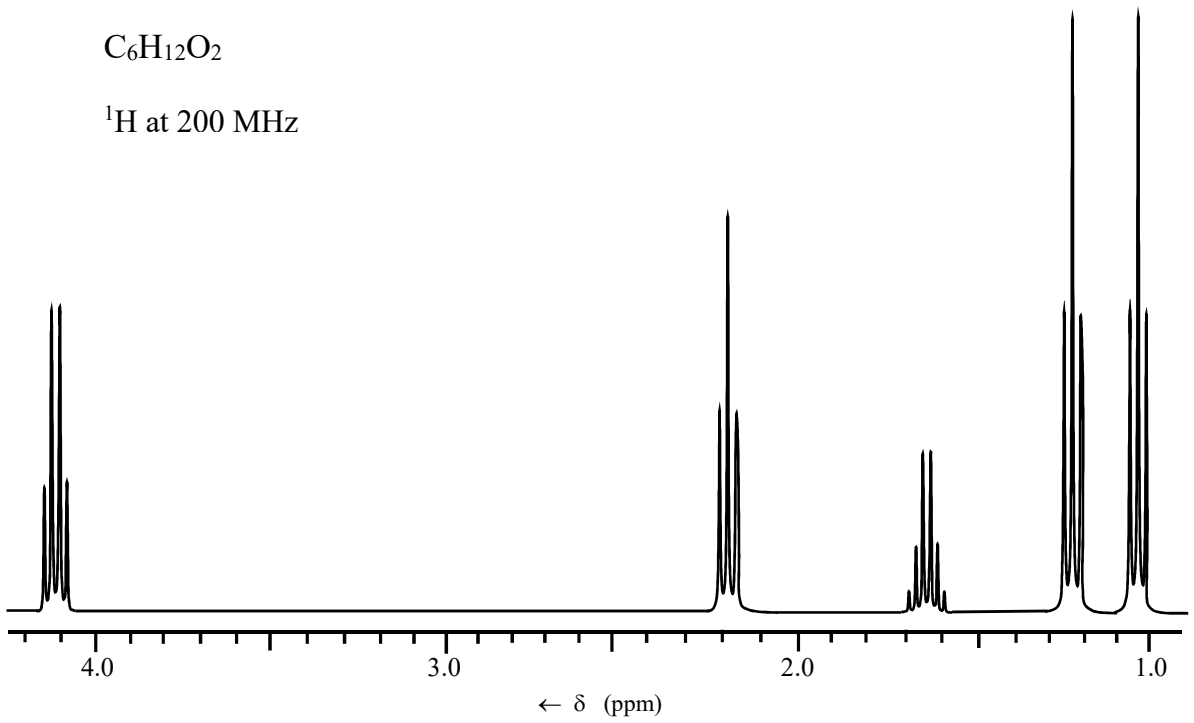


13. Determine the structure of the following compound. The spectrum was acquired at 300 MHz. The down field resonance at 8.01 ppm is a singlet. Expanded spectra of the multiplets are shown below the full spectrum. The $^{13}C$ spectrum has five peaks with the most downfield at 161.2 ppm. [Hint: see the comments about the degree of unsaturation in the previous problem.]

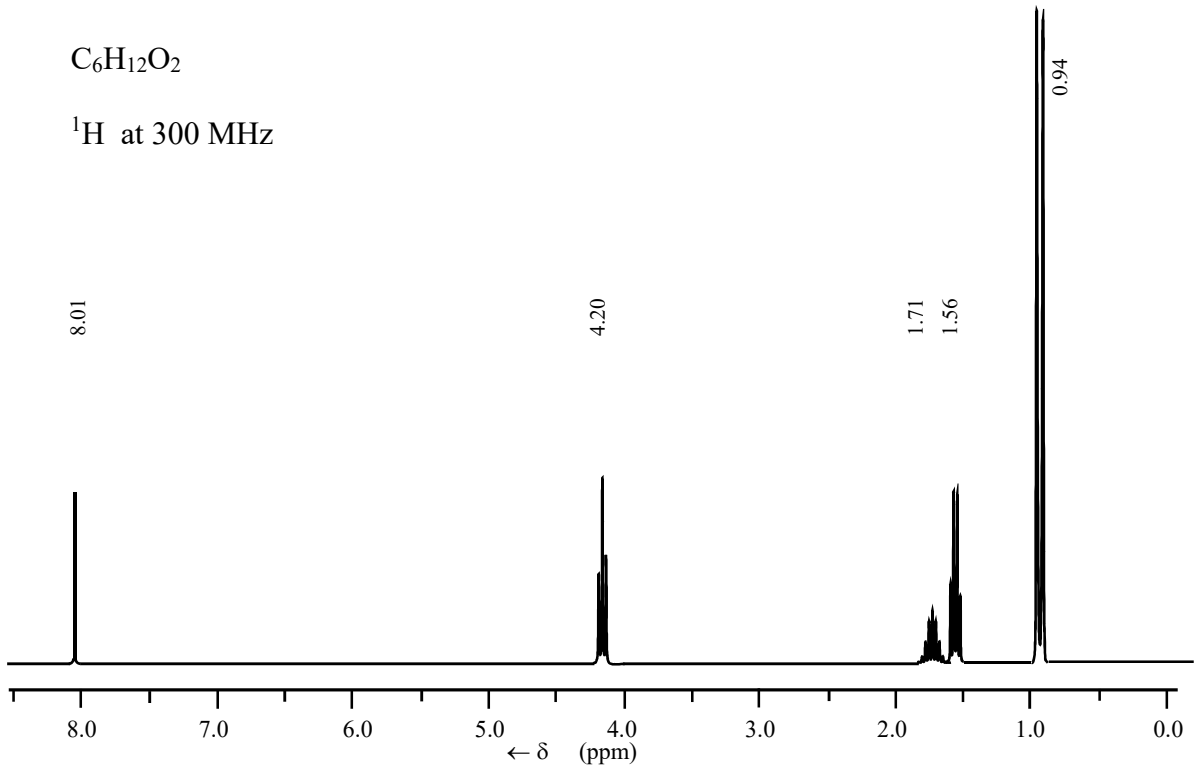

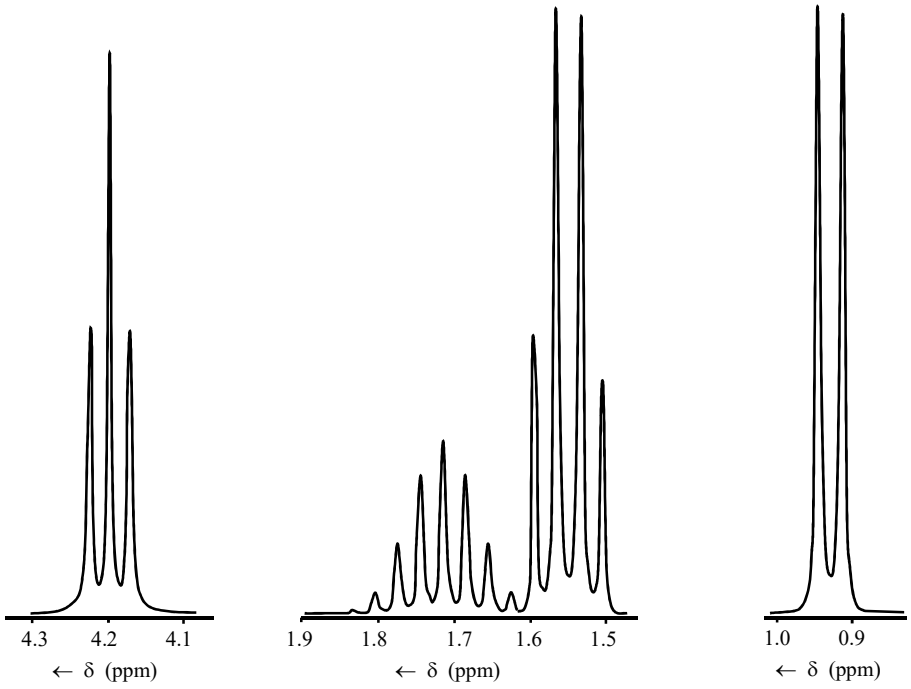


14. Determine the number of proton and carbon resonances that are observed for the following compounds. Determine the corresponding multiplicities of the spin-spin coupling multiplets.

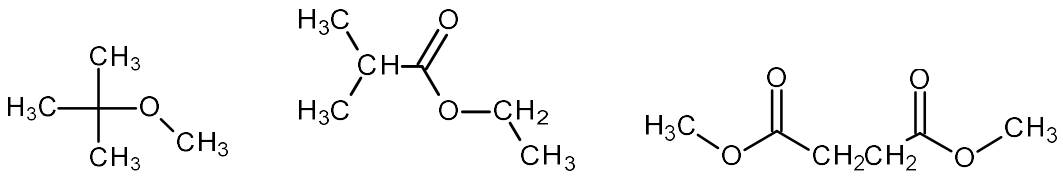

15. *Equivalent Spins Don't Split*: Derive the energy levels and transition frequencies of a system with two equivalent protons. This problem fills in the details of the energy level diagram in Figure 29.1.13. Because the chemical shift differences are not greater than the spin-spin coupling constant, the full spin-spin coupling Hamiltonian must be used for this problem:

$$\hat{\mathcal{H}} = -\nu_A \hat{I}_{zA} - \nu_B \hat{I}_{zB} + J_{AB} \vec{I}_A \cdot \vec{I}_B \qquad (29.1.13)$$

where $\vec{I}_A \cdot \vec{I}_B = \hat{I}_{xA} \hat{I}_{xB} + \hat{I}_{yA} \hat{I}_{yB} + \hat{I}_{zA} \hat{I}_{zB}$.

The allowable spin states for two equivalent spins are the symmetric combinations: $\alpha\alpha$, $1/\sqrt{2}\,(\alpha\beta + \beta\alpha)$, and $\beta\beta$, while the fourth spin state is antisymmetric: $1/\sqrt{2}\,(\alpha\beta - \beta\alpha)$. In Ch. 24.7 we found the relationship between the angular momentum raising and lowering operators and the x and y-components of the angular momentum, Eq. 24.7.18. Expressed explicitly in terms of nuclear angular momentum operators, Eqs. 24.7.18 are recast as:

$$\hat{I}^- = \hat{I}_x - i\,\hat{I}_y \quad \text{(lowering)} \qquad \text{and} \qquad \hat{I}^+ = \hat{I}_x + i\,\hat{I}_y \quad \text{(raising)} \qquad (24.7.18)$$

which have the following effects on the spin wave functions:

$$\hat{I}^+\,\alpha = 0 \qquad \hat{I}^+\,\beta = \alpha$$
$$\hat{I}^-\,\alpha = \beta \qquad \hat{I}^+\,\beta = 0$$

Solving for $\hat{I}_x$ and $\hat{I}_y$ gives for both A and B spins:

$$\hat{I}_x = \tfrac{1}{2}(\hat{I}^+ + \hat{I}^-) \qquad \text{and} \qquad \hat{I}_y = \tfrac{1}{2}\,i(\hat{I}^+ - \hat{I}^-)$$

In a subsequent problem we will prove that the spin-spin interaction can be written as:

$$J_{AB}\,\vec{I}_A\cdot\vec{I}_B = J_{AB}\,[\,\hat{I}_{zA}\,\hat{I}_{zB} + \tfrac{1}{2}(\hat{I}_A^+\,\hat{I}_B^- + \hat{I}_A^-\,\hat{I}_B^+)]$$

(a). For simplicity of notation set $J = J_{AB}$. Show that:

$$J\,\vec{I}_A\cdot\vec{I}_B\,\alpha\alpha = {}^{J}/_{4}\,\alpha\alpha$$
$$J\,\vec{I}_A\cdot\vec{I}_B\,\alpha\beta = -{}^{J}/_{4}\,\alpha\beta + {}^{J}/_{2}\,\beta\alpha$$
$$J\,\vec{I}_A\cdot\vec{I}_B\,\beta\alpha = -{}^{J}/_{4}\,\beta\alpha + {}^{J}/_{2}\,\alpha\beta$$
$$J\,\vec{I}_A\cdot\vec{I}_B\,\beta\beta = {}^{J}/_{4}\,\beta\beta$$

(b). Combine these results to show that:

$$J\,\vec{I}_A\cdot\vec{I}_B\,[{}^{1}/\sqrt{2}(\alpha\beta+\beta\alpha)] = {}^{J}/_{4}\,[{}^{1}/\sqrt{2}\,(\alpha\beta + \beta\alpha)]$$
$$J\,\vec{I}_A\cdot\vec{I}_B\,[{}^{1}/\sqrt{2}(\alpha\beta-\beta\alpha)] = -{}^{3J}/_{4}\,[{}^{1}/\sqrt{2}\,(\alpha\beta - \beta\alpha)]$$

(c). Use these results to verify the energies of the levels shown in Figure 29.1.13.

16. Using the relationships given in the introduction to the previous problem to prove that the spin-spin interaction can be written as:

$$J_{AB}\,\vec{I}_A\cdot\vec{I}_B = J_{AB}\,[\,\hat{I}_{zA}\,\hat{I}_{zB} + \tfrac{1}{2}(\hat{I}_A^+\,\hat{I}_B^- + \hat{I}_A^-\,\hat{I}_B^+)]$$

17. Consider the spin-spin coupling of two inequivalent spins. If the difference in chemical shift is much larger than the spin-spin coupling constant then Eq. 29.1.14 is a good approximation. As seen in Figure 29.1.13, the wave functions αα, αβ, βα, and ββ are then good eigenfunctions of the approximate Hamiltonian, Eq. 29.1.14. If the chemical shift difference is comparable to the spin-spin coupling constant, then the exact Hamiltonian must be used, Eq. 29.1.13. Use the results of Problem 15(b) to determine if αα, αβ, βα, and ββ are eigenfunctions of the exact Hamiltonian. If αα, αβ, βα, and ββ are eigenfunctions of the exact Hamiltonian, then they may be used to determine the energies of the final spin levels directly from the eigenvalues, as we did in Figure 29.1.13. If αα, αβ, βα, and ββ are not eigenfunctions of the exact Hamiltonian, then the exact wave functions are linear combinations of αα, αβ, βα, and ββ. The wave functions must then be determined from the secular equation that is based on the exact Hamiltonian.

18. Use the "*JD: Spin-Spin Splitting Simulation*" applet (jdplot.html) on the course Web site or companion CD to determine the spectrum of an $^1$H AB-system. An AB-system is comprised of two inequivalent spin-spin coupled protons, with the difference in chemical shifts between the

two protons comparable to the spin-spin coupling constant. Assume the two chemical shifts are 1.00 ppm and 1.20 ppm, with the resonance frequency at 60.000 MHz. Use a spin-spin coupling constant of J = 9.0 Hz. Compare the results to the first-order predictions based on the energy levels derived in Figure 29.1.11.

19. A surprising result of strong second-order effects in spin-spin splitting is that more transitions appear than expected based on first-order analysis. Consider a $^1$H $AB_2$ pattern as an example. An $AB_2$ pattern corresponds to two chemical environments, A with one proton and B with two protons, with the difference in chemical shifts between the two environments comparable to the spin-spin coupling constant. In comparison, an $AX_2$ pattern corresponds to the same proton distribution but with the difference in chemical shifts between the two environments much larger than the spin-spin coupling constant. (a). Use the "*JD: Spin-Spin Splitting Simulation*" applet (jdplot.html) on the course Web site or companion CD to determine the spectrum of an $^1$H $AX_2$-system. Assume the two chemical shifts are 3.20 ppm and 1.00 ppm, with the resonance frequency at 60.000 MHz. Use a spin-spin coupling constant of J = 9.0 Hz. Does the resulting spectrum agree with the first-order prediction? (b). Determine the spectrum of an $^1$H $AB_2$-system. Assume the two chemical shifts are 1.20 ppm and 1.00 ppm, with the resonance frequency at 60.000 MHz. Once again, use a spin-spin coupling constant of J = 9.0 Hz. Decrease the line width to 0.75 Hz to better observe the number of transitions. How many transitions are evident?

20. In pulsed NMR, the free induction decay of all the chemical shifts in the spectrum are excited by a short pulse at a single frequency. For example, the proton chemical shift range is ~5000 Hz at a resonance frequency of 400.00 MHz, while the pulse is at a single frequency of 400.000 MHz. Explain how all the chemical shifts in the spectrum can be excited by a short pulse at a single frequency. Assume the pulse length is 15.0 μs.

21. Qualitatively sketch the relative changes in the spectra obtained by Fourier transformation of the second FID as compared to the first:

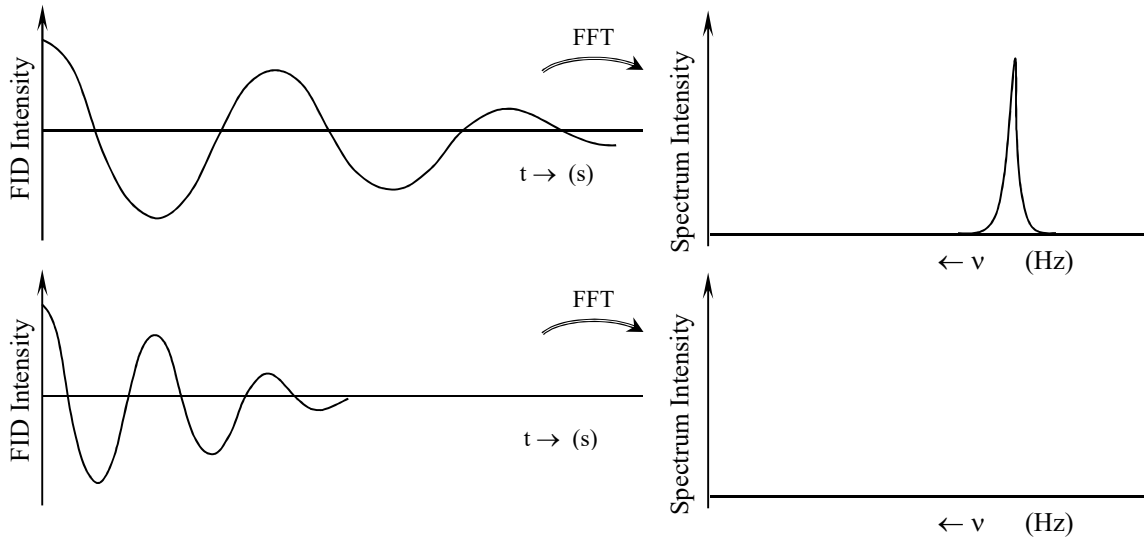

22. The inversion recovery sequence was used to determine the $^1$H spin-lattice relaxation time of the geminal-dimethyl groups of β-ionone. The data is reproduced below. Determine the $T_1$. (Don't bother to get the uncertainty using linest(), just use a linear trendline.)

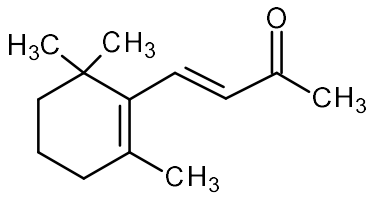


| τ (s) | 0.0625 | 0.2500 | 0.5000 | 1.000 | 2.000 | 8.000 |
|---|---|---|---|---|---|---|
| intensity | -64.8 | -32.2 | 4.43 | 47.4 | 76.9 | 84.1 |

23. Derive Eq. 29.7.3 by integrating Eq. 29.7.2.

24. Consider the following molecule with *tert*-butyl groups as the R-groups:

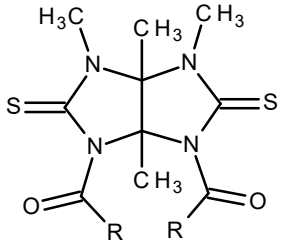


Steric interactions of the *tert*-butyl groups prevent the amide bonds from being planar with each respective ring. The N-methyl groups are not equivalent, because the amide groups are twisted out of plane.[2,3] Rotation about the amide C-N bonds exchanges the chemical environment of the N-methyl resonances. Outline the experimental and data analysis steps necessary to find the activation energy of the chemical exchange process for twisting about the amide bonds.

25. The $^1$H-NMR spectra of the N-methyl compound shown below are plotted at -94°C and -30°C at 300 MHz. The R-groups are *tert*-butyl groups, which force the amide groups to be twisted out of plane, which makes the two N-methyl groups inequivalent. The spectra are taken in deuterated methylene chloride solution. The resonances near 3.2 ppm are the N-methyl groups. The difference in chemical shift at low temperature for the N-methyl groups is 35.0 Hz. Assume that the effective $T_2'$ is 1.5 s. At -94°C, the full-width at half-height of one of the two N-methyl transitions in the exchanging doublet is 13.5 Hz. The coalescence temperature is -70.5°C. The width of the coalesced N-methyl peak at -30°C is 10.4 Hz. Calculate the activation energy for the twisting motion of the amide groups.[2,3]

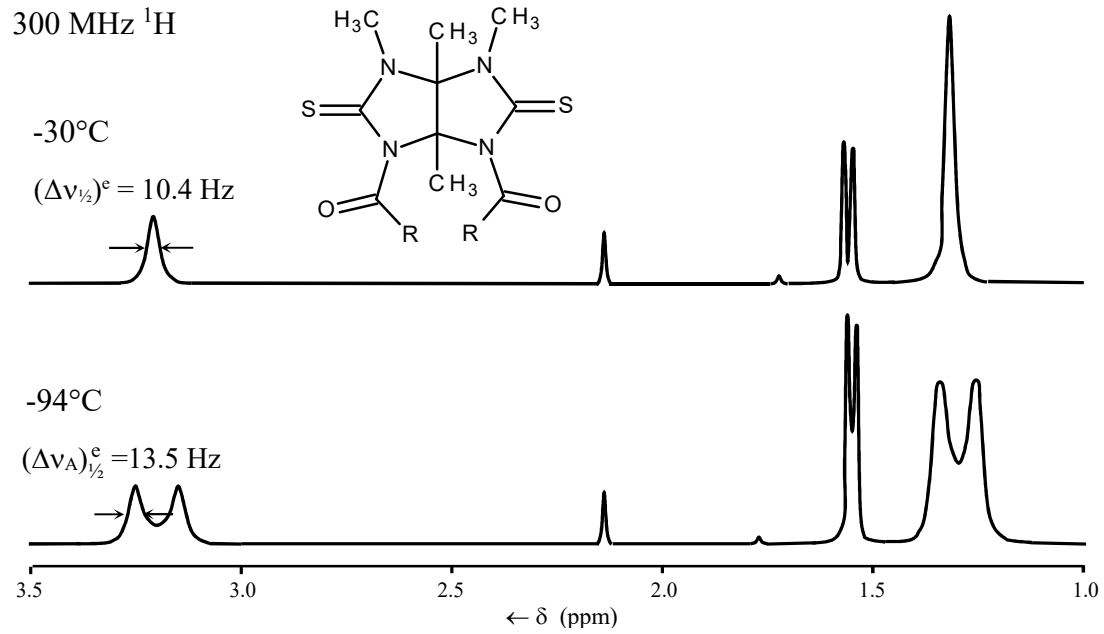


26. Create an Excel spreadsheet to do the time averages to determine the correlation function for a random signal. Generate the random signal at equal time increments, of length Δt, with varying persistence, p:

$$f(t + \Delta t) = f(t) + (1 - p)[(2*RND() - 1) - f(t)]$$

where RND() is the built-in random number generator in Excel and (2*RND() – 1) generates a random number between -1 and +1. Plot $f(t)$ and the corresponding correlation function. Hints for setting up the spreadsheet are given below. Use four different values of the persistence: p = 0, 0.2, 0.5, and 0.8. With p = 0, the signal is purely random with no correlation, $f(t + \Delta t) = (2*RND() - 1)$. Increasing p gives a signal that is increasingly slowly varying. For each value of p, generate several different plots. The results will be different in each plot; you can estimate the equivalent of the ensemble average by "averaging" the successive plots by eye. To generate each new set of random numbers, change the value in any arbitrary unused cell in the spreadsheet. Any unused cell will do, the cell chosen for generating updates shouldn't be used in the main part of the spreadsheet. From your comparison of the results for the different values of p, discuss the relationship among the persistence, the appearance of $f(t)$, and the observed approximate correlation time. You don't need to find a numerical value of the correlation time, discuss the results qualitatively.

An example spreadsheet is shown below. Only the first few rows and the final three rows are shown, to save space. Rows 2-5 and column B are input directly, that is with no formulas. The main time variable t in column B runs in 5 ns increments up to 200 ns in row 46. Seven values of the time delay, τ, are specified in row 3. The number of rows that correspond to the chosen τ value are entered in row 4. For example, 3 rows are required to give a τ delay of 15 ns.

| A1 | B | C | D | E | F | G | H | I | J |
|---|---|---|---|---|---|---|---|---|---|
| 2 | persistence= | 0.5 | | | | | | | |
| 3 | | τ = (ns) | 0 | 5 | 10 | 15 | 20 | 25 | 30 |
| 4 | | offset | 0 | 1 | 2 | 3 | 4 | 5 | 6 |
| 5 | t (ns) | f(t) | f(t+τ)f(t) | f(t+τ)f(t) | f(t+τ)f(t) | f(t+τ)f(t) | f(t+τ)f(t) | f(t+τ)f(t) | f(t+τ)f(t) |
| 6 | 0 | -0.8037 | 0.6459 | -0.0719 | -0.3803 | -0.0622 | -0.1562 | 0.2355 | 0.3560 |
| 7 | 5 | 0.0895 | 0.0080 | 0.0423 | 0.0069 | 0.0174 | -0.0262 | -0.0396 | -0.0567 |
| 8 | 10 | 0.4731 | 0.2238 | 0.0366 | 0.0919 | -0.1386 | -0.2096 | -0.2997 | -0.3480 |
| | ⋮ | | | | | | | | |
| 46 | 200 | 0.0258 | 0.0007 | | | | | | |
| 47 | | | | | | | | | |
| 48 | | average= | 0.1326 | 0.0539 | 0.0126 | 0.0180 | -0.0133 | -0.0164 | 0.0163 |

The starting random value of the signal, $f(t)$, at time zero is in cell C6: =(2*RND()-1)

The subsequent value of $f(t)$ in cell C7 is: = C6 + (1-$C$2)*((2*RND()–1)–C6)

This formula is "filled down" to fill in the values for the remaining rows in column C. The product $f(t+\tau)\,f(t)$ is created using the Excel OFFSET function. The formula in cell D6 is:

=OFFSET($C6:$C$46,D$4,0,1,1)*$C6

The offset is specified in row 4. Make sure to set up the absolute references exactly as shown. This formula is "filled right" for columns E-J and then "filled down" for all the rows up to 46. Some cells near the bottom of the table will read "0" after filling, because there is insufficient data to complete the required calculation for long τ-values. Delete the contents of these zero cells. The averages of each column are calculated in row 48 giving $\overline{f(t+\tau)\,f(t)}$. The formula in cell D48 is: =AVERAGE(D6:D46)

This cell is "filled right" for the remaining columns E-J. Construct a plot of column C versus column B to see the time-varying random signal. Construct a plot of the averages from row 48 on the vertical axis against the τ-values on the horizontal axis.

27. The benzene radical anion, $C_6H_6^-$, is produced at low temperature by reduction of benzene with an alkali metal. Predict the multiplicity of the ESR transition of the benzene radical anion and the corresponding transition intensities of the components of the multiplet.

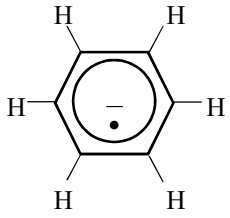


28. Sketch by hand the ESR derivative spectrum of a doublet of doublets, shown below. (Note the positions of the maxima in the absorption spectrum as a basis for the zero-derivative points on the plot.)

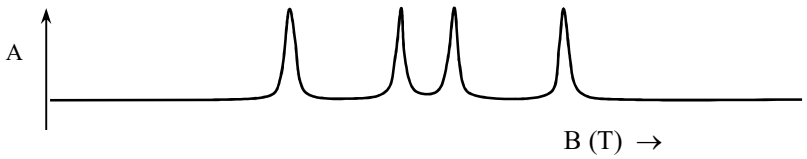


29. The π-systems of the aromatic radicals are extensively delocalized. If the nuclei of the aromatic radical lie in the x-y plane, then the π-orbitals are constructed from the overlap of $2p_z$-orbitals. The hyperfine interaction, $a_H$, is then approximately proportional to the unpaired electron density in the $2p_z$-orbital at each C-H, which is denoted $\rho_\pi$:

$$a_H = Q\rho_\pi \qquad \text{(aromatic hydrocarbons)}$$

where Q is a proportionality constant derived from model compounds. The hyperfine interaction in the benzene radical anion is 0.375 mT, or 3.75 G; assuming a π-electron density of $^1/_6$ gives Q = 2.25 mT = 22.5 Gauss. The hyperfine coupling constants for the naphthalene radical anion are given below. Calculate the π-electron density on the two types of ring positions.

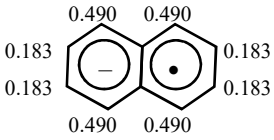


30. The hyperfine coupling constants from the ESR spectra of the radical anion of toluene are shown below. The AM1 level π-molecular orbitals for toluene as a neutral molecule are also diagrammed below. Are the hyperfine constants consistent with the π-molecular orbitals? Orbital 18 is the HOMO and orbital 19 is the LUMO. (In benzene, MO 17 and 18 are degenerate and MO 19 and 20 are degenerate.)

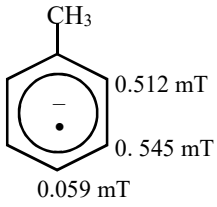


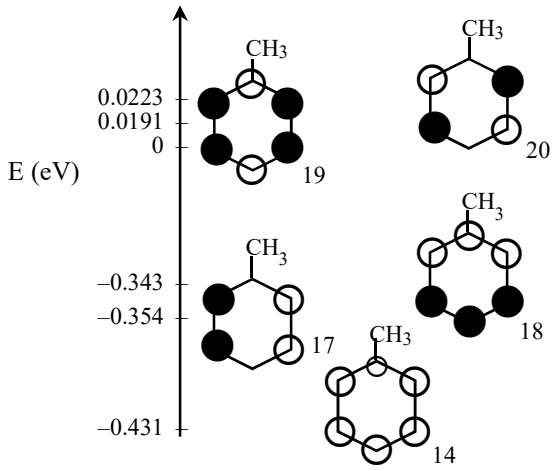


31. The ESR hyperfine coupling constants and low-lying π-molecular orbitals of the toluene anion radical are given in the previous problem. Using Spartan or Gaussian, build and geometry minimize the toluene radical anion (doublet state) at the HF 3-21G level or higher. Request the

molecular orbital coefficients and then generate the "radical density" or "spin density" surface for the toluene radical anion. Does this unpaired electron density surface agree with the hyperfine coupling constants and molecular orbitals listed in the previous problem? (Note that the π-molecular orbital energies depicted in the previous problem are for neutral toluene.)

32. Determine if the following statements are true or false. If the statement is false, describe the changes that are necessary to make the statement true, if possible. If the statement is true but too restrictive, give the more general statement.

(a). The spacing in ppm between the component transitions of a spin-spin splitting multiplet is constant with increasing field strength.

(b). In $^1$H NMR spectroscopy, for a given spin with n-coupled neighboring protons the minimum number of transitions in the multiplet is n+1 and the maximum possible number of transitions in the multiplet is $2^n$. Assume the given spin has a unique chemical shift.

(c). The differences between the exact spin-spin splitting pattern and the first-order prediction are called second-order effects. The exact spin-spin splitting pattern is based on $J_{AB}\ \vec{I}_A \cdot \vec{I}_B$ while the first-order prediction is based on $J_{AB}\ \hat{I}_{zA}\ \hat{I}_{zB}$. Second-order effects are more important at high field (e.g. 500 MHz) than at low field (e.g. 60 MHz).

(d). The spin-lattice relaxation time of a given chemical environment in a $^1$H-spectrum increases with an increase in temperature. Assume that the motion of the molecule that is most important for relaxation is faster than the resonance frequency at the starting temperature.

(e). Consider chemical exchange between two inequivalent chemical environments. The line widths decrease with an increase in temperature if the system is initially at a temperature that is below the coalescence temperature.

(f). The frequency spectrum of fluctuations in the lattice has a maximum at intermediate frequency. If that maximum frequency matches the transition frequency, relaxation is fast.

(g). In spin-lattice relaxation the energy loss of a transition from the upper state to the lower state is absorbed by isofrequency fluctuations of the motions of the lattice.

(h). The fluctuations that drive relaxation exist only in the non-equilibrium state.

(i). In spin-lattice relaxation, the fluctuations of the lattice must have an energetic coupling to the spin system. Magnetic dipole-dipole interactions of the relaxing spin with nearby spins is an example.

(j). High frequency fluctuations of the lattice are more likely than low frequency fluctuations.

(k). The Fluctuation Dissipation theorem only applies to magnetic resonance relaxation.

(l). Fourier transforms resolve the intensity of fluctuations at different frequencies.

(m). The driving forces that change spin states must be aligned perpendicular to the external field direction. Such forces include rf-irradiation and the fluctuating magnetic fields responsible for spin-lattice relaxation.

(n). The correlation function of a random motion follows the value of the coordinate at time t relative to the value at a time delay of τ seconds later.

(o). The ensemble average used in finding the correlation function is necessary because each determination of the time average of $f(t)f(t+\tau)$, for the same τ, gives a different result.

**Literature Cited:**

1. A. Carrington, A. D. McLachlan, *Introduction to Magnetic Resonance*, Harper & Row, New York, NY, 1967. pp. 182-194.
2. A. D. Bain, "Chemical Exchange NMR," *Prog. in N.M.R.*, **2003**, *43*, 67-71.
3. P. A. Duspara, C. F. Matta, S. I. Jenkins, P. H. M. Harrison, "Twisted Amides: Synthesis and Structure of 1,6-Dipivaloyl-3,4,7,8- tetramethyl-2,5-dithioglycoluril," *Org. Lett.*, **2001**, *3(4)*, 495–498.